

UNIVERSIDADE DE LISBOA

FACULDADE DE FARMÁCIA



Development of new screening methodologies and preparation
methods with application in amorphous solid dispersions
and pharmaceutical cocrystals

Íris Daniela Correia da Silva Duarte

Orientador: Prof. Doutor João Fernandes de Abreu Pinto

Coorientador: Doutor Márcio Milton Nunes Temtem

Tese especialmente elaborada para obtenção do grau de Doutor no ramo de
conhecimento de Farmácia, especialidade de Tecnologia Farmacêutica.

Júri:

Presidente: Prof. Doutora Matilde da Luz dos Santos Duque da Fonseca e Castro

Vogais:

- *Prof. Doctor Thomas Rades;*
- Prof. Doutora Ana Isabel Nobre Martins Aguiar de Oliveira Ricardo;
- *Doctor Marco António Dias de Sousa Gil;*
- Prof. Doutor Rogério Paulo Pinto de Sá Gaspar;
- Prof. Doutora Helena Maria Cabral Marques.

Abstract

The number of drugs with solubility limitations under development has been increasing. Limited aqueous solubility is a major challenge in the development of oral-dosage forms, as it may impact oral bioavailability. To circumvent this issue various solubilization strategies have been developed. Two of these strategies are the generation of amorphous solid dispersions and pharmaceutical cocrystals. Amorphous solid dispersions are today one of the most popular solubilization strategies to improve solubility. In contrast, pharmaceutical cocrystals are an emerging technology, but whose acceptance has been increasing in the last years.

In this thesis, new computational screening methods to predict drug-polymer kinetic miscibility and *in vivo* performance were developed to support the early formulation design of amorphous solid dispersions.

Regarding the computational tool to predict kinetic miscibility, this consisted on the implementation of a mathematical model that combined thermodynamic, kinetic and process considerations. The novelty of this model is related with its potential to evaluate a ternary system made of drug, polymer and solvent, as well as, the consideration of time dependent phenomena, such as components' diffusion and solvent evaporation. For considering the evaporation of the solvent, the practical utility of this tool was demonstrated for the early development of amorphous dispersions produced by spray drying. The results obtained with the model not only enabled the ranking of the polymers according to their miscibility capacity with the drug, but also the narrowing of an optimal drug load range within which drug-polymer miscibility is guaranteed. In what accounts the computational tool to predict amorphous solid dispersions *in vivo* performance, this consisted on a statistical model having as input several molecular descriptors of the drug and the polymer, and as output *in vivo* pharmacokinetic data such as the area under the curve (AUC) and the maximum concentration (C_{\max}) achieved in the pharmacokinetic profile. The novelty of this model is related to the fact that the experimental *in vivo* data were obtained from the literature. The results produced generalized performance trends, as well as identified the molecular descriptors with higher influence for the *in vivo* performance.

New and alternative manufacturing methods were also explored in this thesis, for the generation of amorphous solid dispersions and pharmaceutical cocrystals. New technologies that allow the control of the particle size at the nano-scale while maintaining the amorphous state, or technologies with reduced footprint that allow the particle engineering of cocrystals are scarce in the literature.

A novel solvent controlled precipitation process based on microfluidization was assessed to produce nano-sized amorphous solid dispersions. Moreover, an experimental design was conducted to study the effect of different formulation variables (*viz.* polymer type, drug load, and feed solid's concentration) on the particle size and morphology, drug's solid state and drug's molecular distribution within the carrier of the co-precipitated materials produced. Nano-composite aggregated particles were produced after isolation using spray drying. According to the results obtained it was possible to conclude that the particle size of the spray-dried aggregates was dependent on the feed solids' concentration, while the level of aggregation between nanoparticles was dependent on the drug-polymer ratio. Depending on the type of polymeric stabilizer and the drug load in formulation, amorphous nano-solid dispersions or crystalline nano-solid dispersions could be produced. The small particle size at the nano-scale, *i.e.* the high surface area, was found to be a more important factor than the amorphization of the drug, to enhance the dissolution-rate and *in vivo* bioavailability of a model drug whose absorption is dissolution-rate limited.

Spray congealing was the technology evaluated for the production of cocrystals. The work considered a feasibility study, followed by an experimental design to assess the impact of varying atomization and cooling-related process parameters on cocrystals formation, purity, particle size and shape, and bulk powder flow properties. It was demonstrated that spray congealing could be used to produce cocrystals particles. These were compact and spherical particles consisting of aggregates of individual cocrystals fused or adhered to each other. Varying the process parameters did not influence cocrystals formation, but had an impact on cocrystals purity. Moreover, it was demonstrated that cocrystals particle properties can be adjusted in a single process step, by varying the atomization and cooling efficiency, in order to produce particles more suited for incorporation in the final dosage forms.

Resumo

O número de fármacos com solubilidade limitada em desenvolvimento tem vindo a aumentar. A baixa solubilidade é um dos grandes desafios no desenvolvimento de formas farmacêuticas orais, pois pode afetar a biodisponibilidade. De modo a ultrapassar este problema, várias estratégias de solubilização têm sido desenvolvidas. Duas destas estratégias são a produção de dispersões sólidas amorfas e cocrystalis farmacêuticos. As dispersões sólidas amorfas são hoje em dia uma das estratégias de solubilização mais divulgadas para melhorar a solubilidade. Por oposição, os cocrystalis farmacêuticos são uma tecnologia emergente, mas cuja aceitação tem vindo a crescer nos últimos anos.

Nesta tese, novos métodos de rastreio de natureza computacional foram desenvolvidos para prever a miscibilidade cinética e o desempenho *in vivo* de uma dada combinação fármaco-polímero, tendo como objetivo último apoiar o processo de formulação de novas dispersões sólidas amorfas.

A ferramenta computacional para prever a miscibilidade cinética, consistiu na implementação de um modelo matemático que combina parâmetros termodinâmicos, cinéticos e de produção de dispersões sólidas. A novidade deste modelo relaciona-se com o seu potencial para avaliar sistemas ternários compostos por fármaco-polímero-solvente, bem como a consideração de fenómenos dependentes do tempo, tais como a difusão dos componentes da formulação e a evaporação do solvente. Por considerar a evaporação do solvente, a utilidade prática desta ferramenta foi demonstrada para o desenvolvimento de dispersões amorfas produzidas por secagem por aspersão. Os resultados obtidos com o modelo não só permitiram hierarquizar os polímeros de acordo com a sua miscibilidade com o fármaco, mas também reduzir a gama de concentrações de fármaco para uma gama ótima, dentro da qual a miscibilidade fármaco-polímero está garantida. No que toca à ferramenta computacional para prever o desempenho *in vivo* das dispersões sólidas amorfas, esta consistiu no desenvolvimento de um modelo estatístico, tendo como variáveis independentes descritores moleculares do fármaco e do polímero, e como variáveis dependentes dados farmacocinéticos como a área sob a curva e a concentração plasmática máxima atingida. A novidade deste modelo relaciona-se com o facto de considerar dados experimentais *in vivo* obtidos a partir da literatura. Os resultados obtidos permitiram identificar tendências generalizadas ao nível do desempenho que foram transversais a diferentes classes de fármacos e polímeros, bem como a identificação dos descritores moleculares com maior influência no desempenho *in vivo* de uma dispersão sólida amorfa.

Métodos de produção alternativos, robustos, economicamente eficientes e facilmente escaláveis do laboratório para a escala industrial, também foram explorados nesta tese, mais especificamente para a produção de dispersões sólidas amorfas e cocristais farmacêuticos. Tecnologias que permitam o controlo do tamanho de partícula à nano-escala bem como a manutenção do estado amorfo, ou tecnologias com baixo impacto no ambiente e que permitam a engenharia de partículas de cocristais, são escassas de acordo com o estado da arte.

Assim, um novo processo de precipitação controlada por solvente tendo por base a microfluidização foi avaliado para produzir dispersões sólidas amorfas à escala nano. Adicionalmente, foi considerado um desenho experimental para estudar o efeito de variáveis independentes de formulação - tipo de polímero, concentração de fármaco, e concentração de sólidos na solução inicial – nas propriedades finais dos produtos co-precipitados, tais como o tamanho das partículas e sua morfologia, estado sólido do fármaco e distribuição deste último no polímero. O estudo de viabilidade foi demonstrado com sucesso, sendo que partículas agregadas e nano-compósitas foram obtidas após isolamento por secagem por aspersão. De acordo com os resultados obtidos foi possível concluir-se que o tamanho de partícula dos agregados obtidos após secagem foi dependente da concentração de sólidos na solução inicial, enquanto que o nível de agregação entre nanopartículas foi dependente do rácio fármaco-polímero. Dependendo do tipo de polímero e da concentração de fármaco na formulação, para além de nano dispersões sólidas amorfas, foi também possível obter-se nano dispersões sólidas cristalinas. Observou-se que a redução do tamanho de partícula à nano-escala foi um fator mais importante do que a amorfização do fármaco para melhorar a velocidade de dissolução e a biodisponibilidade *in vivo* de um fármaco cuja absorção é limitada pela sua velocidade de dissolução.

O congelamento por aspersão foi a tecnologia avaliada para a produção de cocristais. O trabalho incluiu um estudo de viabilidade, seguido de um desenho experimental de modo a avaliar o efeito de variáveis independentes de processo, relacionadas com a atomização e o arrefecimento, nas propriedades finais, tais como a formação e pureza do cocrystal, tamanho de partícula e morfologia e propriedades do pó. Demonstrou-se que o congelamento por aspersão pode ser usado para produzir cocristais. Obtiveram-se partículas compactas e esféricas, consistindo em agregados de cocristais individuais. A variação dos valores dos parâmetros de processo não influenciaram a formação do cocrystal, mas afetaram a sua pureza. Demonstrou-se que as propriedades das partículas de cocrystal podem ser ajustadas num único passo do processo, manipulando a atomização e o arrefecimento, de modo a otimizar as partículas e facilitar a sua incorporação em formas farmacêuticas orais.

Acknowledgements/Agradecimentos

Chegado ao fim deste ciclo, concluo que foi um caminho longo, com os seus altos e baixos, mas com a certeza porém, de que não teria sido possível chegar onde cheguei, sem a força, ajuda, e compreensão de um conjunto de pessoas muito importante.

Em primeiro lugar, quero agradecer aos meus orientadores, Prof. João Pinto e Márcio Temtem. Ao Prof. João Pinto pela sua orientação, incentivo, disponibilidade e apoio que sempre demonstrou. Obrigada Professor por ter contribuído para meu crescimento enquanto aluna de doutoramento e cientista. Ao Márcio pela orientação e total disponibilidade. Pelo seu entusiasmo pela ciência, pela sua ambição e perseverança, pela paciência, exigência e ritmo que impôs quando foi necessário. Obrigada Márcio pelos ensinamentos, pelo voto de confiança, e por teres sido o meu tutor neste projeto.

Quero também agradecer à Faculdade de Farmácia, Departamento de Tecnologia Farmacêutica e ao iMed.Ulisboa, pela sua simpatia e por me fazerem sentir parte integrante da instituição. Aos colegas de doutoramento da faculdade, nomeadamente ao Gonçalo, à Maria e à Joana Pinto, com quem partilhei momentos trabalho, desanuviados por alguma diversão, obrigada!

À Fundação para a Ciência e Tecnologia pelo financiamento da bolsa de doutoramento em ambiente empresarial.

Um agradecimento especial à empresa Hovione FarmaCiência e seus colaboradores, que de uma forma direta ou indireta me ajudaram na concretização desta tese. Pelo financiamento, pela atenção, pela paciência e disponibilidade demonstradas. Quero agradecer também a **todos** os colegas que passaram pelo grupo do *R&D Drug Product Development* nos últimos anos e que me ajudaram. Ao Conrad, aos colegas do grupo do *Oral Dosage Forms* e Inalação, da Analítica e Técnicos dos laboratórios do B5 e B21, a todos o meu sincero e profundo agradecimento. Aos colegas de doutoramento/mestrado que me acompanharam e apoiaram ao longo deste percurso, nomeadamente ao João, à Kinga, à Cláudia, à Lúcia, ao Tiago, ao Nuno, à Diana e à Beatriz. Obrigada pelas discussões científicas, pelo apoio no laboratório, pela camaradagem, pelo ombro amigo, pelas brincadeiras e gargalhadas!

Por último, quero agradecer à minha família e ao Sérgio, pelo apoio, pela paciência, pelo amor durante estes últimos anos, pois sem eles a realização deste projeto teria sido impossível.

List of Contents

1	Introduction	3
1.1	Amorphous solid dispersions.....	5
1.1.1	General considerations.....	5
1.1.2	Early formulation design	9
1.1.3	Overview of the technologies used to prepare ASDs	18
1.2	Pharmaceutical cocrystals.....	21
1.2.1	General considerations.....	21
1.2.2	Overview of the technologies used to prepare cocrystals.....	23
1.3	Motivations and objectives of the project.....	24
1.4	Hypothesis and thesis layout.....	27
1.5	References.....	28
2	Screening methodologies for the development of spray-dried amorphous solid dispersions	41
2.1	Introduction.....	41
2.2	Materials and Methods.....	41
2.2.1	Materials	41
2.2.2	Methods	42
2.3	Results.....	49
2.3.1	F-H interaction parameter calculation using solubility parameters	49
2.3.2	Drug-polymer kinetic miscibility predictions.....	50
2.3.3	Solvent casting and spray drying experiments	54
2.4	Discussion.....	59
2.4.1	Validation of the TKE model and screening methodology	61
2.5	Conclusions.....	63
2.6	References.....	64

3	Predicting the <i>in vivo</i> performance of amorphous solid dispersions based on molecular descriptors and statistical analysis	71
3.1	Introduction.....	71
3.2	Methodology.....	72
3.2.1	Database.....	72
3.2.2	Molecular descriptors and experimental data	73
3.2.3	Statistical analysis.....	76
3.3	Results and Discussion	77
3.3.1	Dataset overview by Principal Components Analysis (PCA)	77
3.3.2	Finding correlations between molecular descriptors and ASDs <i>in vivo</i> performance using Partial Least Squares (PLS) modeling	79
3.4	Conclusions.....	84
3.5	References.....	85
4	Production of nano-solid dispersions using a novel solvent-controlled precipitation process – benchmarking their <i>in vivo</i> performance with an amorphous micro-sized solid dispersion produced by spray drying.....	93
4.1	Introduction.....	93
4.2	Materials and Methods.....	94
4.2.1	Materials	94
4.2.2	Methods	94
4.3	Results and Discussion	101
4.3.1	Part I - Experimental Design	101
4.3.2	Part II - Benchmarking solid dispersions obtained through SCP and SD processes	108
4.4	Conclusions.....	117
4.5	References.....	118

5 Green production of cocrystals using a new solvent-free approach	
by spray congealing	125
5.1 Introduction.....	125
5.2 Materials and Methods.....	127
5.2.1 Materials	127
5.2.2 Methods	128
5.3 Results and Discussion	131
5.3.1 Feasibility study: cocrystals of 1:1 CAF:SAL and 1:1 CBZ:NIC using spray congealing.....	131
5.3.2 2 ² +1 Experimental design: particle engineering of 1:1 CAF:GLU cocrystals	136
5.4 Conclusions.....	142
5.5 References.....	143
6 Conclusions and future work	149
Supplementary Information.....	154
A. Chapter 2.....	154
B. Chapter 3.....	159
C. Chapter 4.....	160
D. Chapter 5.....	164

List of Abbreviations

AFM	Atomic force microscopy
ANDA	Abbreviated New Drug Application
API	Active pharmaceutical ingredient
ASD	Amorphous solid dispersion
AUC	Area under the curve
BCS	Biopharmaceutical Classification System
CAF	Caffeine
CBZ	Carbamazepine
CED	Circular equivalent diameter
CQA	Critical quality attribute
CSD	Cambridge Structural Database
DCM	Dichloromethane
DCS	Developability Classification System
DMA	Dimethylacetamide
DMF	Dimethylformamide
DoE	Design of Experiments
Eudragit® EPO	Dimethylaminoethyl methacrylate, butyl methacrylate, and methyl methacrylate copolymer
Eudragit® L100	1:1 Methacrylic acid and methyl methacrylate copolymer
FaSSIF	Fasted state simulated intestinal fluid
FDA	Food and Drug Administration
F-H	Flory-Huggins
GI	Gastrointestinal
GLU	Glutaric acid
HCl	Hydrochloric acid
HHSP	Hildebrand and Hansen solubility parameters
HME	Hot melt extrusion
HPH	High pressure homogenization
HPLC	High performance liquid chromatography
HPMCAS	Hydroxypropylmethylcellulose acetate succinate
ITZ	Itraconazole
LOQ	Limit of quantification

(m)DSC	(modulated) Differential scanning calorimetry
MeOH	Methanol
NCE	New chemical entity
NDA	New Drug Application
NIC	Nicotinamide
PBPK	Physiologically-based Pharmacokinetic
PC	Principal component
PCA	Principal components analysis
PDE	Partial differential equation
PK	Pharmacokinetic
PLM	Polarized light microscopy
PLS	Partial least squares method
POL	Polymer
PVP/VA	Polyvinylpyrrolidone-vinyl acetate copolymer
QSAR	Quantitative structure activity relationships
SAL	Salicylic acid
SC	Solvent casting
SCF	Supercritical fluid methods
SCG	Spray congealing
SCP	Solvent controlled precipitation
SD	Spray drying
SDD	Spray dried dispersion
SEDDS	Self-emulsifying drug delivery systems
SEM	Scanning electron microscopy
SP	Solubility parameter
TKE	Thermodynamics, Kinetics and Evaporation model
UCST	Upper critical solution temperature
UV	Ultraviolet
VIP	Variable importance plot
XRPD	X-ray powder diffraction

List of Figures

Figure 1.1. Biopharmaceutical Classification System (BCS, A) and approximate BCS distribution of the new chemical entities (NCEs) and marketed products (B).....	4
Figure 1.2. Representation of the activation energies (E_a) and kinetic barriers that an amorphous drug alone or dispersed in a carrier (<i>i.e.</i> amorphous solid dispersion) need to overcome for recrystallization to take place.	6
Figure 1.3. The supersaturation state: the “spring” and “parachute” effect.	8
Figure 1.4. Hypothetical thermodynamic phase diagram for an API-polymer system.....	14
Figure 1.5. Representation of the experimental screening methodologies applied to evaluate supersaturation: the solvent- or pH-shift method, and the amorphous film dissolution method.....	17
Figure 1.6. Selection of the manufacturing technology based on the drug’s melting point and drug’s solubility in organic solvent.....	19
Figure 1.7. Number of product programs with respect to small molecule, pharmaceutical cocrystals.....	22
Figure 1.8. Most common manufacturing methods to produce cocrystals	23
Figure 2.1. Representation showing the application of the TKE model as a screening tool for the development of amorphous systems.....	44
Figure 2.2. Results from 1D simulations showing the expected final phase behavior of ITZ:HPMCAS-MG, ITZ:PVPVA/64 and ITZ:Eudragit® EPO systems with increasing drug concentration (from left to right).	51
Figure 2.3. Results from 1D and 2D simulations showing the phase composition of ITZ:PVPVA/64 system with increasing drug load within the kinetic miscibility discontinuity boundary (from 45% to 65% ITZ w/w).....	53
Figure 2.4. Results from 1D and 2D simulations presenting the final phase behavior of ITZ:PVPVA/64 system at 52.5% (w/w) ITZ.	54
Figure 2.5. Reversible heat flow thermograms for the 45 and 65% (w/w) ITZ:HPMCAS-MG cast films (SC) and spray-dried materials (SD).	56
Figure 2.6. Reversible heat flow thermograms obtained for the 45, 65 and 85% (w/w) ITZ:PVP/VA 64 cast films (SC) and respective spray-dried materials (SD).....	58

Figure 2.7. Reversible heat flow thermograms obtained for the 15 and 35 (wt.%) ITZ:Eudragit® EPO cast films (SC) and respective spray-dried materials (SD)...	59
Figure 2.8. Theoretical miscibility predictions given by the TKE model and analytical results obtained for the solvent casting films and spray drying products, as a function of drug load.	61
Figure 2.9. Workflow for the early development of a new spray dried amorphous solid dispersion.....	63
Figure 3.1. Representation of the database.....	72
Figure 3.2. Score plot (A) and loading plot (B) of the two first PCs of the PCA dataset.	78
Figure 3.3. Observed data versus predicted data by the PLS model.....	80
Figure 3.4. PLS loading plot (A) and correspondent variable importance plot (B).....	82
Figure 3.5. Scatter plots of two important variables for the model.....	84
Figure 3.6. Workflow showing the application of the PLS model as a screening tool for development of amorphous systems.....	85
Figure 4.1. Representation of the experimental design for the SCP process study.....	95
Figure 4.2. Representation of the solvent/anti-solvent controlled precipitation process, followed by the isolation step in a spray dryer.....	96
Figure 4.3. SEM micrographs corresponding to Tests 1, 2, 3 and Tests 4, 5, 6 of the DoE conducted.	102
Figure 4.4. Representation of a hypothetical ternary phase diagram for the system polymer-solvent-anti-solvent.....	103
Figure 4.5. Mean circular diameter results correspondent to Tests 1, 2, 3 and Tests 4, 5, 6 of the DoE conducted.....	104
Figure 4.6. Powder diffractograms correspondent to Tests 1, 2, 3 and Tests 4, 5, 6 of the DoE conducted.	105
Figure 4.7. Representation of a hypothetical temperature-composition phase diagram for a general drug-polymer binary system.	108
Figure 4.8. Powder dissolution profiles correspondent to the formulations <i>NanoAmorphous</i> (20% CBZ: Eudragit® L100, squares), <i>NanoCrystalline</i> (60% CBZ: Eudragit® L100 diamonds), <i>MicroAmorphous</i> (20% CBZ: Eudragit® L100, triangles), pure crystalline CBZ (circles)	110
Figure 4.9. SEM micrographs corresponding to the <i>NanoAmorphous</i> , <i>MicroAmorphous</i> and <i>NanoCrystalline</i> powders, from left to right.	111

Figure 4.10. Pharmacokinetic profiles, correspondent to the formulations <i>NanoAmorphous</i> (20% CBZ:Eudragit [®] L100, squares), <i>NanoCrystalline</i> (60% CBZ:Eudragit [®] L100, diamonds), <i>MicroAmorphous</i> (20% CBZ:Eudragit [®] L100, triangles), pure crystalline CBZ (circles)	114
Figure 4.11. Powder diffractograms correspondent to the <i>NanoAmorphous</i> and <i>MicroAmorphous</i> formulations after 90 days of storage at 25°C/65% RH (A and B, respectively) and 45°C/75% RH (A.1 and B.1, respectively).....	117
Figure 5.1. Representation of the spray congealing process.	125
Figure 5.2. Chemical structures of the APIs and cofomers considered in the study	127
Figure 5.3. Total heat flow profiles of 1:1 CAF:SAL (A) and 1:1 CBZ:NIC (B)	132
Figure 5.4. Powder diffractograms correspondent of 1:1 CAF:SAL (A) and 1:1 CBZ:NIC (B).....	134
Figure 5.5. Micrographs correspondent of 1:1 CAF:SAL (A) and 1:1 CBZ:NIC (B).....	135
Figure 5.6. Total heat flow profiles correspondent of 1:1 CAF:GLU.....	136
Figure 5.7. XRPD diffractograms correspondent of 1:1 CAF:GLU	138
Figure 5.8. SEM micrographs correspondent to the 1:1 CAF:GLU cocrystals obtained.....	141

List of Tables

Table 1.1. Examples of medicines (oral-dosage forms) according to different solubilization techniques commonly used to circumvent poor water solubility limitations.....	5
Table 1.2. Examples of marketed ASDs-based medicines	7
Table 1.3. Examples of full screening programs reported in the literature	11
Table 2.1. Physicochemical properties of the raw materials considered in this project.....	50
Table 3.1. ASDs considered as observations, with respective abbreviations and references..	74
Table 4.1. Experimental design for the SCP study.....	95
Table 4.2. Results for the surface area for the <i>NanoAmorphous</i> , <i>MicroAmorphous</i> and <i>NanoCrystalline</i> powders.	111
Table 5.1. API/coformer systems tested and process variables defined for each test.	129
Table 5.2. Onset temperatures and enthalpy values of the endothermic events detected in the thermal profiles of the pure components, respective physical mixtures and spray-congealed products	133
Table 5.3. Peak areas measured at $11.8\ 2\theta$ for the 5 wt.% CAF:standard cocrystal physical mixture and for the different tests performed	139
Table 5.4. Number-based circular equivalent diameter distribution, compressibility and pressure drop across the powder bed for Test 1 to Test 5	142

Chapter 1

1 Introduction

Among the various routes of drug administration, oral delivery is invariably the most preferred, due to the ease of use, convenience to patients and clinicians, and general lower manufacturing costs. According to the Food and Drug Administration (FDA), 53% of the new drug approvals in 2015 were solid oral dosage forms, such as tablets or capsules [1]. Moreover, oral drug delivery today represents the largest share of the pharmaceutical market (around 60%), and this position is expected to be maintained in the future [2,3].

One of the most important parameters used to measure oral drug formulation performance is bioavailability. Oral bioavailability can be defined as the percentage of active drug (or metabolite) that enters the systemic circulation and reaches the site of action [4]. Attaining adequate and consistent systemic exposure or bioavailability is important for improving drug's therapeutic efficacy [5].

Upon ingestion and disintegration of the dosage form in the gastrointestinal (GI) tract, there are four main pharmacokinetic stages that characterize a drug's journey through the body – absorption, distribution, metabolism, and excretion (ADME). In particular, absorption, or the fraction of drug absorbed in the GI tract, highly influences bioavailability. Ideally, a drug should present high solubility in the aqueous GI fluids, and high permeability across biological membranes, either via passive diffusion or active transport. According to the Biopharmaceutical Classification System (BCS) these are considered Class I compounds (Figure 1.1 A). BCS Class I compounds are the best candidates to work with for formulation scientists, as there are no physicochemical limitations to their absorption. However, today there are few BCS Class I compounds both in development and market (Figure 1.1 B).

Indeed, current pharmaceutical pipelines are highly populated with new drug candidates belonging to BCS Class II or Class IV, thus presenting low solubility and high permeability, or low solubility and low permeability, respectively. It is estimated that around 70-90% of the new molecules in the pharmaceutical pipeline present at least solubility constraints.

The reasons behind this growing trend of poorly water-soluble drugs are two-fold and include the current drug-receptor targets being addressed and the current drug discovery methodologies. Combinatorial chemistry, *in silico* modelling and high throughput screening techniques started to be routinely used in drug discovery. These methods tend to select drug candidates with certain physicochemical properties that are not compatible with high solubility

and high permeability. New chemical entities (NCEs) are becoming structurally more complex, with high molecular weight and more lipophilic.

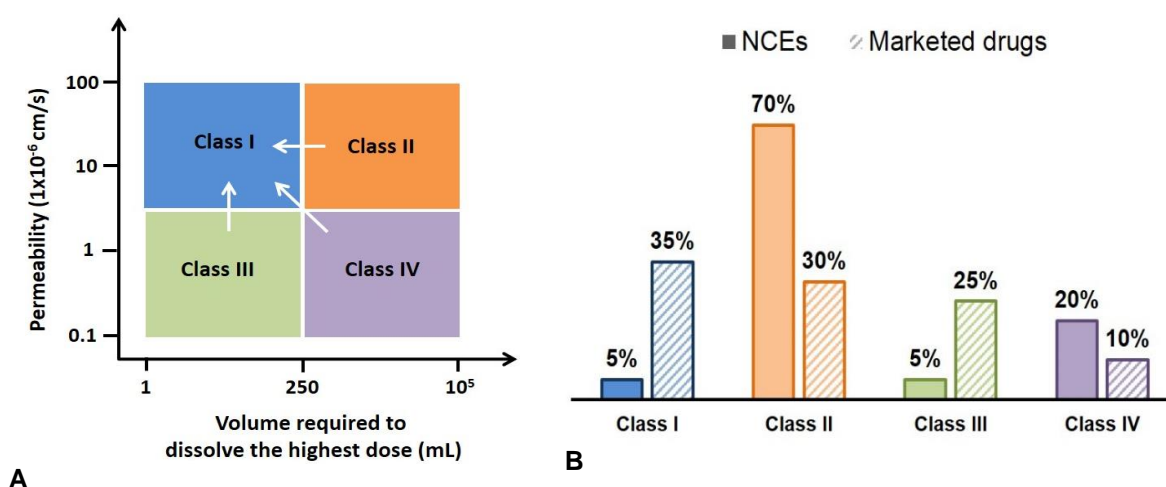


Figure 1.1. Biopharmaceutical Classification System (BCS, A) and approximate BCS distribution of the new chemical entities (NCEs) and marketed products (B) (adapted from [6]).

Limited aqueous solubility has been one of the major hurdles in the development of oral-dosage forms, mainly because poor solubility hinders oral bioavailability. Thus, to circumvent this issue and to continue to provide new therapies for patients, in the last decades, scientists and engineers have explored different formulation strategies with the ability to further increase aqueous drug's solubility and bioavailability. Considering the BCS (Figure 1.1 A), the ultimate goal is to move Class II, Class III and Class IV compounds towards Class I, considered as the best-case scenario in terms of water solubility and permeability properties. Some examples of well-established solubilization technologies are particle-size reduction (such as the production of nanocrystals), complexation with cyclodextrines, lipid-based techniques [such as self-emulsifying drug delivery systems (SEDDS)], and production of solid dispersions (either crystalline or amorphous). Table 1.1 shows some marketed pharmaceutical products obtained by these techniques.

Among the emerging formulation strategies, pharmaceutical cocrystallization became known as an alternative crystal-engineering platform to improve the physicochemical properties of challenging crystalline APIs, and is today an emerging technology for improving the low solubility of modern compounds.

Table 1.1. Examples of medicines (oral-dosage forms) according to different solubilization techniques commonly used to circumvent poor water solubility limitations [7-10].

Product	Drug (BCS Class)	Company	Year of approval
<i>Nanocrystals</i>			
Rapamune [®]	Sirolimus (II)	Wyeth	2000
Emend [®]	Aprepitant (IV)	Merck	2003
TriCor [®]	Fenofibrate (II)	Abbott	2003
Triglide [®]	Fenofibrate (II)	Shionogi	2005
Megace [®] ES	Megestrol acetate	Par Pharm	2005
<i>Cyclodextrin complexes</i>			
Ulgut [®]	Benexate	Shionogi	1987
Pansporin T [®]	Cefotiam hydrochloride	Takeda	1990
Brexin [®]	Piroxicam (II)	Chiesi	1993
Meiact [®]	Cefditoren (IV)	Meiji Seika Pharma	2006
<i>SEDDS</i>			
Sandimmune [®]	Cyclosporin A (IV)	Novartis	1990
Neoral [®]	Cyclosporin (II)	Novartis	1995
Norvir [®]	Ritonavir (IV)	Abbott	1996
Gengraf [®]	Cyclosporin A (IV)	Abbott	2000
Aptivus [®]	Tipranavir (II)	Boehringer Ingelheim	2005
<i>Solid Dispersions</i>			
Gris-PEG [®]	Griseofulvin (II)	Pedinol	1975
Sporanox [®]	Itraconazole (II)	Janssen	1992
Kaletra [™]	Liponavir/Ritonavir (II/IV)	Abbott	2005
Cesamet [®]	Nabilone (II)	Valeant	2006
Certican [®]	Everolimus	Novartis	2010

1.1 Amorphous solid dispersions

1.1.1 General considerations

The production of the amorphous form of the drug is, in certain cases, enough to overcome its solubility issues. Since the amorphous state is a metastable state and because the amorphous materials lack of long-range order, the typical energetic barriers that need to be overcome during the dissolution of crystalline materials (*i.e.* crystal lattice disruption, solvent's cavitation, hydration of drug molecules) are easily surpassed [11]. This is the reason why amorphous materials are more soluble than the crystalline counterparts. However, due to the inherent thermodynamic instability of the amorphous state, this approach is often hindered by

recrystallization of the drug over time. The use of polymeric matrices in order to improve amorphous drug physical stability is an apparently simple alternative that has been attracting formulators' interest. Miscible drug-polymer blends are more resistant to drug crystallization than the amorphous drug alone because the chemical potential of the drug is reduced and the kinetic barrier or activation energy to crystallization increases, as can be seen in Figure 1.2 [12].

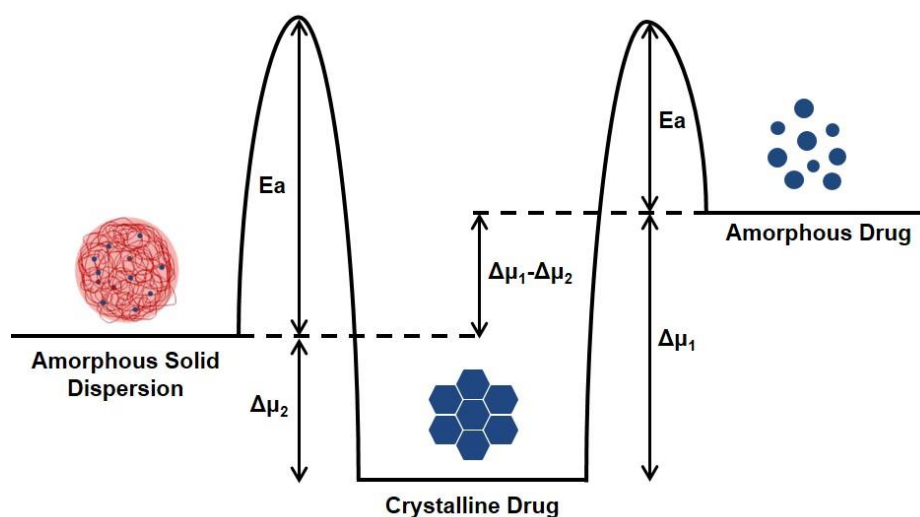


Figure 1.2. Representation of the activation energies (E_a) and kinetic barriers that an amorphous drug alone or dispersed in a carrier (*i.e.* amorphous solid dispersion) need to overcome for recrystallization to take place. The chemical potential (μ) of the amorphous drug in both situations with respect to the crystalline drug is also schematically represented (adapted from [12]).

Indeed, amorphous solid dispersions (ASDs) are today one of the most important solubilization strategies to overcome the limited bioavailability of BSC Class II compounds. Their efficiency and popularity is not only reflected in the increasing percentage of ASDs demonstrating improved bioavailability when compared with the reference products [13], but also in the significant number of amorphous-based medicines reaching the market since its appearance in the early 90's (Table 1.2).

The distinctive advantage of ASDs is that, once the formulation components start to dissolve in the gastro-intestinal fluids, a supersaturated state is obtained and drug concentration in solution may reach values well above its intrinsic solubility. With a higher amount of drug in solution, more drug is available to be absorbed and this will ultimately improve bioavailability. Amorphous formulations presenting up to 100-fold enhancement in bioavailability comparing with the crystalline formulation have been reported in the literature [7,13].

Table 1.2. Examples of marketed ASDs-based medicines [7,8,10,17,18].

Product	Drug (BCS Class)	Company	Technology	Year of approval
Sporanox [®]	Itraconazole (II)	Janssen	Spray Layering ^a	1992
Prograf [®]	Tacrolimus (II)	Astellas	Spray Drying	1994
Rezulin ^{® b}	Troglitazone	Pfizer	-	1997
Kaletra [™]	Lopinavir (II) / Ritonavir (IV)	Abbott	Hot Melt Extrusion	2005
Cesamet [®]	Nabilone (II)	Valeant	-	2006
Fenoglide [™]	Fenofibrate (II)	LifeCycle Pharm	Hot Melt Extrusion	2007
Intelence [™]	Etravirine (IV)	Janssen	Spray Drying	2008
Norvir [®]	Ritonavir (IV)	Abbott	Hot Melt Extrusion	2010
Onmel [™]	Itraconazole (II)	Merz Pharm	Hot Melt Extrusion	2010
Certican [®]	Everolimus	Novartis	Spray Drying	2010
Incivek ^{® b}	Telaprevir (II)	Vertex	Spray Drying	2011
Zelboraf [™]	Vemurafenib (IV)	Roche	Co-precipitation	2011
Kalydeco [™]	Ivacaftor (II or IV)	Vertex	Spray Drying	2012
Noxafil [®]	Posaconazole (II)	Merck	Hot Melt Extrusion	2013
Belsomra [®]	Suvorexant	Merck	-	2014
Viekira [™]	Ombitasvir/Paritaprevir/ Ritonavir/Dasabuvir	Abbott	Hot Melt Extrusion	2014
Harvoni [®]	Ledipasvir/Sofosbuvir	Gilead	-	2014
Orkambi [®]	Lumacaftor/Ivacaftor	Vertex	Spray Drying	2015

^a *i.e.* spray drying on sugar beads; ^b marketed discontinued.

Supersaturation can be explained by the so called “spring” and “parachute” effect [14]. The “spring” effect is the instantaneous peak when the concentration of drug is well above its saturation limit (Figure 1.3). However, the drug in solution will tend to precipitate over time, eventually losing the advantages acquired. The key aspect is to maintain the supersaturated state as long as possible, in order to extend the “parachute” effect, as shown in the blue curve in Figure 1.3.

To retard drug’s precipitation, the presence of stabilizing polymers is crucial. Polymers are capable of hindering drug nucleation and crystal growth in solution either by interacting with the drug via hydrogen bonding and other ionic interactions and/or through the formation of different drug-polymer assemblies, such as nano and micellar structures, where the drug is

safe against recrystallization [15]. The high viscosity of certain polymer grades may also contribute for retarding drug nucleation and crystal growth, by reducing drug's molecular diffusion and molecular collision in solution [16].

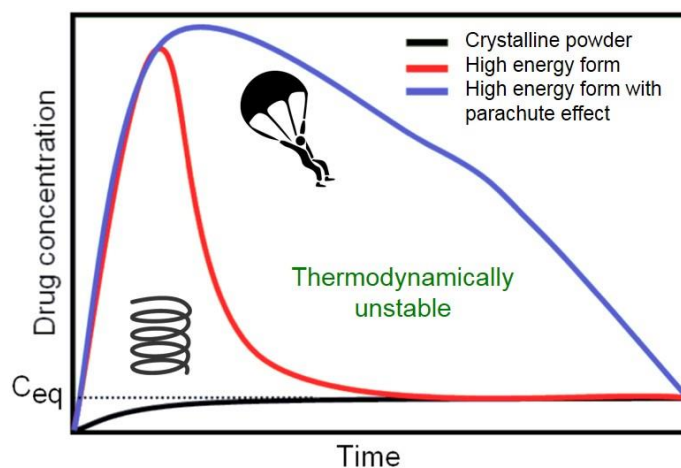


Figure 1.3. The supersaturation state: the “spring” and “parachute” effect.

The use of polymeric excipients is also important in the immobilization of the drug molecules in the solid state or during the shelf-life of the product, keeping the latter separate from each other, and thus preventing the formation of amorphous clusters, nucleation and growing of crystalline material. It has been suggested that the shelf life of the final drug product should be at least two years at 25°C [19]. In order to take the maximum advantage of the stabilization effect of the polymer the drug should be irregularly, preferably molecularly, dispersed within the carrier forming a one-phase system. This not only promotes drug solubilization within the carrier and physical stability during preparation and storage, but also improves wettability and dispersability of the drug when exposed to aqueous media. It is noteworthy that in this situation the drug particle size is reduced to nearly its absolute minimum (*i.e.* molecular level), which also promotes rapid dissolution.

That said, the requirements for the successful development of an ASD from any therapeutic small-molecule, especially those belonging to BCS Classes II/IV, are related with *in vivo* performance and chemical/physical stability aspects. In what regards the performance requirements, an amorphous dispersion formulation should present an improved dissolution profile compared with the crystalline reference and should be capable of sustaining drug supersaturation in solution for a longer time. Both parameters will contribute to an increased amount of drug available for absorption. In what accounts chemical/physical stability, maintaining the integrity of the amorphous drug during solid dispersion preparation,

manipulation and long-term storage must be guaranteed; otherwise, upon administration, the therapeutic effect may be compromised.

1.1.2 Early formulation design

The development of an ASD with the desirable physical stability and performance is a challenging process, due to the wide number of formulation and process variables that influence both physical and chemical properties of the product (*e.g.* several existing polymeric stabilizers, surfactants, different drug-polymer ratios, solvents, preparation methods, temperature, etc). For a long time, the selection of the best formulations was simply based on trial and error experiments, together with the own experience of researchers. Some known polymers were selected and combined with the drug, a wide range of drug-polymer ratios were studied, and a significant number of prototypes were produced using low-throughput laboratory-scale equipment [20-23]. In the end of formulation development a few grams of API were spent and only a few drug-polymer combinations were tested. Therefore, this empirical approach soon demonstrated to be too costly, time-consuming and API demanding.

At a time, in which the competition among the pharmaceutical industry demands for fast turnaround times, lower costs and to reduce the risks associated with the development of new drugs, it became critical the development of new screening methodologies and screening programs for narrowing the scope of formulations and to rapidly identify suitable systems for subsequent pre-clinical evaluation. Today, several screening methodologies are reported in the literature. Some methodologies have been developed to determine (or predict) drug-polymer physical stability (*i.e.* solubility, miscibility) [24], while others to determine drug-polymer performance in solution (*i.e.* supersaturation) [25]. The nature of the reported methodologies varies between medium to high-throughput small-scale experimentation in 96-well plates, and/or computational modeling, making use of theoretical models. The great advantage of these methodologies is the low amount of API needed (in the order of milligrams) and the possibility of running several tests at the same time. This not only allows to save time and resources (manpower), but also to study different drug-polymers combinations, at different drug loads, different solvents, temperatures and even the evaluation of adding a third component, such as surfactants. A more detailed analysis of these methodologies will be made in the following sections.

These methodologies may then be combined to produce full screening programs, in which the best drug-polymer formulations are selected based on a “funnel” approach. This means that

the less promising formulations are successively eliminated along the screening program, and only the best ones - those having acceptable properties in terms of physical stability and/or performance - will follow through the next stages of product development. A significant number of screening programs have also been disclosed in the literature. Some programs focus on the assessment of drug-polymer performance and supersaturation potential of the polymer, while others already attempted to establish broader approaches by combining methodologies that allow them to select the best amorphous formulations based not only on maximum performance but also highest physical stability. Table 1.3 summarizes some of the screening programs that have been reported. Most of them have been purely based on small-scale experimentation, where a wide range of variables can be evaluated at a time, and with minimal API requirements. More recently, some proposed screening programs include a computational screening stage prior to the bench screening [26,27]. It is often beneficial to obtain an early insight into drug-polymer mixture properties by a computational approach. The advantage of computational tools is that there is no consumption of raw materials, and typically only the chemical structure of the components under study needs to be known. In cases where the amount API available is reduced the computational stage can be highly advantageous.

The screening methodologies that have been developed and used in the state of the art to predict both physical stability and performance of ASDs will be described.

1.1.2.1 Predicting physical stability

Two critical parameters that influence the physical stability of an ASD are the selection of the polymeric carrier and definition of the drug load. Regarding the polymer, this should present a high glass transition temperature (T_g), potential hydrogen bonding sites and an acceptable miscibility capacity with the drug [26]. Regarding the drug load, typically, scientists attempt to maximize the drug fraction in the formulation aiming the development of final oral-dosage forms (*i.e.* tablets or capsules) with reduced size [11]. However, apart from drug potency, dose and solubility requirements, the optimal drug loading in the formulation should also take into account the maintenance of the physical state of the ASD.

Table 1.3. Examples of full screening programs reported in the literature.

Reference	Brief description	Throughput	Pros/Cons
Dai <i>et al.</i> [28,29]	Automated and miniaturized solvent-casting (SC) in 96-well plates, followed by kinetic solubility evaluation.	>10 excipients were screen. Drug load, polymers, dilution ratio and media were variables studied. The leading formulation was identified with < 10 mg of API, within 1-2 days.	Pros: wide design space studied; API sparing; fast method / Cons: No physical evaluation of the casted films formed, before the solubility evaluation. In certain cases, SC may result in heterogeneities.
Barillaro <i>et al.</i> [30]	Automated SC in 10 mL vials format, followed by dissolution testing.	12 excipients (7 polymers and 5 surfactants) and 3 drug loads were studied. 108 formulations (triplicates) were evaluated in 1 day, with a minimum amount of materials.	Pros: wide design space studied; API sparing; fast method / Cons: No physical evaluation of the casted films formed, before the solubility evaluation. In certain cases, SC may result in heterogeneities.
Shanbhag <i>et al.</i> [31]	Automated and miniaturized SC in 96-well plates. Casted films are held at room temperature overnight prior to dissolution. Next, a melt-press method is applied as an additional “confirmatory step” to identify suitable formulations for HME. Films follow for dissolution testing.	For the SC step, 14 binary and 48 ternary formulations were studied (6 polymers and 8 surfactants). 60 µg compound per sample. For the melt-press step, 13 ternary formulations were tested. 10 mg compound per sample.	Pros: an aging step was added to the program in order to give the most unstable formulations an opportunity to begin to recrystallize / Cons: Longer storage times or accelerated storage conditions should be used to promote aging.

Wytttenbach <i>et al.</i> [16]	Two-step screening: (1) miniaturized SC in 96-well plates, followed by dissolution; (2) A. miniaturized SC in 100 μ L DSC pans, followed by spectroscopy (FTIR); B. melt-quenched films on glass slides, followed by imaging (AFM)	28 different binary combinations studied. API requirement \sim 500 mg, within \sim 2 weeks.	Pros: detailed analysis of molecular interactions, molecular homogeneity and stability / Cons: No physical evaluation of the casted films formed, before dissolution evaluation. In certain cases, SC may result in heterogeneities.
Chiang <i>et al.</i> [32]	Miniaturized SC in 96-well plates (duplicated plates). One plate follows for physical stability assessment (XPRD) and the other plate is used for solubility measurement. The plates are transferred for stability ovens for long-term storage evaluation under stress conditions.	Minimal compound requirement to evaluate optimal drug load in 3 different polymers. The first results are obtained within 1-2 days. The time for complete screening is dependent on the number of time-points for the long-term stability.	Pros: physical stability and kinetic solubility assessment are run in parallel; long-term physical stability is evaluated / Cons: using the 96-well plate format, a dissolution profile is not possible to be obtained due to volume constraints.
Hu <i>et al.</i> [33]	Miniaturized co-precipitation screening in 1 mL glass vials in a 96 position insert. Suspensions are filtered on 96-well filter plates (duplicated plates), then the wet-solids washed and dried. One plate follows for physical stability assessment (XPRD and Raman) and the other plate is used for kinetic solubility measurement.	In one 96-well plate, it can evaluate 96 experimental conditions using only 200 mg of material. Within 1 week, it can select the best performing polymer, drug loading and solvent/anti-solvent ratio.	Pros: efficient screening tool to guide formulation development of amorphous formulations using co-precipitation; physical stability and kinetic solubility assessment are run in parallel / Cons: the residual solvent/anti-solvent content after drying may impact amorphous physical stability.

In this respect, the determination of the equilibrium crystalline drug solubility in the polymer and the drug-polymer amorphous miscibility is of great importance [34].

From a theoretical point of view, an ASD should be prepared, preferably, at a drug concentration below the equilibrium solid solubility of its crystalline form in the polymer in order to prevent supersaturation of the system and recrystallization. According to the hypothetical drug-polymer thermodynamic phase diagram represented in Figure 1.4, this equilibrium solubility of drug crystals in the polymer is represented by the solid-liquid curve. The area above this curve represents the temperature-composition region where the crystalline drug is dissolved in the polymer and both form an unsaturated solution, while the area below means that the drug is supersaturated in relation to the polymer [35].

Several screening methodologies have been proposed to predict the solid-liquid curve or the solubility of the crystalline drug in polymers at room temperature, which represents the typical storage temperature during the shelf-life of the product [36-41]. Some predictive methods are based on the determination of the solubility of the drug in a liquid monomer of the polymer [36,37] or polymer solution [41], on the determination of drug's melting point depression in drug-polymer physical mixtures [36,38,39], or on the determination of the demixing kinetics of a supersaturated drug-polymer amorphous dispersion [40]. However, the equilibrium crystalline drug concentration in polymer is typically quite low - in the range of 2-8% [42,43]- and thus incompatible with the production of tablets and/or capsules with an acceptable size to be ingested. This is the reason why, in most of the cases, formulators work above the equilibrium of drug solubility.

Now, when quench-cooling a melt composed of a drug and a polymer to a temperature below the solid-liquid curve, amorphous (liquid-liquid) phase separation may take place when entering the two-phase metastable/unstable regions, as represented in Figure 1.4 [35]. The same situation applies with the rapid evaporation of the solvent(s) from a solution containing the drug and polymer *e.g.* during a spray drying process. So, it is important to obtain information on the drug-polymer miscibility limits in order to prevent the formation of drug- and polymer-rich amorphous phases in the solid dispersion once produced, otherwise any subsequent perturbation will further cause recrystallization of the drug. Another important variable, still related to the latter, is the kinetic miscibility limit. In real terms, most ASDs are kinetically "stabilized" in a non-equilibrium state, not only due to polymeric hindrance, but also due to the process and dynamic factors related to the typical energy-intensive methods of preparation (*e.g.* hot-melt extrusion or spray drying) [44]. This is the reason why the market is crowded with amorphous

formulations composed of drug loads typically above the thermodynamic solubility and miscibility limits.

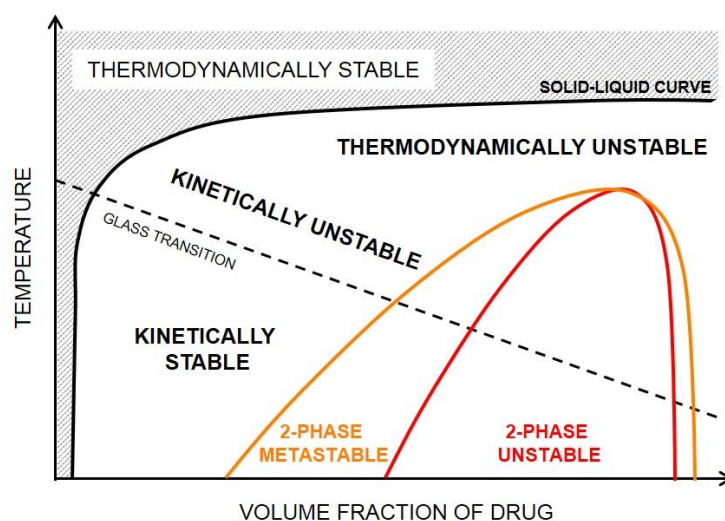


Figure 1.4. Hypothetical thermodynamic phase diagram for an API-polymer system. The black solid line represents the solid-liquid equilibrium curve or the maximum solubility of crystalline API in the polymer. The colored curves represent the API-polymer demixing or two-phase amorphous regions. The dashed line represents the glass transition temperature of hypothetically homogenous API-polymer mixtures.

Current literature describes different screening methods to predict drug-polymer miscibility. The screening strategies developed can vary between the simple implementation of theoretical models (*e.g.* solubility parameters, Flory-Huggins model) [45,46], the combination of the latter with some experimentation in order to obtain the input variables (*e.g.* melting point depression) [36,37], or the use of small-scale experimentation associated with the use of advance analytical techniques (*e.g.* DSC, Raman, AFM) [47,48].

Regarding the use of theoretical models to assess drug/polymer miscibility, the analysis of the Hildebrand and Hansen Solubility Parameters (HHSP) is one of the oldest methods considered [45,46]. Drug-polymer miscibility can be assessed qualitatively through the difference in the solubility parameters of two materials. Materials with similar values are likely to be miscible. Typically, differences ≤ 7.0 (MPa)^{1/2} is an indication of miscibility [45]. As the difference in the solubility parameters between the drug and the polymer increases, the tendency for immiscibility also increases. This method, however, possess some limitations and recent studies suggested poor correlation between the HHSP and experimental miscibility [36,46]. Nevertheless, this method is still used for an initial and rapid estimation of drug-polymer miscibility. The implementation of the Flory-Huggins lattice model has also shown utility on

the quantitative assessment of the thermodynamics of drug-polymer mixing and miscibility. The Flory-Huggins theory was initially developed to describe the phase behavior of polymer solutions but today is being widely used to study drug-polymer systems [36]. With the use of Flory-Huggins interaction parameter (χ), the temperature-composition phase diagram, as represented in Figure 1.4, can be obtained. Several authors have reported the construction of the phase diagrams as a guide for polymer ranking, selection of initial drug-polymer ratios, evaluation of manufacturing-ability and definition of storage temperatures [35,49-53]. The Flory-Huggins interaction parameter, at room temperature, is typically estimated using the Hildebrand solubility parameters, or at higher temperatures, using the experimental melting point depression method [36,37]. Both methods for estimating the interaction parameter also present limitations, which can impact the predicted drug-polymer miscibility [54]. The Flory-Huggins theory itself also fails for not considering specific drug-polymer molecular interactions, such as hydrogen bonding or ionic interactions [37]. Recently, more advanced thermodynamic models, such as the Perturbed-Chain Statistical Associating Fluid Theory (PC-SAFT), have been reported in order to give a step forward when it comes to predicting drug-polymer miscibility [55].

For the determination of the real or kinetic miscibility during screening, the traditional analytical techniques that are routinely used to characterize ASDs have been used. The main difference is that, during screening, these are applied in solvent-casted [47,56] or quench-cooled films [48], in order to spend less of API and obtain preliminary information on miscibility and stabilization in less time. The gold standard tests for evaluating amorphous miscibility are differential scanning calorimetry (DSC) and X-ray powder diffraction (XRPD). DSC is typically used for detecting amorphous formation and amorphous phase separation based on the detection one or two glass transition temperatures (T_g). It is generally accepted, that the presence of two T_g 's is indicative of phase separation, whereas a single T_g is often taken as an evidence of the formation of a one-phase homogenous blend. The limitation of this technique is its inability to discriminate phase-separation at the nano-scale (amorphous domains < 30 nm), and for being a thermal method it can alter miscibility during heating [57]. The XRPD complements the DSC analysis and it is used for detecting crystalline material in amorphous samples, based on the detection of the sharp crystalline peaks. The XRPD of a general amorphous material shows a broad halo characteristic of materials lacking of long-range order, but still presenting some short-range order. This technique is however unable to detect phase separation, and due to this, it is now being used in combination with computational methods such as the pair-distribution function (PDF) in order to better assess the miscibility of drug-

polymer mixtures [58]. Another limitation of the XRPD techniques is its low level of detection for trace crystallinity. The limitations of these techniques are even more pronounced when dealing with small samples, as commonly obtained during miniaturized screening (in the order of a few milligrams of material). Alternative analytical techniques that have been used to discriminate between the formation of one-phase or two-phase drug-polymers systems are Raman and Atomic Force Microscopy (AFM). Both provide information on the spatial molecular structure of drug-polymers mixtures, phase homogeneity, and surface properties on the micrometer to nanometer scales [48]. The use of solid-state NMR (ssNMR) has also been recently explored to evaluate miscibility at the nano-scale [59,60]. This analysis is based on the measurement of the relaxation times in the solid state reflecting the mobility in the sample. For example, if a single relaxation time is obtained for the sample it means that drug-polymer are completely miscible [59].

1.1.2.2 Predicting performance

The ultimate goal when developing an ASD is to provide a clinical benefit to the patient, by increasing drug's bioavailability. The *in vivo* performance of an ASD will greatly depend on the stability of the drug's supersaturated state and on the kinetics of precipitation in solution. As long as supersaturation is maintained at high levels, more time is given for the drug to be absorbed, and this will ultimately improve bioavailability.

One of the critical parameters that highly influences the supersaturated state is the selection of the polymeric excipient. By selecting the right polymer the formulator can modulate the creation and maintenance of the supersaturated state. Thus, during the screening stage, it is of interest to evaluate different polymers in terms of their supersaturation potential and precipitation inhibition capacity.

Commonly used strategies to early assess the performance of ASDs consist in the implementation of medium to high-throughput bench screening experiments, using smaller volumes apparatus, typically in the 96-well plate format, and wherein the API requirements are reduced to the minimum. There are experimental methods based on the induction of supersaturation in solution, such as the solvent-shift [61-64] and pH-shift assays [65,66], or methods based on the dissolution of amorphous casted films [30,31,16], where supersaturation is not induced, but should be an inherent characteristic of the system (Figure 1.5). In the end, the degree of supersaturation is measured or evaluated as a kinetic solubility time profile that works as a surrogate of *in vivo* performance.

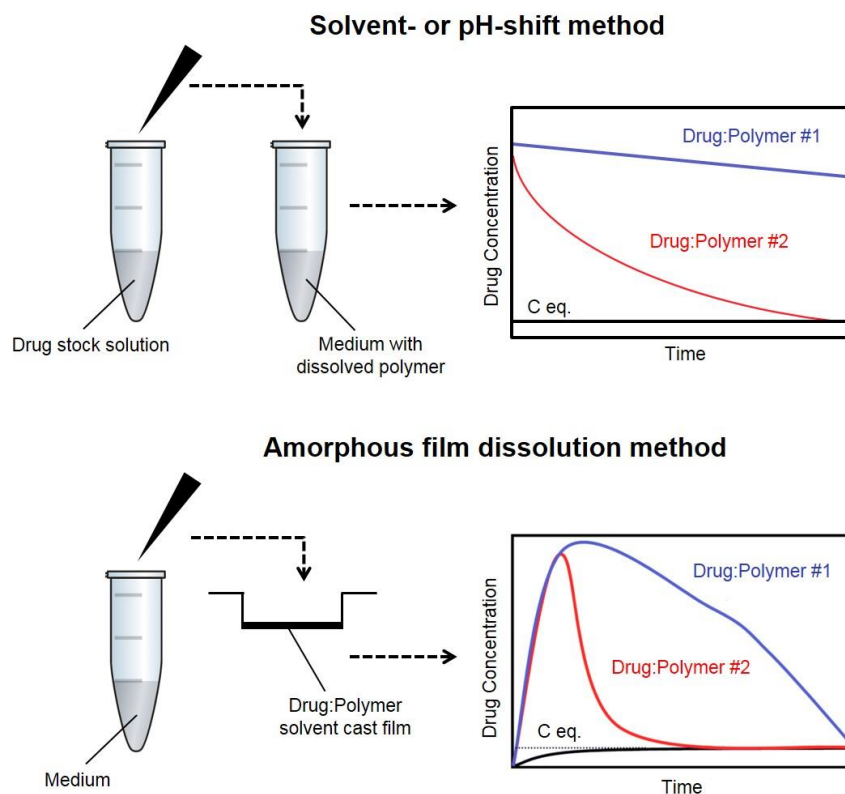


Figure 1.5. Representation of the experimental screening methodologies applied to evaluate supersaturation: the solvent- or pH-shift method, and the amorphous film dissolution method. The hypothetical kinetic solubility time profiles obtained for different drug-polymer combinations are also represented.

Briefly, in the solvent-shift method, the drug is first dissolved in a highly polar water-miscible organic solvent, such as dimethylacetamide (DMA) [61] or dimethylformamide (DMF) [64], to form a concentrated stock solution. A small aliquot of this latter solution is then transferred and dispersed in the aqueous-based medium to induce supersaturation. The medium can vary between a simple buffer [64] or biorelevant fluid [63] to improve predictability, and already contains the polymer dissolved at a pre-defined concentration. The pH-shift assay follows the same methodology, but instead of inducing supersaturation via a shift in solvent, is via a shift in pH, by reducing drug's ionization in the receptor medium. This method is typically used for ionizable drugs. Typical analytical methods used to measure drug concentration over time include turbidimetry [62], UV spectroscopy [61] or liquid chromatography [63]. Reported limitations of this method are related with the use of the organic solvent, which may act as a co-solvent and may interfere with the kinetics of precipitation, and the fact that supersaturation creation and maintenance is highly dependent on the drug and polymer initial concentrations.

Alternatively, in the cast film dissolution method, different drug-polymer films, at different drug loads, are prepared by solvent casting in 96-well plates. A small-volume of the dissolution medium is then transferred to each well, and drug concentration is measured over time. Typical analytical methods used include UV spectroscopy [31] or liquid chromatography [30]. The limitations of this method are related with the heterogeneity that can be formed during solvent casting, thus a prior assessment of the physical stability of the films should be made.

In terms of the use of computational tools for the prediction of the *in vivo* performance of ASDs, the existing physiologically-based pharmacokinetic (PBPK) models, such as GastroPlus™ or Simcyp®, have been successfully used [25]. However, these models need to be combined with accurate *in vitro/in vivo* dissolution experiments as input data, only typically obtained at advanced stages of formulation development. Thus, from an early screening perspective, there are few works reported in the literature demonstrating a theoretical rationale for the selection of the best polymers with precipitation inhibition effect. One of these works, if not the only one reported in the literature so far, was the work developed by Warren *et al.* [62]. Warren and co-workers first used a solvent-shift method combined with turbidity measurements to monitor the precipitation kinetics of 9 model drugs in presence of various polymers, from 42 different polymeric classes. Then, using multivariate data analysis tools such as principal components analysis (PCA) applied to the results generated together with a series of physicochemical descriptors of the polymers, the authors identified interesting performance trends, such as that cellulose-based polymers provide robust precipitation inhibition across different drug classes [62]. However, the authors did not attempt to establish any correlations with *in vivo* data.

1.1.3 Overview of the technologies used to prepare ASDs

Among the existing production methods to obtain ASDs, spray drying (SD) and hot melt extrusion (HME) are the most widely used. Both are mature and well-established techniques in the pharmaceutical industry. They are also compatible with continuous manufacturing processes, which is an important aspect, given the recent efforts of regulators in promoting this initiative aimed at increasing productivity and reducing costs [67].

At the moment of selecting the best manufacturing technique several aspects should be taken into consideration. For example, SD allows particle engineering during processing, enabling the control of product attributes such as particle size and density, and supports a broad variety of applications [68]. By opposition, when selecting HME, the downstream processing

of amorphous extrudates typically requires an additional milling or pelletization step, which can affect drug product physical stability [69]. In terms of processing time and costs, these are typically higher in SD due to the larger processing equipment footprint and the need for a secondary drying step to remove residual solvents. In this regard HME is economically more advantageous and environmentally friendly because it is a solvent-free production method. Simple physicochemical properties of the drug under development, such as the solubility in organic solvents and melting temperature, may also determine the selection of a given technique to the detriment of the other, as shown in Figure 1.6.

For instance, due to the operating principles of HME, this technique is not suitable for processing drugs that present high melting points ($\geq 200^{\circ}\text{C}$) due to thermal instability, or drugs that are shear sensitive. Even in the cases where the drug is dissolved by the polymer at lower temperatures, the drug may not be resistant to heat and/or may not dissolve completely in the excipient. For such compounds, SD is certainly a better option for operating at moderate temperatures and relatively short residence times. However, one of the prerequisites for the production of spray dried ASDs is that the drug should be sufficiently stable and soluble in volatile organic solvents; otherwise the final chemical and physical stability of the drug product may be compromised [71].

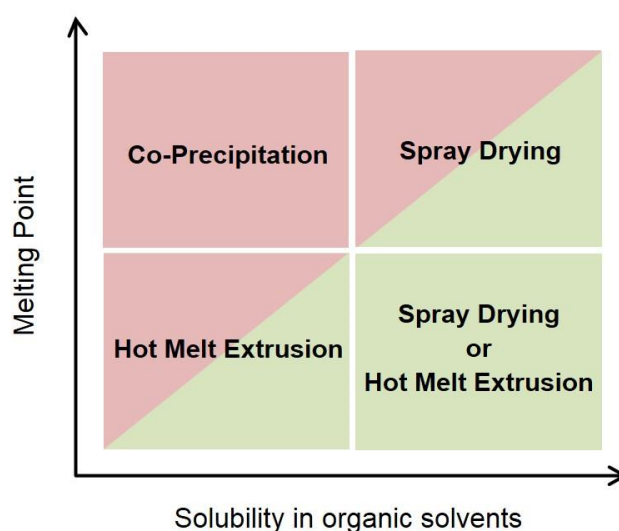


Figure 1.6. Selection of the manufacturing technology based on the drug's melting point and drug's solubility in organic solvent (adapted from [70]).

A particular type of poorly water-soluble compounds whose incidence in pharmaceutical development has been increasing, are those that neither have adequate solubility

in volatile organic solvents nor a melting temperature below 200°C. These difficult-to-formulate compounds are often designated as “brick dust”, and their conversion to the amorphous form may be too risky or even impossible when using the traditional techniques. Motivated by the need of solving this problem, the solvent controlled precipitation (SCP) process has recently come into play associated with the development of an ASD of vemurafenib, that ended up being converted into a successful commercial product for the treatment of late-stage melanoma (Zelboraf[®], Roche) [42]. SCP is a scalable technology, readily adaptable from batch to continuous processing. In general terms it consists in the mixing of an organic homogenous solution containing the drug and the stabilizer (*i.e.* polymer or surfactant) with an anti-solvent. Due to the insolubility of the pharmaceutical components in the anti-solvent, when both streams interact, supersaturation is generated inducing rapid precipitation of amorphous particles [72]. One of the advantages of this technology when compared with SD is that polar solvents with high boiling points, such as DMA or DMF, can be used to dissolve such “brick dust” molecules as far as their chemical stability is not compromised. Another advantage relates to the fact that it is not necessary to dissolve both pharmaceutical components in the same solvent or solvent system, as the stabilizer can be dissolved in the anti-solvent. These can significantly improve the process throughput and the drug load in the formulation. When compared with HME, SCP is a low temperature process suitable for thermolabile compounds, not only because the anti-solvent is cooled to reduce solubility and improve precipitation, but also the final suspension passes through a heat exchanger for heat removal [71].

In large-scale production, SCP has been conducted in high volume stirred reactors preferably using high shear mixing to promote effective contact between the organic solution and the anti-solvent. The final properties of the co-precipitated particles are highly dependent on the operational conditions (*i.e.* shear rate, temperature, mixing time) and formulation variables (*i.e.* properties of the drug, the polymer, drug-polymer interactions, solvent-anti-solvent ratio and interactions). For example, the amorphous microparticles of vemurafenib produced by SCP using high shear mixing are highly porous, due to the “extraction” or “substitution” process of the organic solution by the antisolvent that occurs during particle precipitation [73]. Consequently, these microparticles present the advantage of having a very high specific surface area with improved wetting properties and enhanced dissolution rate when compared with spray-dried particles or melt extrudates.

1.2 Pharmaceutical cocrystals

1.2.1 General considerations

Pharmaceutical cocrystals are an emerging crystal-engineering strategy, used with success by chemists and formulators to enhance the poor physicochemical properties of modern APIs. The rapid acceptance of this strategy was noticed since the early 2000s, as evidenced by the increasing number of annual citations in CAS SciFinder containing the search term “pharmaceutical cocrystals”. These results demonstrate the general interest of bringing cocrystals to the same level of typically used formulation platforms, such as ASDs.

Cocrystals are multicomponent crystals of, at least, two molecules combined in a stoichiometric ratio in which one is the active API and the other the cofomer. The cofomer can be another API or a pharmaceutical excipient, vitamin, amino acid, but is generally limited to compounds in the Generally Regarded as Safe (GRAS) list [74]. API and cofomer form a stable molecular complex typically interacting via hydrogen bonding, Van der Waals forces or π -stacking [75]. Cocrystals have shown efficacy on improving the aqueous solubility, and thus bioavailability, hygroscopicity, stability, taste, and downstream processing capacity [76-79]. They also represent a business opportunity for intellectual property and lifecycle management [80].

Up to date, there is no final drug product in the market that has been intentionally developed as a cocrystal. The one that is indicated in Figure 1.7 is an antidepressant product from Lundbeck (Cipralex[®], 2002) that was developed and filled as a salt, but it is now known that it is actually a cocrystal from a salt of an API [81]. Nevertheless, there are already a few cocrystal formulations in advanced stages of drug product development, such as Esteve’s cocrystal of tramadol and celecoxib (Phase II) [82].

The entrance of cocrystal products into the market has also been somehow hindered by an uncertain regulatory framework and lack of consensus regarding nomenclature. It was only in April 2013, that the FDA released a guidance for industry on the regulatory classification of pharmaceutical cocrystals for new drug applications (NDAs) and abbreviated drug applications (ANDAs) [83]. According to the FDA’s guidance, pharmaceutical cocrystals are classified as a drug product intermediate, similarly to ASDs. By opposition, for the European Medicines Agency (EMA) cocrystals should be classified as drug substances, even though any definitive regulatory framework has not been issued yet [84].

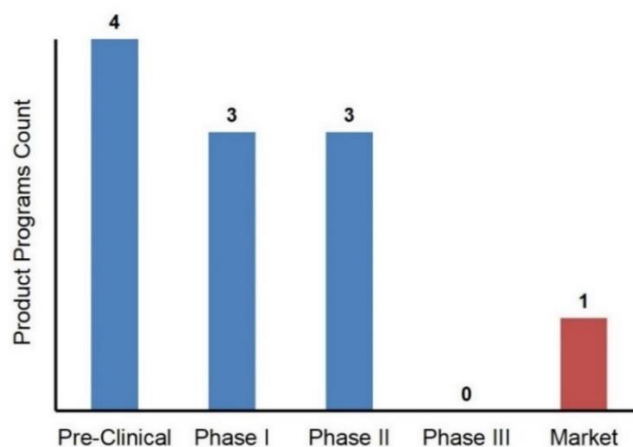


Figure 1.7. Number of product programs with respect to small molecule, pharmaceutical cocrystals (adapted from Pharmacircle.com)

The lack of harmonization between regulatory agencies increases the perceived risk associated with developing new cocrystal-based products. Nevertheless, the FDA first step on the release of a guidance for industry on pharmaceutical cocrystals has already contributed to a better definition of the current regulatory framework, bringing hope to those who (1) need to improve poor physicochemical properties of potential therapeutic APIs when alternatives formulation platforms have failed, (2) whose market position is the development of generic products or (3) pharmaceutical companies seeking for life cycle management opportunities. For example, a new cocrystal comprising an API of a brand product can lead to the possibility of filling an ANDA, rather than the NDA, which is mandatory for new cocrystals of new APIs. This is an advantage for generic companies because it will expedite market entrance and gain advantage over competitors. In life cycle management, patenting and intellectual property protection are major concerns for extending market position as much as possible. Circumventing the original patent with a cocrystal that has the same API as the brand product is challenging, but patenting a cocrystal with improved properties is an opportunity and typically easier to make it possible. Additional benefits of the current FDA guidance are the potential regulatory acceptance of cocrystallization between excipients, in opposition to the conventional API-based cocrystals, thus leading to the development of novel functional excipients.

1.2.2 Overview of the technologies used to prepare cocrystals

Pharmaceutical cocrystals have been prepared by different manufacturing methods, briefly summarized in Figure 1.8. Classical approaches for the production of cocrystals include solution-based methods (*e.g.* reaction, recrystallization via slow evaporation, cooling or anti-solvent addition) and mechano-chemical methods (*e.g.* neat and liquid-assisted grinding). These are by far the most commonly used techniques. By opposition, cocrystallization from slurry conversion, sublimation, or crystallization from the undercooled melt are less used [85].

Although the majority of these methods have shown to be useful in the production and screening of cocrystals at a small-scale (milligrams to grams), the scale-up is in most cases difficult or even impossible, due to the inherent limitations of the techniques. For example, in solution crystallization approaches the API and the coformer may undergo undesired interactions with organic solvents that may be incorporated into the crystal lattice with the possibility of solvate/hydrate formation [86]. With the grinding methods the intensive energy input may generate some degree of amorphization and/or cocrystal defects, limiting the formation of the cocrystal [87].

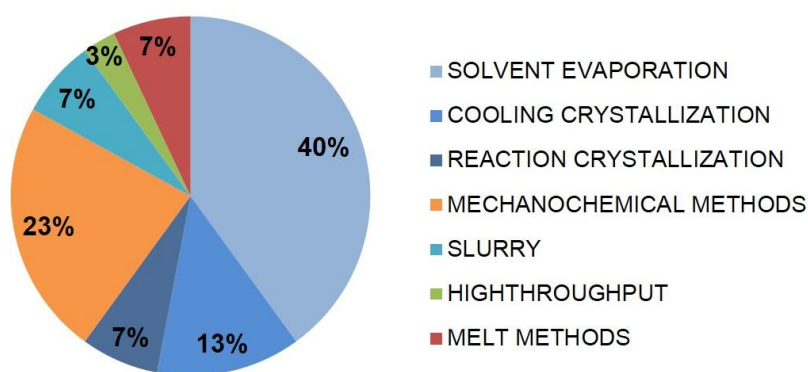


Figure 1.8. Most common manufacturing methods to produce cocrystals (adapted from [44]).

Currently, with the intensive research and fast development observed in this area, the assessment of manufacturing techniques that allow the direct scale-up of cocrystals, in a reproducible and cost-effective way has been encouraged. In fact, progress in this field has already been made. For example, the use of High Pressure Homogenization (HPH) or Hot Melt Extrusion (HME) allows the scale-up of cocrystals in a continuous mode [88,89]. The advantage of using HPH when compared with HME is that it enables the particle engineering of cocrystals in the particulate form, which facilitates their incorporation in the final dosage

forms (*e.g.* capsules or tablets). Using HME, downstream processing of cocrystal extrudates usually requires additional steps such as milling, granulation or pelletization. Currently, the development of scalable processes that allow for particle engineering during processing are of utmost importance to minimize downstream operations. Particle engineering is not usually associated to greener processes, however, the delivery of material with the target properties such as particle size without additional downstream processes allows for a significant reduction in development costs and waste treatment. The major disadvantage of HPH is the fact that is a solvent-based process and an additional drying step is required to isolate the powder from the suspension obtained. In this regard HME is more advantageous and environmentally friendly because it is a solvent-free production method, which may provide real cost benefits.

Other methods that have been assessed for the production of cocrystals are Spray Drying (SD) and Supercritical Fluid CO₂-based methods (SCF) [90-92]. Both methods offer the possibility of controlling cocrystal particle's properties (*e.g.* particle size, shape or density). Although SD is a common technology in industrial pharmaceutical facilities, it should not be neglected the fact that SD has associated the limitations of a common solvent-based method (*i.e.* process time, costs, environmental impact). In this respect SCF is considered a more environmental friendly process due to the use of "green" solvents, however is still limited due to the often poor solubility of pharmaceutical compounds in supercritical CO₂, and/or the existing challenges of processing feeds with gases at high pressures. In the case of SCF methods where supercritical CO₂ is used as the anti-solvent, further limitations include the need of using organic solvent(s) to dissolve the pharmaceutical compounds, and said solvent(s) should be miscible with supercritical CO₂, thus limiting the solvents' selection.

1.3 Motivations and objectives of the project

The development of new ASDs to address the current solubility/bioavailability challenges is increasing at a fast pace. Considering the high number of variables that influence the production of an amorphous dispersion with optimized stability and performance, the implementation of screening methodologies from the early beginning of formulation development is of critical importance. These strategies help to "build quality into the product", thereby reducing empiricism, development time, risk and costs. Few screening programs have been reported combining computational modeling and experimental miniaturization for evaluating drug-polymer physical stability and *in vivo* performance. The use of computational

tools contributes for the reduction in API consumption and can serve as a first level screen in terms of polymer selection and drug load definition.

Regarding the prediction of drug-polymer miscibility, currently applied computational methods include the analysis of the HHSPs and the use of the Flory-Huggins thermodynamic model. One of the limitations of these models is their inability to predict miscibility for drug-polymer mixtures forming highly directional interactions, such as hydrogen bonding and ionic interactions. Moreover, these models do not take into account the influence of the preparation methods nor the process parameters (*e.g.* evaporation rate, mixing effect) on drug-polymer kinetic miscibility. This may impact drug load optimization during screening, as one may not be taking full advantage of the amount of drug that the polymer can really “dissolve” or “incorporate”. Thus, for a more accurate estimation of kinetic miscibility during screening, new theoretical models capable of describing both kinetic (typically process related factors) and thermodynamic considerations on the phase separation of a drug-polymer system should be developed.

Regarding the prediction of *in vivo* performance of ASDs, current screening methodologies are essentially based on experimentation at a small-scale level. The development of computational tools that accurately predict oral absorption is a challenging task, due to the complexity of *in vivo* drug behavior. Existing PBPK mathematical models to predict *in vivo* absorption have been successfully used, however these models require accurate *in vitro* and/or *in vivo* input data typically obtained at advanced stages of formulation development. Thus, the state of the art would benefit from the development of computational screening methodologies for guiding the selection of polymers with appropriate supersaturation potential and precipitation inhibition capacity. Moreover, it would also be interesting to assess any relationships between the properties of the API, the polymer and the final amorphous dispersion *in vivo* performance.

After the screening stage, the most promising amorphous formulations in terms of physical stability and performance are identified. Typically only a small group of formulations follow for the production at the laboratory-scale, in order to obtain a few grams of the product for further evaluation and characterization. At this stage, an adequate selection of the preparation method is also important for the success of the program. Traditional methods for producing ASDs vary between SD and HME. However, with the recent approval of the first co-precipitated amorphous product in the market, a lot of attention has turned to the SCP process. SCP enables the production of ASDs with unique properties, especially in terms of surface area, a property with a big impact on the dissolution rate. In the context of large-scale production,

SCP has been limited to stirred reactors together with high shear mixing. The number of reproducible and cost-effective co-precipitation processes to produce ASDs is still scarce in the state of the art.

Regarding the use of pharmaceutical cocrystals, their understanding is increasing at a fast pace. On one hand, the knowledge and interest on pharmaceutical cocrystals is increasing thanks to solid-state chemists and pharmaceutical scientists who have been actively working in this field, but on the other hand, there are still some important legal and scientific issues that are hampering the extensive use of cocrystals by the pharmaceutical industry. The legal issues are related with the current regulatory scheme and uncertainties when dealing with a relatively new technology and crystal form. Among the scientific issues is the scarcity of suitable large-scale production methods and lack of robust and cost-effective processes.

Given the present research problems in state of the art, the following general goals were defined for this thesis:

- ✚ *To evaluate the applicability of a new computational tool that relies on fundamental thermodynamic and kinetic equations and manufacturing considerations to describe the influence of formulation and process conditions on drug-polymer miscibility;*
- ✚ *To develop a statistically-based model for predicting the in vivo performance of ASDs based on reported information and past history and to find correlations between the molecular descriptors of the APIs, the polymer and the in vivo pharmacokinetic parameters;*
- ✚ *To investigate a novel solvent-controlled precipitation process that uses microfluidization to produce amorphous dispersions, as well as, to study the effect of common formulation variables on typical critical quality attributes of ASDs, namely particle size/morphology, physical stability, in vitro and in vivo performance;*
- ✚ *To evaluate the use of the spray congealing technology to produce pharmaceutical cocrystals, as well as, to study the effect of critical process variables on cocrystal formation, purity, particle size, shape and powder flow properties.*

1.4 Hypothesis and thesis layout

Hypothesis: The physical stability and in vivo performance of amorphous solid dispersions can be described by mechanistic and statistical screening methodologies. Amorphous solid dispersions and pharmaceutical cocrystals presenting unique characteristics can be manufactured by novel production methods.

In order to meet the objectives proposed, this thesis is organized in six chapters. The contents and goals of each chapter can be briefly summarized, as follows:

Chapter 1: Consists on a general literature review on amorphous solid dispersions and pharmaceutical cocrystals, with emphasis on the existent screening methods to accelerate the formulation development of amorphous dispersions and current preparation methods to produce both amorphous dispersions and cocrystals.

Chapter 2: Describes the implementation and validation of a mechanistically-based computational screening method to predict amorphous physical stability, intended to be used in the early development of spray-dried amorphous solid dispersions.

Research question: Can a model that combines thermodynamic, kinetic and manufacturing considerations be used to obtain estimates of the miscibility and phase behavior of spray-dried ASDs?

Chapter 3: Describes the development of a statistically-based computational screening method to predict amorphous *in vivo* performance, intended to be used in the early development of amorphous solid dispersions.

Research question: Can the in vivo performance of ASDs based on molecular descriptors and statistical analysis be predicted?

Chapter 4: Describes and assesses an alternative solvent controlled-precipitation process to obtain amorphous solid dispersions, together with the analysis of the influence of formulation variables on critical quality attributes of co-precipitated ASDs. The *in vitro* and *in*

in vivo performances of the co-precipitated materials produced were compared with an amorphous dispersion manufactured by spray drying.

Research question: How formulation variables influence typical critical quality attributes of co-precipitated ASDs? In terms of in vivo performance, how is a co-precipitated amorphous product compared with a spray dried amorphous dispersion?

Chapter 5: Describes the assessment of the spray-congealing process to obtain pharmaceutical cocrystals, together with the analysis of the influence of process variables on quality attributes of cocrystals.

Research question: Is it possible to obtain cocrystals using spray congealing? How process variables influence the quality attributes of cocrystals? Is it possible to fine tune process variables in order to manipulate particle properties?

Chapter 6: Presents the conclusions and complementary perspectives on the subject.

1.5 References

- [1] Food and Drug Administration Center for Drug Evaluation and Research (CDER). [Online]. "<http://www.fda.gov/downloads/Drugs/DevelopmentApprovalProcess/DrugInnovation/UCM485053.pdf>" (Accessed January 2016).
- [2] T. Wright. Contract Pharma. [Online]. "http://www.contractpharma.com/issues/2015-03-01/view_features/solid-dosage-manufacturing-trends--724749" (Accessed March 2015).
- [3] GBI Research. Contract Pharma. [Online]. "http://www.contractpharma.com/issues/2012-06/view_features/oral-drug-delivery-market-report" (Accessed March, 2015).
- [4] J. H. Lin and A. Y. H. Lu, "Role of Pharmacokinetics and Metabolism in Drug Discovery and Development" *Pharmacological Reviews* , vol. 49, no. 4, pp. 404-440, 1997.
- [5] C. Giliyar, D. T. Fikstad, and S. Tyavanagimatt, "Challenges & Opportunities in Oral Delivery of Poorly Water-Soluble Drugs" *Drug Development & Delivery*, vol. 6, no. 1, pp. 57-63, 2006.

-
- [6] L. Z. Benet, C.-Y. Wu, and J. M. Custodio, "Predicting Drug Absorption and the Effects of Food on Oral Bioavailability" *Bulletin Technique Gattefossé*, vol. 99, pp. 9-16, 2006.
- [7] Y. Kawabata, K. Wada, M. Nakatani, S. Yamada, and S. Onoue, "Formulation design for poorly water-soluble drugs based on biopharmaceutics classification system: Basic approaches and practical applications" *International Journal of Pharmaceutics*, vol. 420, no. 1, pp. 1-10, 2011.
- [8] A. Singh, Z. Worku, and G. Van den Mooter, "Oral formulation strategies to improve solubility of poorly water-soluble drugs" *Expert Opinion on Drug Delivery*, vol. 8, no. 10, pp. 1-18, 2011.
- [9] T. Loftsson and M. E. Brewster, "Pharmaceutical applications of cyclodextrins: basic science and product development" *Journal of Pharmacy and Pharmacology*, vol. 62, pp. 1607-1621, 2010.
- [10] C. Brough and R. O. Williams III, "Amorphous solid dispersions and nano-crystal technologies for poorly water-soluble drug delivery" *International Journal of Pharmaceutics*, vol. 453, pp. 157-166, 2013.
- [11] G. Van den Mooter, "The use of amorphous solid dispersions: A formulation strategy to overcome poor solubility and dissolution rate" *Drug Discovery Today: Technologies*, vol. 9, no. 2, pp. e79-e85, 2012.
- [12] P. Harmon *et al.*, "Amorphous solid dispersions: Analytical challenges and opportunities" *AAPS News Magazine*, pp. 14-20, September 2009.
- [13] A. Newman, G. Knipp, and G. Zografi, "Assessing the Performance of Amorphous Solid Dispersions" *Journal of Pharmaceutical Sciences.*, vol. 101, pp. 1355-77, 2012.
- [14] H. R. Guzmán *et al.*, "Combined Use of Crystalline Salt Forms and Precipitation Inhibitors to Improve Oral Absorption of Celecoxib from Solid Oral Formulations" *Journal of Pharmaceutical Sciences*, vol. 96, no. 10, pp. 2686-2702, 2007.
- [15] S. R. K. Vaka *et al.*, "Excipients for Amorphous Solid Dispersions" in *Amorphous Solid Dispersions: Theory and Practice*, Navnit Shah *et al.*, Springer, 2014.
- [16] N. Wyttenbach *et al.*, "Miniaturized screening of polymers for amorphous drug stabilization (SPADS): Rapid assessment of solid dispersion systems" *European Journal of Pharmaceutics and Biopharmaceutics*, vol. 84, no. 3, pp. 583-598, 2013.

- [17] T. Vasconcelos, S. Marques, J. das Neves, and B. Sarmento, "Amorphous solid dispersions: Rational selection of a manufacturing process" *Advanced Drug Delivery Reviews*, vol. 100, pp. 85-101, 2016.
- [18] A. C. F. Rumondor, S. S. Dhareshwar, and F. Kesisoglou, "Amorphous Solid Dispersions or Prodrugs: Complementary Strategies to Increase Drug Absorption" *Journal of Pharmaceutical Sciences*, 2016, In Press
- [19] R. Lipp, "The Innovator Pipeline: Bioavailability Challenges and Advanced Oral Drug Delivery Opportunities" *American Pharmaceutical Review*, vol. 16, no. 3, 2013.
- [20] M. Moneghini, A. Carcano, G. Zingone, and B. Perissutti, "Studies in dissolution enhancement of atenolol. Part I" *International Journal of Pharmaceutics*, vol. 175, no. 2, pp. 177-183, 1998.
- [21] D. A. Miller, J. C. DiNunzio, W. Yang, J. W. McGinity, and R. O. Williams III, "Targeted Intestinal Delivery of Supersaturated Itraconazole for Improved Oral Absorption" *Pharmaceutical Research*, vol. 25, no. 6, pp. 1450-1459, 2008.
- [22] J. C. DiNunzio, D. A. Miller, W. Yang, J. W. McGinity, and R. O. Williams III, "Amorphous Compositions Using Concentration Enhancing Polymers for Improved Bioavailability of Itraconazole" *Molecular Pharmaceutics*, vol. 5, no. 6, pp. 968-980, 2008.
- [23] D. Engers *et al.*, "A Solid-State Approach to Enable Early Development Compounds: Selection and Animal Bioavailability Studies of an Itraconazole Amorphous Solid Dispersion" *Journal of Pharmaceutical Sciences*, vol. 99, no. 9, pp. 3901-3922, 2010.
- [24] F. Meng, V. Dave, and H. Chauhan, "Qualitative and quantitative methods to determine miscibility in amorphous drug-polymer systems" *European Journal of Pharmaceutical Sciences*, vol. 77, pp. 106-111, 2015.
- [25] J. Bevernage, J. Brouwers, M. E. Brewster, and P. Augustijns, "Evaluation of gastrointestinal drug supersaturation and precipitation: Strategies and issues" *International Journal of Pharmaceutics*, vol. 453, no. 1, pp. 25-35, 2013.
- [26] A. Paudel, Z. A. Worku, J. Meeus, S. Guns, and G. Van den Mooter, "Manufacturing of solid dispersions of poorly water soluble drugs by spray drying: Formulation and process considerations" *International Journal of Pharmaceutics*, vol. 453, no. 1, pp. 253-284, 2013.

-
- [27] N. Shah *et al.*, "Structured Development Approach for Amorphous Systems" in *Formulating Poorly Water Soluble Drugs*, Robert O. Williams III, Alan B. Watts, and Dave A. Miller, Springer, 2012, pp. 267-310.
- [28] W.-G. Dai, C. Pollock-Dove, L. C. Dong, and S. Li, "Advanced screening assays to rapidly identify solubility-enhancing formulations: High-throughput, miniaturization and automation" *Advanced Drug Delivery Reviews*, vol. 60, pp. 657-672, 2008.
- [29] W.-G. Dai *et al.*, "Parallel screening approach to identify solubility-enhancing formulations for improved bioavailability of a poorly water-soluble compound using milligram quantities of material" *International Journal of Pharmaceutics*, vol. 336, pp. 1-11, 2007.
- [30] V. Barillaro *et al.*, "High-Throughput Study of Phenytoin Solid Dispersions: Formulation Using an Automated Solvent Casting Method, Dissolution Testing, and Scaling-Up" *Journal of Combinatorial Chemistry*, vol. 10, pp. 637-643, 2008.
- [31] A. Shanbhag *et al.*, "Method for screening of solid dispersion formulations of low-solubility compounds-Miniaturization and automation of solvent casting and dissolution testing" *International Journal of Pharmaceutics*, vol. 351, pp. 209-218, 2008.
- [32] P.-C. Chiang *et al.*, "Evaluation of Drug Load and Polymer by Using a 96-Well Plate Vacuum Dry System for Amorphous Solid Dispersion Drug Delivery" *AAPS PharmSciTech*, vol. 13, no. 2, pp. 713-722, 2012.
- [33] Q. Hu, D. Soon Choi, H. Chokshi, N. Shah, and H. Sandhu, "Highly efficient miniaturized coprecipitation screening (MiCoS) for amorphous solid dispersion formulation development" *International Journal of Pharmaceutics*, vol. 450, no. 1-2, pp. 53-62, 2013.
- [34] F. Qian, J. Huang, and M. A. Hussain, "Drug-Polymer Solubility and Miscibility: Stability Consideration and Practical Challenges in Amorphous Solid Dispersion Development" *Journal of Pharmaceutical Sciences*, vol. 99, no. 7, pp. 2941-2947, 2010.
- [35] D. Lin and Y. Huang, "A thermal analysis method to predict the complete phase diagram of drug-polymer solid dispersions" *International Journal of Pharmaceutics*, vol. 399, pp. 109-115, 2010.
- [36] P. J. Marsac, S. L. Shamblin, and L. S. Taylor, "Theoretical and Practical Approaches for Prediction of Drug-Polymer Miscibility and Solubility" *Pharmaceutical Research*, vol. 23, no. 10, 2006.

- [37] A. Paudel, J. V. Humbeeck, and G. Van den Mooter, "Theoretical and Experimental Investigation on the Solid Solubility and Miscibility of Naproxen in Poly(vinylpyrrolidone)" *Molecular Pharmaceutics*, vol. 7, no. 4, pp. 1133-1148, 2010.
- [38] Y. Sun, J. Tao, G. G. Zhang, and L. Yu, "Solubilities of Crystalline Drugs in Polymers: An Improved Analytical Method and Comparison of Solubilities of Indomethacin and Nifedipine in PVP, PVP/VA, and PVAc" *Journal of Pharmaceutical Sciences*, vol. 99, no. 9, pp. 4023-4031, 2010.
- [39] R. A. Bellantone *et al.*, "A Method to Predict the Equilibrium Solubility of Drugs in Solid Polymers near Room Temperature Using Thermal Analysis" *Journal of Pharmaceutical Sciences*, vol. 101, no. 12, pp. 4549-4558, 2012.
- [40] A. Mahieu, J.-F. Willart, E. Dudognon, F. Danède, and M. Descamps, "A New Protocol To Determine the Solubility of Drugs into Polymer Matrixes" *Molecular Pharmaceutics*, vol. 10, no. 2, pp. 560-566, 2013.
- [41] M. M. Knopp *et al.*, "A Promising New Method to Estimate Drug-Polymer Solubility at Room Temperature" *Journal of Pharmaceutical Sciences*, 2016, In Press.
- [42] N. Shah *et al.*, "Improved Human Bioavailability of Vemurafenib, a Practically Insoluble Drug, Using an Amorphous Polymer-Stabilized Solid Dispersion Prepared by a Solvent-Controlled Coprecipitation Process" *Journal of Pharmaceutical Sciences*, vol. 102, no. 3, pp. 967-981, 2013.
- [43] M. Manne Knopp *et al.*, "Comparative Study of Different Methods for the Prediction of Drug-Polymer Solubility" *Molecular Pharmaceutics*, vol. 12, p. 3408-3419, 2015.
- [44] A. Paudel, E. Nies, and G. Van den Mooter, "Relating Hydrogen-Bonding Interactions with the Phase Behavior of Naproxen/PVP K 25 Solid Dispersions: Evaluation of Solution-Cast and Quench-Cooled Films" *Molecular Pharmaceutics*, vol. 9, no. 11, pp. 3301-3317, 2012.
- [45] D. J. Greenhalgh, A. C. Williams, P. Timmins, and P. York, "Solubility parameters as predictors of miscibility in solid dispersions" *Journal of Pharmaceutical Sciences*, vol. 88, no. 11, pp. 1182-90, 1999.
- [46] J. Albers, K. Matthée, K. Knop, and P. Kleinebudde, "Evaluation of Predictive Models for Stable Solid Solution Formation" *Journal of Pharmaceutical Sciences*, vol. 100, no. 2, pp. 667-680, 2011.

-
- [47] B. Van Eerdenbrugh and L. S. Taylor, "Small Scale Screening To Determine the Ability of Different Polymers To Inhibit Drug Crystallization upon Rapid Solvent Evaporation" *Molecular Pharmaceutics*, vol. 7, no. 4, pp. 1328-1337, 2010.
- [48] M. E. Lauer *et al.*, "Atomic Force Microscopy-Based Screening of Drug-Excipient Miscibility and Stability of Solid Dispersions" *Pharmaceutical Research*, vol. 28, pp. 572-584, 2011.
- [49] Y. Zhao, P. Inbar, H. P. Chokshi, A. W. Malick, and D. S. Choi, "Prediction of the Thermal Phase Diagram of Amorphous Solid Dispersions by Flory–Huggins Theory" *Journal of Pharmaceutical Sciences*, vol. 100, no. 8, pp. 3196-3207, 2011.
- [50] K. Bansal, U. S. Baghel, and S. Thakral, "Construction and Validation of Binary Phase Diagram for Amorphous Solid Dispersion Using Flory–Huggins Theory" *AAPS PharmSciTech*, vol. 17, no. 2, pp. 318-327, 2016.
- [51] Y. Tian *et al.*, "Construction of Drug–Polymer Thermodynamic Phase Diagrams Using Flory–Huggins Interaction Theory: Identifying the Relevance of Temperature and Drug Weight Fraction to Phase Separation within Solid Dispersions" *Molecular Pharmaceutis*, vol. 10, no. 1, pp. 236-48, 2013.
- [52] Y. Tian, V. Caron, D. S. Jones, A.-M. Healy, and G. P. Andrews, "Using Flory–Huggins phase diagrams as a pre-formulation tool for the production of amorphous solid dispersions: a comparison between hot-melt extrusion and spray drying" *Journal of Pharmacy and Pharmacology*, vol. 66, no. 2, pp. 256-274, 2014.
- [53] J. M. Keen *et al.*, "Investigation of process temperature and screw speed on properties of a pharmaceutical solid dispersion using corotating and counter-rotating twin-screw extruders" *Journal of Pharmacy and Pharmacology*, vol. 66, no. 2, pp. 204-217, 2014.
- [54] M. M. Knopp, N. E. Olesen, Y. Huang, R. Holm, and T. Rades, "Statistical Analysis of a Method to Predict Drug–Polymer Miscibility" *Journal of Pharmaceutical Sciences*, 2015, In Press.
- [55] A. Prudic, Y. Ji, and G. Sadowski, "Thermodynamic Phase Behavior of API/Polymer Solid Dispersions" *Molecular Pharmaceutics*, vol. 11, no. 7, pp. 2294-2304, 2014.
- [56] N. Li and L. S. Taylor, "Nanoscale Infrared, Thermal, and Mechanical Characterization of Telaprevir–Polymer Miscibility in Amorphous Solid Dispersions Prepared by Solvent Evaporation" *Molecular Pharmaceutics*, vol. 13, no. 3, pp. 1123-1136, 2016.

- [57] J. A. Baird and L. S. Taylor, "Evaluation of amorphous solid dispersion properties using thermal analysis techniques." *Advanced Drug Delivery Reviews*, vol. 64, no. 5, pp. 396-421, 2012.
- [58] S. Bates *et al.*, "Analysis of Amorphous and Nanocrystalline Solids from Their X-Ray Diffraction Patterns" *Pharmaceutical Research*, vol. 23, no. 10, pp. 2333-2349, 2006.
- [59] X. Yuan, D. Sperger, and E. J. Munson, "Investigating Miscibility and Molecular Mobility of Nifedipine-PVP Amorphous Solid Dispersions Using Solid-State NMR Spectroscopy" *Molecular Pharmaceutics*, vol. 11, no. 1, pp. 329-337, 2014.
- [60] S. Qi *et al.*, "Characterisation and Prediction of Phase Separation in Hot-Melt Extruded Solid Dispersions: A Thermal, Microscopic and NMR Relaxometry Study" *Pharmaceutical Research*, vol. 27, pp. 1869-1883, 2010.
- [61] R. Vandecruys, J. Peeters, G. Verreck, and M. E. Brewster, "Use of a screening method to determine excipients which optimize the extent and stability of supersaturated drug solutions and application of this system to solid formulation design" *International Journal of Pharmaceutics*, vol. 342, pp. 168-175, 2007.
- [62] D. B. Warren, C. A. S. Bergström, H. Benameur, C. J. H. Porter, and C. W. Pouton, "Evaluation of the Structural Determinants of Polymeric Precipitation Inhibitors Using Solvent Shift Methods and Principle Component Analysis" *Molecular Pharmaceutics*, vol. 10, p. 2823-2848, 2013.
- [63] T. Yamashita, S. Ozaki, and I. Kushida, "Solvent shift method for anti-precipitant screening of poorly soluble drugs using biorelevant medium and dimethyl sulfoxide" *International Journal of Pharmaceutics*, vol. 419, pp. 170-174, 2011.
- [64] S. Janssens *et al.*, "Formulation and characterization of ternary solid dispersions made up of Itraconazole and two excipients, TPGS 1000 and PVPVA 64, that were selected based on a supersaturation screening study" *European Journal of Pharmaceutics and Biopharmaceutics*, vol. 69, no. 1, pp. 158-66, 2008.
- [65] T. Yamashita, T. Kokubo, C. Zhao, and Y. Ohki, "Antiprecipitant Screening System for Basic Model Compounds Using Bio-Relevant Media" *Journal of Laboratory Automation*, vol. 15, no. 4, pp. 306-312, 2010.
- [66] S. Carlert *et al.*, "Predicting Intestinal Precipitation-A Case Example for a Basic BCS Class II Drug" *Pharmaceutical Research*, vol. 27, pp. 2119-2130, 2010.

- [67] S. L. Lee *et al.*, "Modernizing Pharmaceutical Manufacturing: from Batch to Continuous Production" *Journal of Pharmaceutical Innovation*, vol. 10, pp. 191-199, 2015.
- [68] F. Gaspar, J. Vicente, F. Neves, and J.-R. Authelin, "Spray Drying: Scale-Up and Manufacturing" in *Amorphous Solid Dispersions: Theory and Practice*, Navnit Shah *et al.*, Springer New York, 2014, pp. 261-302.
- [69] C. Brown *et al.*, "HME for Solid Dispersions: Scale-Up and Late-Stage Development" in *Amorphous Solid Dispersions: Theory & Practice*, Navnit Shah *et al.*, Springer New York, 2014, pp. 231-260.
- [70] H. Sandhu, N. Shah, H. Chokshi, and A. Waseem Malick, "Overview of Amorphous Solid Dispersion Technologies" in *Amorphous Solid Dispersions: Theory and Practice*, Navnit Shah *et al.*, Springer New York, 2014, pp. 91-122.
- [71] H. Sandhu, N. Shah, H. Chokshi, and A. Waseem Malick, "Overview of Amorphous Solid Dispersion Technologies" in *Amorphous Solid Dispersions: Theory & Practice*, Navnit Shah *et al.*, Springer New York, 2014, pp. 91-122.
- [72] N. Shah *et al.*, "MBP Technology: Composition and Design Considerations" in *Amorphous Solid Dispersions: Theory & Practice*, Navnit Shah *et al.*, Springer New York, 2014, pp. 323-350.
- [73] R. Diodone, H. J. Mair, H. Sandhu, and N. Shah, "MBP Technology: Process Development and Scale-Up" in *Amorphous Solid Dispersions: Theory & Practice*, Navnit Shah *et al.*, Springer New York, 2014, pp. 351-371.
- [74] Food and Drug Administration. [Online].
"<http://www.accessdata.fda.gov/scripts/fdcc/?set=SCOGS>" (Accessed July 2014).
- [75] N. Qiao *et al.*, "Pharmaceutical cocrystals: An overview" *International Journal of Pharmaceutics*, vol. 419, pp. 1-11, 2011.
- [76] A. V. Trask, W. D. S. Motherwell, and W. Jones, "Pharmaceutical Cocrystallization: Engineering a Remedy for Caffeine Hydration" *Crystal Growth & Design*, vol. 5, no. 3, pp. 1013-1021, 2005.
- [77] A. V. Trask, W. D. S. Motherwell, and W. Jones, "Physical stability enhancement of theophylline via cocrystallization" *International Journal of Pharmaceutics*, vol. 320, pp. 114-123, 2006.
- [78] R. Thakuria *et al.*, "Pharmaceutical cocrystals and poorly soluble drugs" *International Journal of Pharmaceutics*, vol. 453, no. 1, pp. 101-125, 2013.

- [79] C. Calvin Sun and H. Hou, "Improving Mechanical Properties of Caffeine and Methyl Gallate Crystals by Cocrystallization" *Crystal Growth & Design.*, vol. 8, no. 5, pp. 1575-1579, 2008.
- [80] Ö. Almarsson, M. L. Peterson, and M. Zaworotko, "The A to Z of pharmaceutical cocrystals: a decade of fast-moving new science and patents" *Pharmaceutical Patent Analyst*, vol. 1, no. 3, pp. 313-327, 2012.
- [81] Chris Frampton, "Cocrystal clear solutions" [Online].
[http://www.soci.org/Chemistry-and-Industry/CnI-Data/2010/5/Cocrystal-clear solutions](http://www.soci.org/Chemistry-and-Industry/CnI-Data/2010/5/Cocrystal-clear%20solutions)
(Accessed July 2014).
- [82] C. Challener, "Scientific Advances in Cocrystals are Offset by Regulatory Uncertainty" *Pharmaceutical Technology*, vol. 38, no. 5, pp. 42-45, 2014.
- [83] Food and Drug Administration. [Online].
<http://www.fda.gov/downloads/Drugs/.../Guidances/UCM281764.pdf> (Accessed July 2014)
- [84] European Medicines Agency. [Online].
"http://www.ema.europa.eu/docs/en_GB/document_library/Scientific_guideline/2014/07/WC500170467.pdf" (Accessed July 2014).
- [85] A. Y. Sheikh, S. A. Rahim, R. B. Hammond, and K. J. Roberts, "Scalable solution cocrystallization: case of carbamazepine-nicotinamide I" *CrystEngComm*, vol. 11, pp. 501-509, 2009.
- [86] T. Rager and R. Hilfiker, "Cocrystal Formation from Solvent Mixtures" *Crystal Growth & Design.*, vol. 10, no. 7, pp. 3237–3241, 2010.
- [87] S. Rehder *et al.*, "Investigation of the Formation Process of Two Piracetam Cocrystals during Grinding" *Pharmaceutics*, vol. 3, no. 4, pp. 706-722, 2011.
- [88] M. P. Fernández-Ronco, J. Kluge, and M. Mazzotti, "High Pressure Homogenization as a Novel Approach for the Preparation of Co-Crystals" *Crystal Growth & Design.*, vol. 13, pp. 2013-2024, 2013.
- [89] A. Paradkar, A. Kelly, P. Coates, and P. York, "Method and Product" WO/2010/013035, February 4, 2010.

- [90] A. Alhalaweh *et al.*, "Theophylline Cocrystals Prepared by Spray Drying: Physicochemical Properties and Aerosolization Performance" *AAPS PharmSciTech*, vol. 14, no. 1, pp. 265-276, 2013.
- [91] L. Padrela, M. A. Rodrigues, S. P. Velaga, H. A. Matos, and E. G. de Azevedo, "Formation of indomethacin–saccharin cocrystals using supercritical fluid technology" *European Journal of Pharmaceutical Sciences*, vol. 38, pp. 9-17, 2009.
- [92] K. C. Müllers, M. Paisana, and M. A. Wahl, "Simultaneous Formation and Micronization of Pharmaceutical Cocrystals by Rapid Expansion of Supercritical Solutions (RESS)" *Pharmaceutical Research*, vol. 32, pp. 702-713, 2015.

Chapter 2

The results described in this chapter have been published total or partially in the following communications:

- I. Duarte, J. L. Santos, J.F. Pinto and M. Temtem, “Screening methodologies for the development of spray dried amorphous solid dispersions” *Pharmaceutical Research*, vol. 32, no. 1, pp. 222-237, 2015;
- 2 international conferences as an oral communication;
- 4 international conferences as a poster communication.

Authors' contribution:

I.D. was involved in the conception, design, production and analysis of data. I.D. wrote the manuscript and led the revision of the article particularly on proposing the journal's reviewers questions and comments.

2 Screening methodologies for the development of spray-dried amorphous solid dispersions

2.1 Introduction

The study presented proposes a new screening methodology intended to be used in the early development of ASDs. This part of the work consists on the implementation of a computational tool, based on diffuse interface theories, to guide rationale polymer selection and narrow the drug load range with potential to form homogenous amorphous systems. The most significant difference over other approaches (*e.g.* the use of the F-H theory alone) is the potential to evaluate a ternary system made of a drug, polymer and solvent, by comparison with the traditional two-component system and the consideration of time-dependent phenomena, such as components mass diffusion and solvent evaporation. For assessing the effect of Thermodynamics, Kinetics and Evaporation (*i.e.* process variables) on the phase behavior of drug-polymer amorphous systems, this model (hereafter named TKE) was regarded as a pre-formulation tool in the development of amorphous dispersions using spray drying. To assess the applicability of this tool and have experimental evidence of the kinetic miscibility estimates, solid dispersions of a BCS Class II model drug - itraconazole (ITZ) - and structurally different polymers, known for having different compatibilities with ITZ, were produced using different solvent-based methods of solvent casting and spray drying.

2.2 Materials and Methods

2.2.1 Materials

Crystalline ITZ was obtained from Chongqing Huapont Pharm.Co., Ltd (Chongqing, China). Three commercially available polymers with different chemical and physical properties were selected: polyvinylpyrrolidone-vinyl acetate copolymer (PVP/VA 64, BASF, Ludwigshafen, Germany), dimethylaminoethyl methacrylate, butyl methacrylate, and methyl methacrylate co-polymer (Eudragit[®] EPO, Evonik Röhm GmbH, Darmstadt, Germany), and hydroxypropylmethylcellulose acetate succinate (HPMCAS grade MG, AQOAT[®], Shin-Etsu Chemical Co., Ltd., Tokyo, Japan). The solvents used were methylene dichloride (DCM) and methanol (MeOH), both of analytical grade.

2.2.2 Methods

2.2.2.1 Theoretical considerations

This section summarizes the underlying theory and mathematical formalism of the model presented in this work. For more details on the derivation of the model, readers are referred to the work of Saylor *et al.* [1,2].

TKE model is a system of partial differential equations (PDEs) based on diffuse interface theories (*i.e.*, Cahn-Hilliard and Allen-Cahn) to describe drug-polymer microstructure evolution. The physical basis of the model relies on fundamental thermodynamic, kinetic, evaporation equations to describe the influence of process conditions during microstructure formation.

Accounting for the thermodynamic contribution to microstructure evolution, the latter is related with the free energy density (*i.e.*, free energy per volume). The free energy (ΔG) is then modeled based on the F-H theory equation for a ternary system and is given by:

$$\frac{\Delta G}{nRT} = \phi_d \ln \phi_d + \phi_s \ln \phi_s + \frac{\phi_p}{m_p} \ln \phi_p + \chi_{ds} \phi_d \phi_s + \chi_{sp} \phi_s \phi_p + \chi_{dp} \phi_d \phi_p \quad \text{Equation 2.1}$$

where, n is total number of mole, R is the ideal gas constant, T is the absolute temperature, ϕ is the volume fraction of each of the components in the mixture (drug, polymer and solvent), m_p is the degree of polymerization and χ_{ij} is the F-H interaction parameter which accounts for the enthalpy of mixing.

Kinetic contributions are expressed by means of the diffusivities of the components, which are related with the implementation of the classic Fick's second law of diffusion:

$$\frac{\partial \phi_i}{\partial t} = \nabla \cdot D_{ij} \nabla \phi_j \quad \text{Equation 2.2}$$

where, t is the time and D_{ij} is the concentration-dependent diffusion coefficient of each of the components in the mixture. To comply with classical Fickian diffusion theory, two assumptions had to be considered, namely ideal mixing and interfaces were absent. The latter assumption implies that the systems are completely amorphous during microstructure formation. To complete the derivation of this model, the following evaporation model was implemented:

$$\frac{\partial h}{\partial t} = k_e \phi_s \quad \text{Equation 2.3}$$

where, h is the height of the solution film, k_e is the evaporation rate coefficient and ϕ_s is the volume fraction of the solvent. The evaporation of the solvent is homogenous across the liquid-vapor boundary and the solvent removal is described by a first-order rate coefficient.

Gathering all the equations together the system's microstructure evolution is governed by iteratively solving the PDEs, while aiming the minimization of the free energy of the system as a function of time. The simulations can be run in one or two-dimensions (1D or 2D, respectively) using a PDE solver software, such as FiPy version 3.1 (NIST, Gaithersburg, Maryland, USA) [3].

2.2.2.2 Implementation of the TKE model

The application of the TKE model within the formulation field of new ASDs is anticipated to support the early identification of the theoretical kinetic miscibility region in which the amorphous system is homogeneously mixed.

A representation demonstrating a proposed flowchart for the application of the model, as a pre-formulation tool for the early development of ASDs is shown in Figure 2.1.

To run a simulation one must start with the definition of the input variables that are dependent upon the drug-polymer-solvent(s) system under study. These variables include thermodynamic and kinetic material-properties and process parameters. The material-properties are the F-H interaction parameters (χ_{ij}), the molar volume (V_m^i) and the diffusion coefficient of each component (D_i). To calculate these properties it is necessary to have information on the molecular structure of the formulation constituents. The process variables are the evaporation rate coefficient (k_e) of the spray drying process and the initial volume fraction of each component in the solution (ϕ_i). All of these input parameters were calculated using the correlations described in the following sections.

Then, 1D simulations are run at the beginning of the process to screen the different systems and/or variables considered. In order to fine-tune the output or to improve clarity about phase-separation, 2D simulations should be considered. The latter are in general more time-consuming than the former.

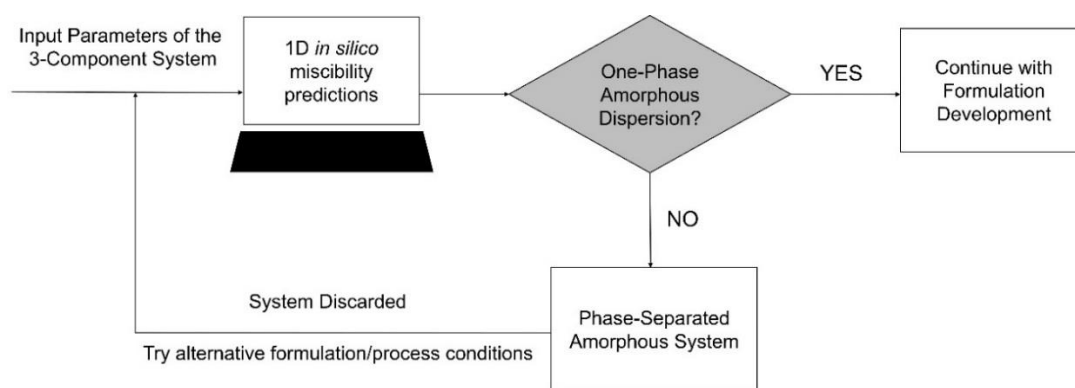


Figure 2.1. Representation showing the application of the TKE model as a screening tool for the development of amorphous systems.

Whether in one or two dimensions, once the computational simulation starts, the solvent evaporates across the liquid surface and the drug-polymer microstructure begins to evolve by diffusion, according to the molecular affinity between the ingredients. The final 1D microstructures are represented on a x-y plot, where the y-axis represents the final volume fraction of drug, polymer and solvent ($0 < \phi_i < 1$) along the film's height, h_{film} (x-axis). On the contrary, the final 2D microstructures can be described as a matrix of volume fractions (drug, polymer or solvent) or composition map, where the y-x axes correspond to height and width (L_{film}) of the liquid film, respectively. In 1D simulations, homogeneity after solvent evaporation is characterized by relatively constant bulk volume fractions (drug and polymer) along the film height, while heterogeneity or phase-separation is indicated by abrupt shifts of the drug and polymer volume fraction curves along the x-axis. In case of 2D simulations, a homogenous system is represented as a composition map depicting a uniform color correspondent to a single final volume fraction, whereas different structures at sharp variations in colors correspond to the formation of different amorphous regions with different levels of drug concentration.

After conducting a computational simulation, if a homogenous amorphous mixture is obtained, such drug-polymer system can be considered a good starting point for further formulation development. Conversely, if the simulation indicates a phase-separated system with two distinct amorphous domains, the drug-polymer system may be considered physically unstable and alternative combinations (*e.g.* polymer, drug-polymer ratio, solvent composition) or changes of the process conditions should be considered (*e.g.* solution concentration, temperature).

2.2.2.3 Obtaining the input variables of the model

2.2.2.3.1 F-H interaction parameters

Three different F-H interaction parameters per system should be determined to apply the TKE model. These are the interaction parameters for the drug-polymer (χ_{dp}), drug-solvent (χ_{ds}) and polymer-solvent (χ_{ps}) pairs.

The interaction parameters can be calculated according to the following equation, using the Hildebrand solubility parameters:

$$\chi_{ij} = \frac{V_m^i}{RT}(\delta_i - \delta_j)^2 \quad \text{Equation 2.4}$$

where, V_m^i is the molar volume of the smaller component within the ij pair and δ is the Hildebrand solubility parameter.

In this work, χ_{ds} and χ_{ps} were calculated using Equation 2.4 with the data provided in Table 2.1. When the solubility parameters are estimated using group contribution values, the respective interaction parameter obtained is an estimative at 298 K [26]. Due to this, it was decided to calculate χ_{dp} at the spray drying outlet temperature. This value will be more representative of the thermodynamic affinity during the formation of the microstructure.

To calculate an interaction parameter at non-ambient conditions, it is necessary to obtain the dependence of χ with temperature. According to the F-H theory and for polymer blends showing an upper critical solution temperature (UCST) behavior, it is accepted the following χ -T relation [5,6]:

$$\chi_{ij} = A + \frac{B}{T} \quad \text{Equation 2.5}$$

where, A and B are fitting parameters that need to be determined in order to obtain χ_{ij} at any temperature.

Assuming that drug-polymer systems also exhibit an UCST, the temperature dependence of χ_{dp} can be described by Equation 2.5. The parameters A and B were determined by fitting a linear regression between two χ_{dp} 's obtained at two different temperatures. These temperatures were around the melting point of the drug (T_1), and at room temperature or 298 K (T_2). To obtain $\chi(T_1)$ the melting point depression method was used for being a simple experimental method to obtain the interaction parameter at higher temperatures [7], while $\chi(T_2)$

was obtained using the Hildebrand solubility parameters (Table 2.1). The experimental protocol for the melting point depression studies and associated results are presented in Supplementary Information A.

2.2.2.3.2 Diffusivity of the components

The diffusivity of the solutes in the solvent was approximated to the diffusivity of the smaller component (*i.e.* drug) at 298 K, since its molecular mobility is much higher when compared with the mobility of the polymer [8].

The drug's diffusivity was estimated using the Wilke-Chang equation [9]:

$$D_{ds} = \frac{7.4 \times 10^{-8} \cdot T \cdot \sqrt{\alpha_s \cdot MW_s}}{\eta_s \cdot V_{m,d}^{0.6}} \quad \text{Equation 2.6}$$

where, D_{ds} is the diffusivity of the drug in the solvent, α_s is the association coefficient of the solvent and η_s the viscosity of the solvent.

2.2.2.3.3 Evaporation rate coefficient

The evaporation rate on the spray dryer was estimated according to the correlation for the drying of a single droplet in still air, according to Equation 2.7 [10]:

$$\frac{dW}{dt} = \frac{k_d A MW_s}{RT} (P_{wb} - p_w) \quad \text{Equation 2.7}$$

where, k_d is the mass transfer coefficient, A is the droplet's surface area, T the drying temperature, P_{wb} is the vapor pressure of the solvent at the wet bulb temperature and p_w corresponds to the partial pressure of the solvent in the surrounding drying gas.

Equation 2.8 describes the mass transfer correlation for a spherical droplet in still air:

$$Sh = \frac{k_d d}{D_{sg}} = 2 \quad \text{Equation 2.8}$$

where, d is the droplet diameter, which was considered to be 30 μm [11], and D_{sg} is the diffusivity of the solvent vapor in the drying gas, which was estimated using the Fuller *et al.* Correlation [12].

Regarding the estimation of P_{wb} and p_w , the former was calculated using Antoine's equation [12], and the latter was considered to be 10% of P_{wb} . The wet bulb temperature was estimated according to reference [13].

In the case of a solvent mixture, the evaporation rate was considered to be the evaporation rate of the solvent with the lowest vaporization enthalpy.

2.2.2.3.4 Volume fraction

The initial volume fraction of each component in the solution can be calculated from the respective weight fraction (w_i) and the true density (ρ_i), based on Equation 2.9:

$$\phi_i = \frac{w_i / \rho_i}{w_i / \rho_i + w_j / \rho_j + w_z / \rho_z} \quad \text{Equation 2.9}$$

2.2.2.4 Solvent casting (SC)

Cast films of ITZ and each polymer were obtained from solutions with 10, 15, 35, 45, 65 and 85% (w/w) ITZ. The total solids fraction was constant at 10% (w/w). The system ITZ:HPMCAS-MG was dissolved in a mixture of DCM:MeOH in a proportion of 80:20 (wt.%), whereas ITZ:PVP/VA and ITZ:Eudragit® EPO were dissolved in pure DCM.

A volume of approximately 40 μ L of each stock solution was pipetted to a DSC aluminum pan to expedite direct analysis. At least three replicates of each drug-polymer system, at each drug fraction, were prepared. The sample holder was placed in a tray dryer oven at 40°C for 1h, under vacuum to promote the rapid evaporation of the solvent. The goal was to design a SC experimental method as close as possible in terms of evaporation rate, to the subsequent spray drying process. The aluminum pans were sealed with the respective lids (pinholed) and directly placed in the sample tray of the calorimeter to be analyzed for the physical stability and experimental or kinetic drug-polymer miscibility capacity.

2.2.2.5 Spray drying (SD)

Spray-dried prototypes of ITZ were produced at 45% and 65% (w/w) load with HPMCAS-MG, 45%, 65% and 85% (w/w) drug load with PVP/VA 64, and 15% and 35% (w/w) ITZ with Eudragit® EPO. Solutions of ITZ and each of the polymers were prepared with

10% w/w concentration of solids. The solvents used in the SD experiments were the same as those used in the SC tests.

Spray dried dispersions (SDDs) were produced in a laboratory scale spray dryer (BÜCHI Mini Spray Drier B-290, Switzerland). The spray drying unit was operated with nitrogen in single pass mode, *i.e.* without recirculation of the drying nitrogen. The drying gas fan was set at 100% of its capacity (flow rate at maximum capacity is approximately 40 kg/h). A flow rate of 0.76 kg/h was set for the atomization with nitrogen. The feed flow rate was set to 30% in the peristaltic pump (about 12mL/min of liquid feed). The inlet temperature was adjusted to achieve an outlet temperature of 40°C. The SDDs were subjected to a post-drying step in a tray dryer oven with a temperature of 40°C for approximately 12 h, under vacuum.

At the end of the process, SDD powders were sampled and DSC pinholed aluminum pans were prepared. The products were analyzed for their physical stability and kinetic miscibility, according to the DSC analysis protocol described below. Powders were also analyzed by polarized light microscopy (PLM) to evaluate the presence of crystalline material.

2.2.2.6 Differential Scanning Calorimetry (DSC)

Conventional and modulated DSC (mDSC) experiments were performed in a TA Q1000 (TA Instruments, New Castle, Delaware, USA) equipped with a Refrigerated Cooling System (RCS). The enthalpy response was calibrated using indium. Three replicates of each sample, weighing between 5 and 10 mg were analyzed under continuous dry nitrogen purge (50 mL/min). Data was analyzed and processed using the TA Universal Analysis 2000 Software. The glass transition temperature was taken as the inflection point in the heat capacity change (ΔC_p) observed in the reversible heat flow, while exothermic and endothermic peaks were identified in the total heat flow.

Pure raw materials (ITZ and polymers) were analyzed using a modulated heating ramp from -10°C to 250°C at a heating rate of 5°C/min using a period of 60s and amplitude of 0.8°C. It should be pointed out that crystalline ITZ had to be first subjected to a heat-cool-heat cycle (conventional DSC) to render the product amorphous, before applying the modulation cycle. Cast films and spray dried dispersions (SDDs) were analyzed using mDSC, while for the latter the modulation conditions were the same as the ones used for the pure components, the amplitude used for the cast films was 1.6°C (*i.e.*, two times 0.8°C) in order to increase sensitivity.

DSC was applied to detect key indicators of homogeneity and phase separation of the cast films and SDDs. The number of amorphous phases present in the mixtures was defined

based on the following generally accepted rules in the literature [14-16]. If a single T_g value between the T_g 's of the pure components is detected in the reversible heat flow, then one can consider that drug and polymer are homogeneously mixed and a true amorphous solid solution (*i.e.* glass solution) was formed. Conversely, if two distinct T_g 's corresponding to the pure components were detected, one can consider that amorphous-amorphous phase separation had occurred and an amorphous (or glass) suspension with polymer and drug rich phases was produced. For systems with higher drug loading is also common to detect other thermal events characteristic of phase-separation, namely recrystallization and melting during heating of the sample. Such events may correspond to the presence of crystalline material in the raw sample or may have been triggered by heating during the DSC run.

In this work, the detection of amorphous-amorphous phase separation can be facilitated by the fact that the molecule (ITZ) presents a mesophase (*i.e.* two endothermic peaks in the reversible heat flow around $69.6 \pm 1.0^\circ\text{C}$ and $84.7 \pm 1.0^\circ\text{C}$) [17].

2.2.2.7 Polarized Light Microscopy (PLM)

The SDDs powders were analyzed in a Nikon Labophot-2 Polarizing Microscope (Nikon, Japan) in order to detect crystalline material in the samples, by the presence of birefringence. Micrographs were taken using a TCA-9.0 Color Camera (Tucsen Imaging Technology Co. Ltd, China). Images were taken using the TSview 6.2.2.6 software.

2.3 Results

2.3.1 F-H interaction parameter calculation using solubility parameters

The F-H interaction parameter (χ_{ij}) accounts for the enthalpic contribution for the Gibbs free energy of mixing (ΔG) and is a measure of the cohesive (intramolecular) and adhesive (intermolecular) interactions within the ij pair. Table 2.1 compiles important physicochemical properties of the solid compounds and solvents used in this work, to calculate the three F-H interactions parameters - drug-polymer (χ_{dp}), drug-solvent (χ_{ds}) and polymer-solvent (χ_{ps}) pairs.

Table 2.1. Physicochemical properties of the raw materials considered in this project.

Substance	MW [gmol ⁻¹]	ρ [gcm ⁻³]	V_m [cm ³ mol ⁻¹] ^a	δ [(MPa) ^{1/2}] ^b	T_g [°C] ^c
ITZ	706	1.27 ^d	556	24.77	59.2±0.3
HPMCAS-MG	18,000 ^e	1.29 ^e	13,846	23.49	120.3±0.7
PVP/VA 64	55,000 ^e	1.2 ^e	45,833	22.92	107.9±0.3
Eudragit® EPO	47,000 ^e	1.1 ^f	42,727	19.62	55.8±2.1
DCM	85	1.33	64	20.2	-
MeOH	32	0.79	40	29.7	-

MW: Molecular weight; ρ : True density; V_m : Molar volume; δ : Hildebrand solubility parameter; T_g : Glass transition temperature.

^a Calculated dividing the molecular weight by the true density;

^b Drug and Polymers: estimated at according to [18]; Solvents: taken from reference [19];

^c Obtained by mDSC – Mean± s.d., n=3;

^d From reference [20];

^e Supplier Information;

^f From reference [21].

2.3.2 Drug-polymer kinetic miscibility predictions

The phase behavior of the simulated systems will depend on the strength of the interaction between species and the process variables. The latter will dictate the formation of a homogenous and molecularly mixed ASD (*i.e.* amorphous solid solution), or on the other hand, an amorphous system showing phase separation of a drug- and polymer rich region (*i.e.* an amorphous suspension). The formation of two distinct amorphous regions is an indication of physical instability, and recrystallization may be observed when producing the respective dispersion [16]. Thus, the model will only return one of two possible outcomes: homogeneity/heterogeneity, one-phase system/two-phase system or miscibility/immiscibility.

Figure 2.2 presents the sequence of 1D simulations for the drug-polymer systems in this study. A comparison of the kinetic miscibility predictions among the three pharmaceutical mixtures shows differences in drug-polymer phase behavior at the drying temperature.

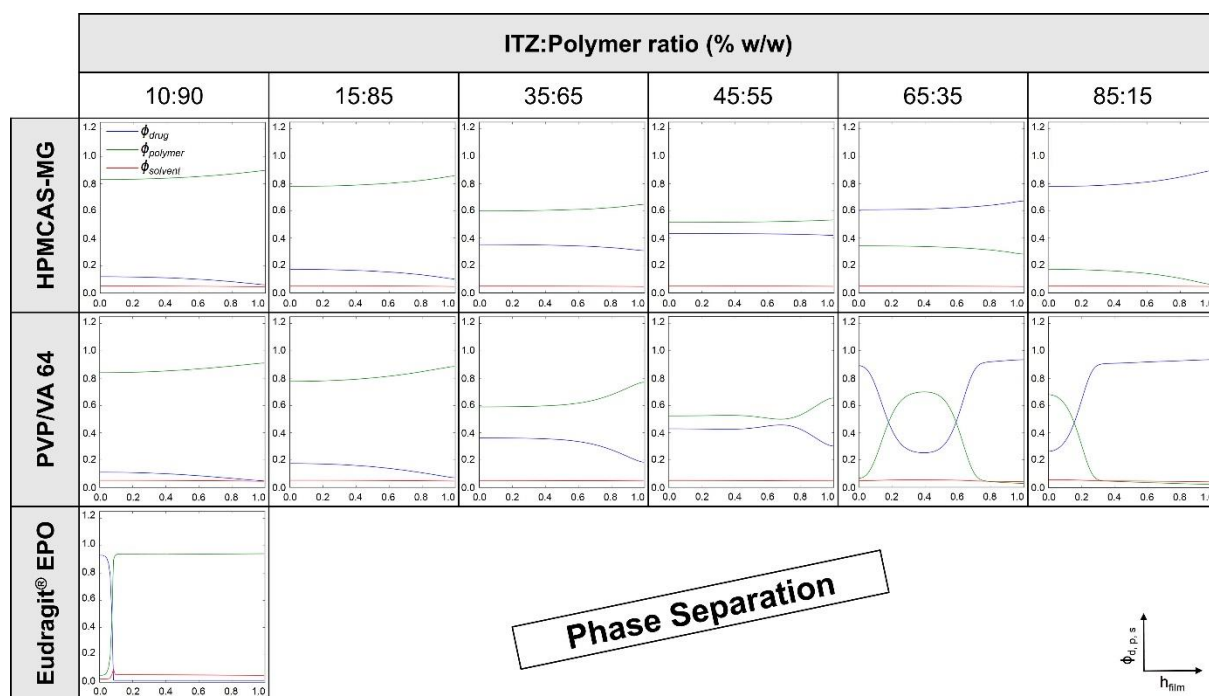


Figure 2.2. Results from 1D simulations showing the expected final phase behavior of ITZ:HPMCAS-MG, ITZ:PVPVA/64 and ITZ:Eudragit® EPO systems with increasing drug concentration (from left to right). The 1D simulations show the final drug (blue), polymer (green) and solvent (red) volume fraction curves along the film height (horizontal axis).

In the case of the ITZ:HPMCAS-MG system, after solvent evaporation, both components remained homogeneously mixed up to 85% ITZ. The drug and polymer volume fraction curves in the 1D ITZ:HPMCAS-MG figures remained almost constant and parallel along the film height. No additional simulations were run for drug loads above 85% ITZ.

In the case of the ITZ:PVPVA 64 system, the drug and polymer remained homogeneously mixed up to 45% ITZ. For 35% ITZ load the results suggest a potential for the system to separate into two phases, with the drug and polymer volume fraction curves showing an abrupt change in trend along the film height when compared to lower drug loads. With an ITZ concentration higher than 65%, the system was considered to be phase-separated, which was indicated by the formation of drug and polymer-rich amorphous regions along the film height.

Considering the results obtained, it can be said that the ITZ:PVPVA 64 system was partial or locally miscible at the drying temperature and showed a miscibility discontinuity with increased drug loading. At this point, this miscibility discontinuity could be seen as a set of ITZ loads comprehended between 45% and 65% drug fraction, which contained the maximum drug concentration from which the miscibility-immiscibility transition was observed.

Among the different drug-polymer systems studied, the pair ITZ:Eudragit[®]EPO presented the lowest drug-polymer kinetic miscibility, taking into account that the phase-separation was observed at the lowest drug load tested – 10% ITZ. In this case, it can be postulated that a miscibility discontinuity exists for drug loads lower than 10% ITZ. Drug loads lower than 10% were considered to be below those used in practice, thus no further simulation was carried out for this system. By opposition, the reasons for not having run additional computational simulations for drug loads above 10% ITZ:Eudragit[®] EPO were different. For drug-polymer systems presenting a miscibility behavior with a UCST (one of the assumptions considered in this work), above the critical temperature (T_c) drug and polymer form a homogenous system, while below T_c the drug-polymer system phase-separates. Analyzing the drug-polymer phase-diagrams reported in the literature by different authors, one can observe that they are highly asymmetric and shifted towards high drug loads [5,6,15,22, 23]. The critical compositions (ϕ_c) are generally above 80% (volume or weigh fraction) and the critical temperatures (T_c) are well above temperatures of interest with respect to spray drying processing ($>100^\circ\text{C}$). These assume that for the drug-polymer systems under study and considering the temperature at which the kinetic miscibility predictions were run ($T_{\text{drying}}=40^\circ\text{C}$), once the formation of a two-phase system occurred, heterogeneity was continuous up to 85% drug load, or another predefined upper bound by the user. The results from the 1D simulations of the ITZ:PVP/VA 64 corroborated the latter statement, showing drug-polymer phase separation above 65% ITZ.

2.3.2.1 Optimization of drug load – ITZ:PVP/VA 64 Case-study

In this section the drug load of the ITZ:PVP/VA 64 system was optimized within the miscibility transition range determined in the 1D simulations (45% to 65% w/w).

The first row in Figure 2.3 shows the final 1D microstructures obtained after the evaporation of the solvent, while the second row corresponds to the final 2D microstructures with respect to the volume fraction of one of the components of the system, which in this specific case is the volume fraction of the drug (ϕ_d). The 2D microstructures respecting the volume fraction of polymer and solvent (ϕ_p and ϕ_s , respectively) are not shown for sake of simplicity. The final polymer composition is the inverse of the drug, *i.e.* ($1 - \phi_d$), while the solvent fraction is ≈ 0 in the whole domain.

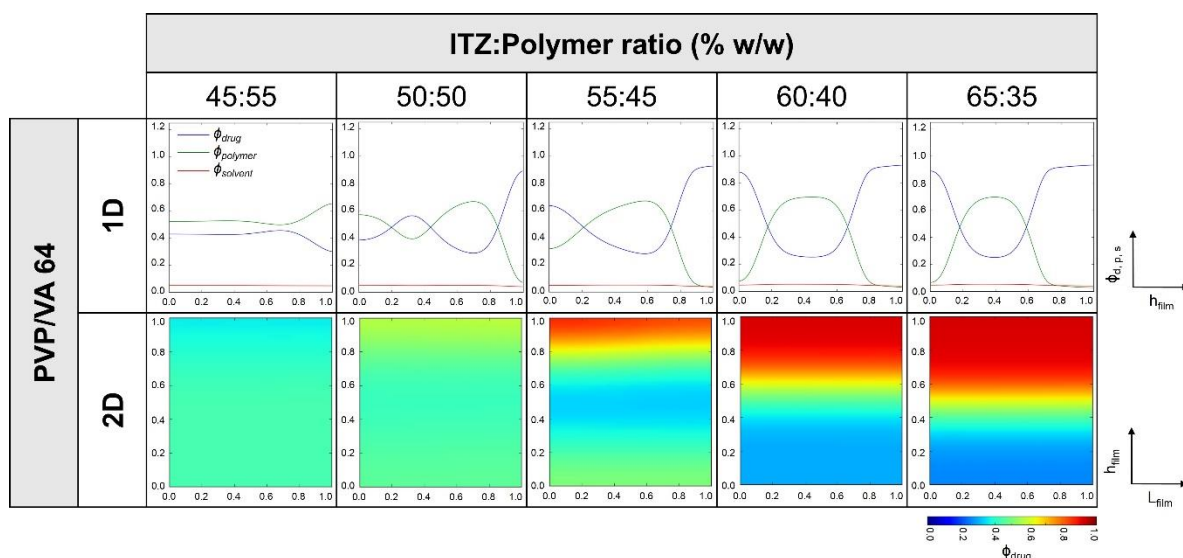


Figure 2.3. Results from 1D and 2D simulations showing the phase composition of ITZ:PVPVA/64 system with increasing drug load within the kinetic miscibility discontinuity boundary (from 45% to 65% ITZ w/w).

Increments of 5% ITZ were simulated in one- and two-dimensions starting with the 50% up to 60% ITZ:PVP/VA 64 systems. The 1D and 2D figures obtained for 45% and 65% loads were also included in Figure 2.3 for comparison purposes.

The analysis of the 1D simulations in Figure 2.3, indicates that phase-separation would occur above 50% ITZ due to the formation of different layers or amorphous domains along the film thickness. However, the analysis of the respective 2D simulations has shown that, although apparent different amorphous regions have been formed in the 1D calculations, the 50% ITZ system could be considered as a one-phase homogenous system in the 2D simulation, for presenting an overall constant volume fraction of drug around 0.4-0.5 along the film. This specific case illustrates well the importance and usefulness of 2D simulations if drug load optimization is desired.

At this point, the miscibility discontinuity or the drug load interval that contains the maximum theoretical drug load expected for the ITZ:PVP/VA 64 system was comprehended in the range between 50-55% ITZ, and it could have been further narrowed down by executing an additional simulation at 52.5% ITZ (Figure 2.4).

Comparing the 1D simulations at 50% and 52.5% ITZ, the final microstructures formed were fairly similar. According to the 2D simulations at 52.5% ITZ, phase-separation with a clear segregation of two amorphous regions was more obvious, with one phase enriched in drug and the other in polymer. The drug load window from 50% to 52.5% ITZ was now narrowed

down so that one can infer that the theoretical maximum drug load the system can admit without compromising miscibility was $\approx 50\%$ ITZ.

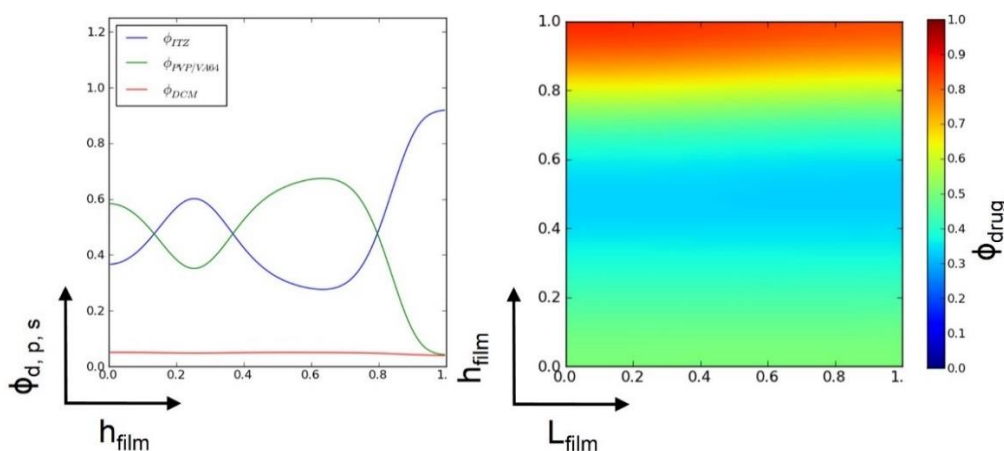


Figure 2.4. Results from 1D and 2D simulations presenting the final phase behavior of ITZ:PVPVA/64 system at 52.5% (w/w) ITZ.

2.3.3 Solvent casting and spray drying experiments

To assess the validity of the TKE model and to produce experimental evidence of the kinetic miscibility estimates, SC experiments were performed. The cast films produced were analyzed using mDSC to define the level of ITZ that could be added to the ASD before signs of phase-separation appear (either amorphous-amorphous or recrystallization). The drug load range between the maximum drug load added to the mixture before phase separation occurred, and the minimum drug load tested that exhibited signs of phase separation was defined as the SC miscibility discontinuity. Subsequently to the SC screening phase, SD prototypes were also produced. Drug-polymer spray drying experiments were undertaken according to the limits of the SC miscibility discontinuity. Only an additional ITZ:PVP/VA 64 SDD system was produced due to the detection of a false-negative result. This will be explained in more detail later in the text.

The DSC heat flow curves correspondent to the thermal analysis of the cast films and spray dried materials with drug loads equal to the SC miscibility discontinuity limits are presented in Figure 2.5, Figure 2.6 and Figure 2.7, for the systems ITZ:HPMCAS-MG, ITZ:PVP/VA 64 and ITZ:Eudragit[®] EPO, respectively. More detailed information (*i.e.* temperatures and micrographs) regarding the analytical characterization of the casted films and spray dried powders produced is presented as Supplementary Information A.

Figure 2.5 shows the mDSC profiles for the 45% and 65% ITZ mixtures with HPMCAS-MG prepared by solvent casting and subsequent spray drying. In what regards the cast films, at 45% ITZ the product presented a single glass transition temperature (T_g) in the reversible heat flow (shown by an arrow) and a single relaxation endotherm in the non-reversible heat flow (not shown). No signs of amorphous-amorphous phase separation or crystallization were observed in the thermograms. Profiles for the 10, 15 and 35% ITZ loading cast films were identical to the 45% ITZ.

The results suggest that ITZ was homogeneously mixed and molecularly dispersed within HPMCAS-MG up to 45% drug load. In the case of 65% ITZ:HPMCAS-MG cast films, the only change in heat capacity detected in the reversible heat flow profile was around $26.7 \pm 4.2^\circ\text{C}$, a temperature significantly below from the one expected, considering the T_g of the pure components or even considering the mixed T_g value decay due to increasing ITZ loading, according to the Gordon-Taylor equation [24]. No phase-separation or recrystallization events were detected during heating, but an endothermic peak at $151.6 \pm 1.2^\circ\text{C}$ was observed. This endothermic peak might correspond to the melting of ITZ ($T_m = 162.6 \pm 0.2^\circ\text{C}$). The melting point depression observed was due to the presence of the polymer that lowered the chemical potential of the drug and led to a decrease of its melting temperature [25,26].

The existence of an endothermic event without the observation of a prior exothermic recrystallization also presupposes the presence of a starting crystalline material in the sample. This observation could be related to the absence of a mixed T_g , thus with the formation of heterogeneities along the cast film due to *e.g.* poor drying conditions, inefficient process of amorphization or residual solvent plasticizing the product. The 85% ITZ:HPMCAS-MG casted films showed a single T_g value near the T_g of pure ITZ, but considering that neither the drug mesophase nor the T_g of the polymer were detected, a homogeneous amorphous system might have been formed. However, the system evolved into recrystallization followed by melting of the drug, during the heating cycle. Recrystallization triggered by heating is a consequence of increased molecular mobility and molecular rearrangement in amorphous systems with high drug load and insufficient polymeric stabilization [27]. Such systems are considered less stable and are more prone to phase-separation and drug crystallization triggered by external variables (*e.g.* temperature, humidity) [28,29].

Both the thermograms of the 45% ITZ cast film and the SDD presented a single T_g in the reversible heat flow without signs of amorphous-amorphous phase separation or recrystallization, suggesting the formation of an amorphous solid solution. Moreover, no birefringence was observed in the sample. The thermogram of 65% ITZ SDD has shown that

the heterogeneities formed during SC disappeared and gave place to a clear mixed T_g with the respective relaxation endotherm in the non-reversible heat flow (not shown).

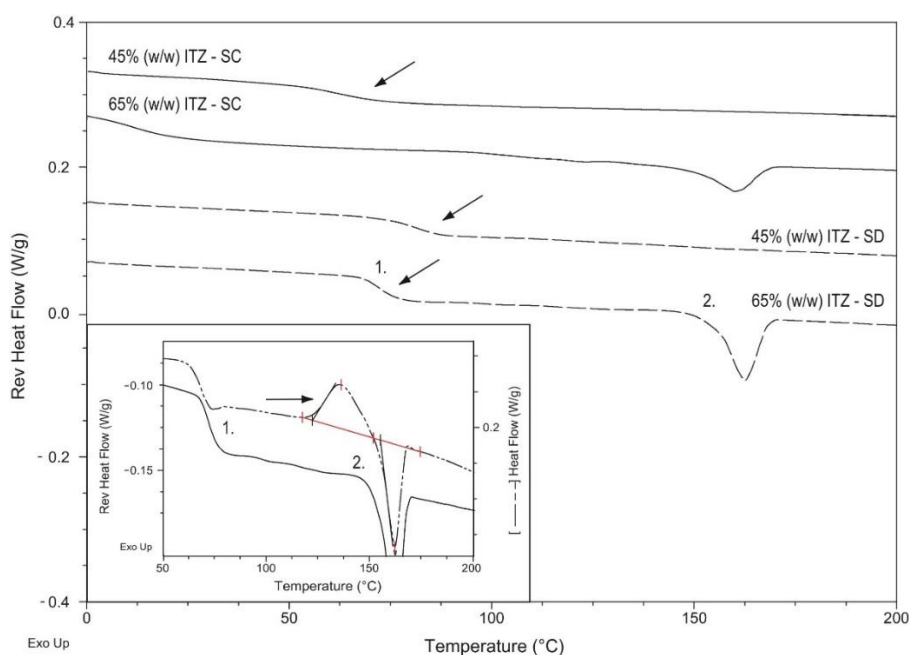


Figure 2.5. Reversible heat flow thermograms for the 45 and 65% (w/w) ITZ:HPMCAS-MG cast films (SC) and spray-dried materials (SD). Arrows indicate the T_g 's.

The absence of birefringence by microscopy also indicated the formation of a homogenous ASD. However, this system like the one with 85% ITZ cast film was not stable on heating; the drug recrystallized prior to melting (Figure 2.5, insert). Although SD promoted a more efficient amorphization process with a faster entrapment of the components of the solution, the high drug load in formulation may present a higher risk of structure destabilization and physical instability.

Figure 2.6 presents the mDSC thermograms for the ITZ:PVP/VA 64 binary mixtures manufactured by the solvent casting and spray drying processes. For casted films with 45% ITZ no recrystallization or melting endotherms were detected and only a single mixed T_g was observed. On the other hand, for lower drug loads (10, 15 and 35% drug load) no conclusion regarding the physical-state of these systems can be drawn by the analysis of the thermograms. In the three replicates, unexpected endothermic events appeared at 80°C and 150°C in the total heat flow. Janssens *et al.* also observed endothermic events in the range of 40°C and 100°C in the mDSC thermograms of ternary systems made up of 10, 20 and 40% ITZ load in 25/75 (w/w) TPGS 1000/PVPVA 64 [30]. These authors justified the appearance of such events as relaxation enthalpy peaks correspondent to the formation of amorphous inhomogeneities in the samples.

To validate this hypothesis, they performed a heat-cool-heat cycle with those materials in the calorimeter, and the endothermic peaks disappeared in the second heating run. This second heating eliminated the thermal history of the samples and potential amorphous phases present in the raw material disappeared [14].

In this work, amorphous inhomogeneities may have also been formed in the cast films. Although additional tests could have been performed, the indication of the production of an amorphous and homogenous system containing a higher drug load [*i.e.* 45% (w/w)] was sufficient to move forward with the screening method.

Increasing the ITZ potency to 65% and 85%, the cast films presented a single T_g and considering the absence of a drug mesophase or second T_g in both systems, this was a strong indication that the drug was homogeneously mixed with the polymer. Still, upon increasing the drug loading to 65%, a slight melting endotherm was detected, while increasing the ITZ potency to 85% caused a large melting endotherm. Both compositions have shown a recrystallization exotherm when analyzing the total heat flows.

The SD results from the respective SDDs with 45% and 65% ITZ exerted a single mixed T_g and no signs of amorphous-amorphous phase separation or crystallization, which suggests that amorphous solid solutions were formed. Consequently, one can refer that the cast film with 65% ITZ was a false-negative result. This observation reinforces the fact that although solvent casting can provide useful preliminary information on kinetic miscibility and physical stability, premature conclusions should not be drawn from the analytical results of the cast films; again, one may be neglecting the real solubilization capacity offered by the polymer. This shows the importance of confirming the SC results with the production of the respective SDDs.

In order to determine the experimental kinetic miscibility limit of the ITZ:PVP/VA 64 mixture, an additional SD experiment at 85% ITZ was performed. Upon increasing the ITZ loading, despite the detection of a mixed T_g , a recrystallization peak followed by melting was observed. No glassy ITZ clusters were detected, but according to the PLM results, ITZ crystallites were present. The results obtained indicate that at 85% ITZ, even using such drying process conditions, the drug cannot be completely stabilized by the polymer. Comparing with the 85% ITZ:PVP/VA 64 cast film, the thermal results were similar.

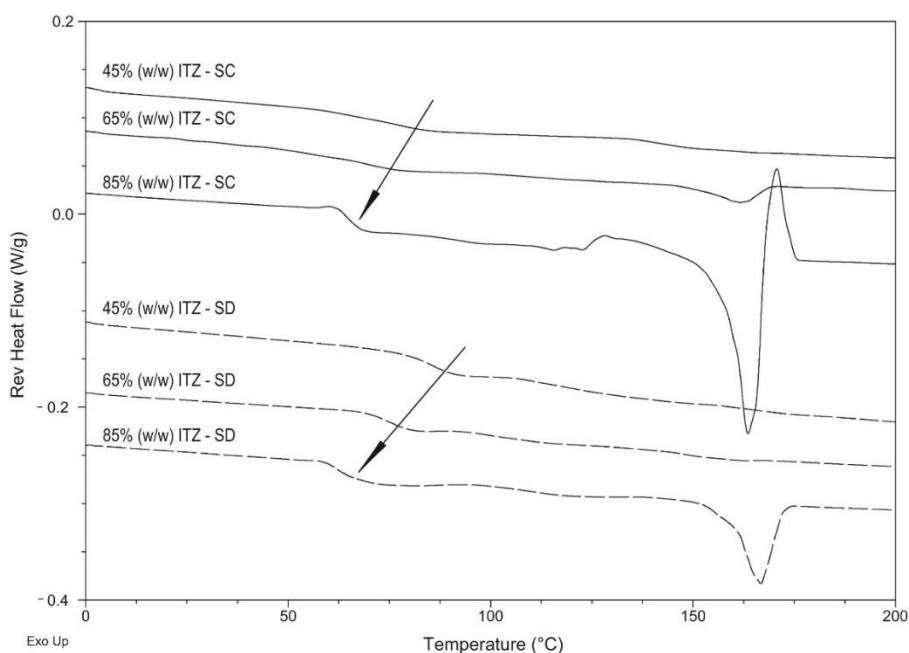


Figure 2.6. Reversible heat flow thermograms obtained for the 45, 65 and 85% (w/w) ITZ:PVP/VA 64 cast films (SC) and respective spray-dried materials (SD). Arrows indicate the T_g 's.

Finally, Figure 2.7 shows the thermal results for the 15% and 35% ITZ:Eudragit[®] EPO cast films and respective spray dried powders. Amorphous solid solutions without the detection of key indicators of physical instability were produced via SC, up to and including 15% drug load. Contrarily, when increasing the ITZ load to 35% two single T_g 's and the ITZ mesophase were detected in the reversible heat flow. The zoom in Figure 2.7 shows the relaxation endotherms correspondent to the phase-separation event. The 45% cast films also present signs of amorphous segregation within the same temperature range. It is difficult to conclude with certainty if these two T_g 's correspond to the complete segregation of two phases or to the formation of amorphous clusters of ITZ, still with a certain percentage of drug molecularly dispersed within the polymer (glass suspension/solution) [31,32]. It was also noted that, while the 35% ITZ cast films remained kinetically stable as phase-separated systems and any additional events were detected during heating, the 45% system presented drug recrystallization and melting. For the 65% and 85% cast films, the formation of drug amorphous clusters was observed (detection of mesophase), however only one T_g was detected. For those cases, the detection of two single T_g 's may be hidden by the detection of a broad T_g value.

The results obtained for the spray-dried materials produced were consistent with the respective SC profiles. At 15% ITZ load a single-phased amorphous system was obtained with

no observation of further events during heating, while at 35%, though the SDD presented one single T_g it has evolved into crystallization of the drug during the heating cycle.

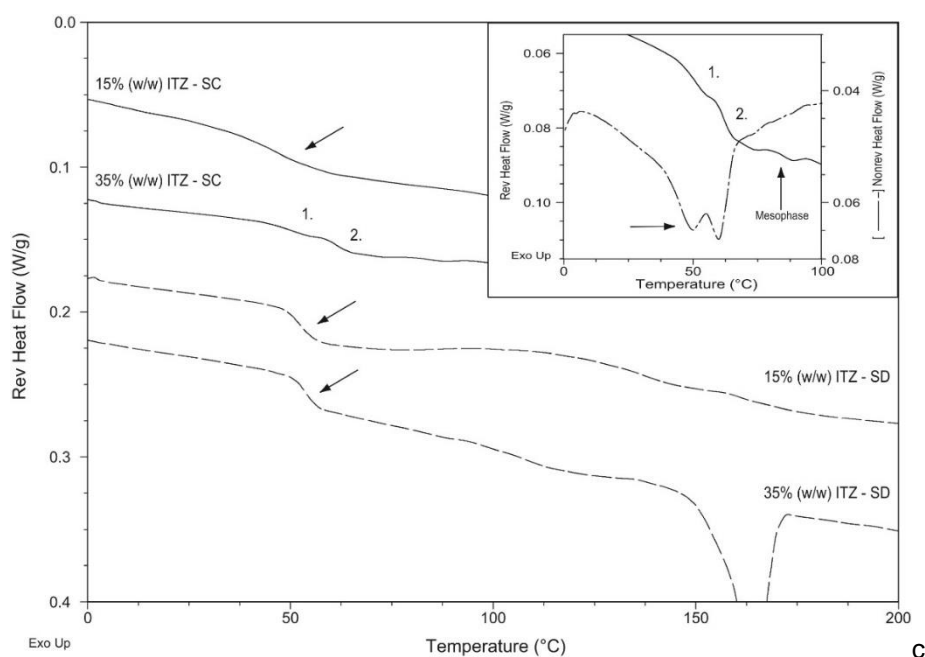


Figure 2.7. Reversible heat flow thermograms obtained for the 15 and 35 (wt.%) ITZ:Eudragit[®] EPO cast films (SC) and respective spray-dried materials (SD). Arrows indicate the T_g 's.

2.4 Discussion

Over the last few years, there was a growing interest by the pharmaceutical industry, in the implementation of screening methodologies to support the development of ASDs. The basis for this change might be related to the application of Quality by Design (QbD) principles and concepts, where one of the main goals is to *build quality into the product*, thereby reducing empiricism, development time, risk and costs [33].

Screening methodologies should include, but not be limited to, the assessment of the thermodynamic drug solubility in the polymer and drug-polymer kinetic amorphous miscibility. Effective screening tools should provide the answer to key questions, such as, what are the most suitable polymers and process variables that allow the manufacturing of high-dose formulations showing improved physical stability during product development and long-term storage.

The study presented proposes a new screening methodology intended to be used in the early development of ASD produced by spray drying. The novelty of this work is the implementation of a computational tool to guide rationale polymer selection and the narrowing

of drug load ranges with the potential to form miscible binary systems. The major differences of the TKE model implemented from commonly applied methodologies to predict the solubility and miscibility of a drug in a polymeric carrier are the assessment of the thermodynamics of mixing of a drug-polymer-solvent system, the inclusion of kinetic material properties and process variables (*i.e.*, components diffusion and evaporation rate, respectively). The use of this model allows the definition of the kinetic drug-polymer system phase boundaries, as it will also provide detailed information regarding the influence of important process variables (*e.g.* selection of the solvent, concentration of solids in the solvent, drying temperature) on the limits of this miscibility region.

As a first assessment of the validity of the TKE model, three amorphous pharmaceutical systems composed of ITZ and PVP/VA-64, HPMCAS-MG and Eudragit[®] EPO were tested. 1D computational simulations were run, and in order to have an experimental evidence of the kinetic miscibility estimates a SC experimental protocol was developed. Cast films were produced with the same drug-polymer systems, at the same drug loads and process conditions (*i.e.* drying temperature) as the computational simulations tested. Then, the scale-up of the systems correspondent to the limits of the SC miscibility discontinuity using spray drying further confirmed the validity of the model and the screening methodology as a whole.

In order to analyze the results obtained together, Figure 2.8 compiles in a single schematic representation the theoretical predictions provided by the TKE model and the analytical results obtained for the casted films and spray dried products for the different ITZ amorphous systems studied.

The results are depicted by means of continuous bars, which represent the kinetic miscibility behavior as a function of drug loading for each ITZ system studied. According to the results that have already been described in previous sections, grey bars were extended up to the maximum drug load tested that each polymer could stabilize without the existence of signs of physical instability. By opposition, black bars were extended from the minimum drug load tested with the detection of two amorphous regions (A-A) or the presence of crystalline material suspended in the amorphous matrix (C-A). The presence of crystalline drug in the product may have origin from incomplete amorphization, or recrystallization during the DSC heating run.

The uncertain region bars correspond to what was defined as the miscibility discontinuity or the region that includes the drug loading from which phase separation is observed or inferred from the results.

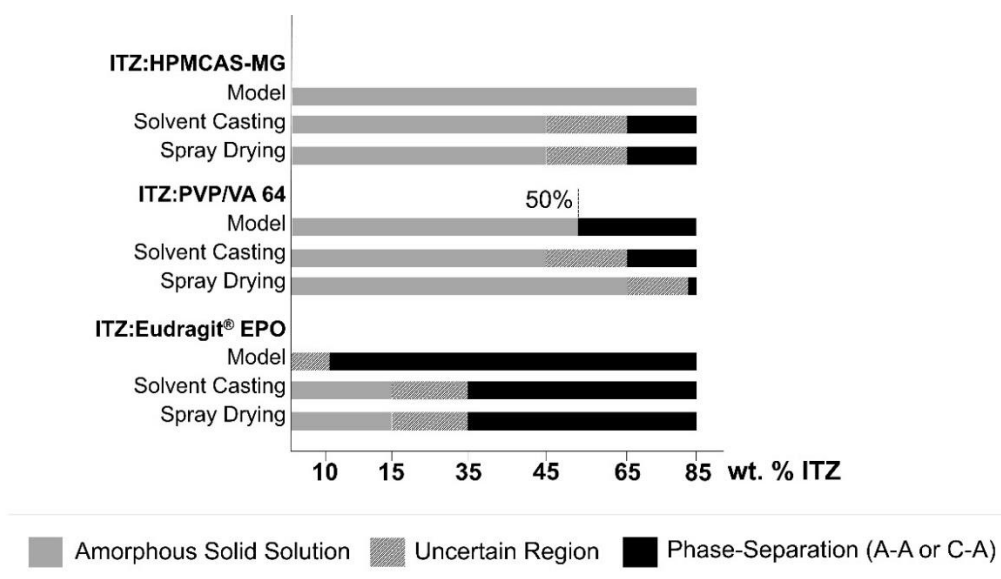


Figure 2.8. Theoretical miscibility predictions given by the TKE model and analytical results obtained for the solvent casting films and spray drying products, as a function of drug load.

It should be noted that the representation of the bars are supported on discrete experimental points, bearing in mind that a lower number of tests were performed for the representation of the spray drying bars. It is assumed that these miscibility interpolations can be considered and that these are valid within the assumption that drug-polymer pharmaceutical systems in general present a typical temperature-composition phase diagram, *i.e.* the asymmetrical “inverted U” presenting only an UCST, shifted for higher drug loads [5,6,15,22,23].

2.4.1 Validation of the TKE model and screening methodology

Analyzing Figure 2.8 and comparing the miscibility estimates and the experimental results of the casted films and spray-dried products of each drug-polymer system, it can be seen that the TKE is able to globally describe the amorphous drug-polymer compatibility and phase behavior. For example, the drug-polymer pairs which exhibited a higher experimental miscibility capacity, *i.e.* around 45% for the ITZ:HPMCAS-MG and 65% for the ITZ:PVP/VA 64 system, were those which simulations indicated the formation of a homogenous amorphous systems for higher drug loads [85% and 50% (w/w) TZ, respectively]. In a similar way, the drug-polymer mixture which presented its maximum of experimental miscibility at lower drug loads, *i.e.* around 15% for the ITZ:Eudragit® EPO system, was the one where the model predicted phase-separation for lower drug loads [10% (w/w) ITZ].

These results suggest that the TKE model can be used successfully to rank the best polymers for amorphous drug stabilization. In this study, the following ranking would be obtained by ascending order of kinetic miscibility capacity for the ITZ systems tested: Eudragit® EPO << PVP/VA 64 < HPMCAS-MG.

As far as the maximum miscibility values obtained are concerned, some differences were identified for the predicted and observed results. Despite including the influence of thermodynamic, kinetic and dynamic factors on the final phase behavior of ASDs, TKE may not fully capture the complexity of drug-polymer particle formation. The causes that contribute for these differences may be seen from a three level perspective, *i.e.* starting from the global design and structure of the computational tool taking into account the objectives for which the model was originally developed, considering simultaneously the limitations and assumptions of the models applied, especially in what regards the F-H theory and the evaporation model, and finally the simple experimental methods and correlations used to estimate part of the system-dependent input parameters. Thus, the accuracy of the predictions should be analyzed in light of the limitations and assumptions of the computational system.

Although validation from a quantitative standpoint should not be made at this point of the work, it is still possible to use the kinetic miscibility estimates obtained from the model to create some guidelines to define a narrow drug load range to be tested using solvent casting or spray drying. Moreover, we can use all the information gathered (TKE+SC) to improve the experimental design with reduction of the experimental work [15,34]. For instance, for systems partially miscible up to a proper relevant drug dose (*e.g.* ITZ:PVP/VA 64), a small number of solvent casting experiments with solutions containing a concentration of drug around the maximum value before phase-separation is detected, could be sufficient to provide useful information on experimental miscibility and ASD stabilization. Conversely, for systems that experience spontaneous phase-separation already at low drug loads (*e.g.* ITZ:Eudragit® EPO), it would probably be a poor decision to experimentally test systems with drug loads well above the minimum tested, due to the high probability of drug-polymer immiscibility. Finally, estimates such as the ones obtained for the ITZ:HPMCAS-MG system, where the model predicted total miscibility for the entire drug load range, should not be over interpreted because a formulation with 85% (w/w) drug concentration may present a higher risk of drug recrystallization, as observed for ITZ.

Based on these results, it can be verified that optimal spray dried ASDs can be produced using less time and resources, owing to the early implementation of screening methodologies that work as important decision-making elements for the rationale design of new amorphous

products. Through a correct validation of the proposed methodology, it can be used not only to rank the best polymers and define a safe drug load/miscibility window, but also to study the influence of changing the solvent(s), solution composition and drying temperature on the final phase behavior of ASDs. A workflow demonstrating the implementation of the screening program developed in this work is shown in Figure 2.9.

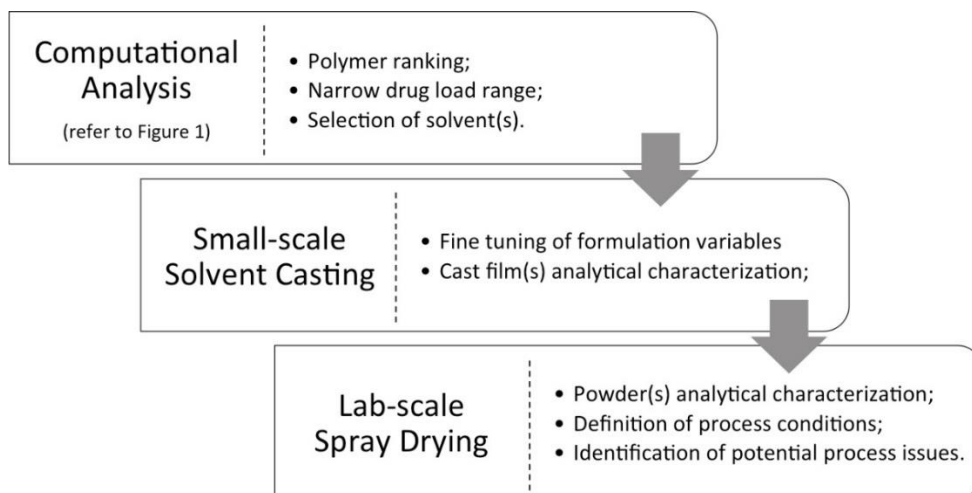


Figure 2.9. Workflow for the early development of a new spray dried amorphous solid dispersion.

2.5 Conclusions

In this work, a screening methodology was developed to support the early development of spray dried amorphous solid dispersions. One of the main improvements in relation with other screening methodologies is the application of a computational tool based on diffuse interface theories for studying drug-polymer microstructure evolution.

Simulations were run for three ITZ-based systems (at increasing drug loading), with the Thermodynamic, Kinetic and Evaporation (TKE) model being able to globally describe the amorphous drug-polymer compatibility and phase behavior on the basis of the computational predictions and experimental results obtained through solvent casting and spray drying. The polymer ranking by ascending order of physical stability as determined by the model - Eudragit® EPO << PVP/VA 64 < HPMCAS-MG – was consistent with the experimental data. The miscibility of ITZ in PVP/VA 64 was higher than HPMCAS-MG, or Eudragit® EPO. Despite differences observed in the absolute maximum miscibility values obtained, it is still possible to use the information given by the TKE model to create guidelines to define a narrow

drug load range to be tested in the following stages of process development, thus saving time and resources.

2.6 References

- [1] D. M. Saylor, C.-S. Kim, D. V. Patwardhan, and J. A. Warren, "Diffuse-interface theory for structure formation and release behavior in controlled drug release systems" *Acta Biomaterialia*, vol. 3, pp. 851-864, 2007.
- [2] D. M. Saylor, "Predicting Microstructure Evolution in Controlled Drug Release Coatings" in *FDA/NHLBI/NSF Workshop on Computer Methods for Cardiovascular Devices*, USA, 2010.
- [3] J. E. Guyer, D. Wheeler, and J. A. Warren, "FiPy:Partial Differential Equations with Python" *Computing in Science & Engineering*, vol. 11, no. 3, pp. 6-15, 2009.
- [4] D. W. van Krevlen and K. te Nijenhuis, *Properties of Polymers*. Amsterdam: Elsevier, 2009.
- [5] Y. Tian *et al.*, "Construction of Drug–Polymer Thermodynamic Phase Diagrams Using Flory-Huggins Interaction Theory: Identifying the Relevance of Temperature and Drug Weight Fraction to Phase Separation within Solid Dispersions" *Molecular Pharmaceutics*, vol. 10, pp. 236-248, 2013.
- [6] D. Lin and Y. Huang, "A thermal analysis method to predict the complete phase diagram of drug-polymer solid dispersions" *International Journal of Pharmaceutics*, vol. 399, no. 1-2, pp. 109-115, 2010.
- [7] P. Marsac, S. Shamblin, and L. S. and Taylor, "Theoretical and practical approaches for prediction of drug-polymer miscibility and solubility" *Pharmaceutical Research*, vol. 23, no. 10, pp. 2417-2426, 2006.
- [8] K. Kawakami *et al.*, "Competition of Thermodynamic and Dynamic Factors During Formation of Multicomponent Particles via Spray Drying" *Journal of Pharmaceutical Sciences*, vol. 102, no. 2, pp. 518-529, 2013.
- [9] C. R. Wilke and P. Chang, "Correlation of diffusion coefficients in dilute solutions" *AICHE Journal*, pp. 264-270, 1955.
- [10] K. Masters, *Spray Drying in Practice*. Denmark: SprayDry Consult, 2002.

- [11] A. M. Goula and K. G. Adamopoulos, "Influence of Spray Drying Conditions on Residue Accumulation - Simulation Using CFD" *Drying Technology*, vol. 22, no. 5, pp. 1107-1128, 2004.
- [12] B. E. Poling, J. M. Prausnitz, and J. P. O'Connell, *The Properties of Gases and Liquids.*: McGraw-Hill, 2001.
- [13] R. S. Miller, K. Harstad, and J. Bellan, "Evaluation of equilibrium and non-equilibrium evaporation models for many-droplet gas-liquid flow simulations" *International Journal of Multiphase Flow*, vol. 24, pp. 1025-1055, 1998.
- [14] A. Paudel, J. Van Humbeeck, and G. Van den Mooter, "Theoretical and Experimental Investigation on the Solid Solubility and Miscibility of Naproxen in Poly(vinylpyrrolidone)" *Molecular Pharmaceutics*, vol. 7, no. 4, pp. 1133-1148, 2010.
- [15] Y. Tian, V. Caron, D. S. Jones, A.-M. Healy, and G. P. Andrews, "Using Flory-Huggins phase diagrams as a pre-formulation tool for the production of amorphous solid dispersions: a comparison between hot-melt extrusion and spray drying" *Journal of Pharmacy And Pharmacology*, vol. 66, no. 2, pp. 256-274, 2014.
- [16] J. A. Baird and L. S. Taylor, "Evaluation of amorphous solid dispersion properties using thermal analysis techniques" *Advanced Drug Delivery Reviews.*, vol. 64, no. 5, pp. 396-421, 2012.
- [17] K. Six *et al.*, "Investigation of thermal properties of glassy itraconazole: identification of a monotropic mesophase" *Thermochimica Acta* , vol. 376, pp. 175-181, 2001.
- [18] R. F. Fedors, "A Method for Estimating Both the Solubility Parameters and Molar Volumes of liquids" *Polymer Engineering and Science* , vol. 14, no. 2, pp. 147-154, 1974.
- [19] A. F. M. Barton, *Handbook of Solubility Parameters and Other Cohesion Parameters*. Florida: Boca Raton, CRC Press, 1983.
- [20] S. Janssens, H. Novoa de Armas, W. D'Autry, A. Van Schepdael , and G. Van den Mooter, "Characterization of ternary solid dispersions of Itraconazole in polyethylene glycol 6000/polyvidone-vinylacetate 64 blends" *European Journal of Pharmaceutics and Biopharmaceutics*, vol. 69, pp. 1114-1120, 2008.
- [21] P. Marsac, T. Li, and L. S. Taylor, "Estimation of drug polymer miscibility and solubility in amorphous solid dispersions using experimentally determined interaction parameters" *Pharmaceutical Research*, vol. 26, no. 1, pp. 139-151, 2009.

- [22] Y. Zhao, P. Inbar, H. P. Chokshi, A. W. Malick, and D. S. Choi, "Prediction of the thermal phase diagram of amorphous solid dispersions by Flory-Huggins theory" *Journal of Pharmaceutical Sciences*, vol. 100, no. 8, pp. 3196-3207, 2011.
- [23] J. M. Keen *et al.*, "Investigation of process temperature and screw speed on properties of a pharmaceutical solid dispersion using corotating and counter-rotating twin-screw extruders" *Journal of Pharmacy and Pharmacology*, vol. 66, no. 2, pp. 204-217, 2014.
- [24] K. Six, G. Verreck, J. Peeters, M. Brewster, and G. Van den Mooter, "Increased Physical Stability and Improved Dissolution Properties of Itraconazole, a Class II Drug, by Solid Dispersions that Combine Fast- and Slow-Dissolving Polymers" *Journal of Pharmaceutical Sciences*, vol. 93, no. 1, pp. 124-131, 2004.
- [25] A. Paudel, E. Nies, and G. Van den Mooter, "Relating hydrogen-bonding interactions with the phase behavior of naproxen/PVP K 25 solid dispersions: Evaluation of solution-casted and quench-cooled films" *Molecular Pharmaceutics*, vol. 9, no. 11, pp. 3301-3317, 2012.
- [26] P. Marsac, T. Li, and L. S. Taylor, "Estimation of drugpolymer miscibility and solubility in amorphous solid dispersions using experimentally determined interaction parameters. " *Pharmaceutical Research*, vol. 26, no. 1, pp. 139-151, 2009.
- [27] K. A. Overhoff, A. Moreno, D. A. Miller, K. P. Johnston, and R. O. Williams III, "Solid dispersions of itraconazole and enteric polymers made by ultra-rapid freezing" *International Journal of Pharmaceutics*, vol. 336, pp. 122-132, 2007.
- [28] P. J. Marsac *et al.*, "Effect of Temperature and Moisture on the Miscibility of Amorphous Dispersions of Felodipine and Poly(vinyl pyrrolidone)" *Journal of Pharmaceutical Sciences*, vol. 99, no. 1, pp. 169-185, 2010.
- [29] A. C. F. Rumondor, H. Wikström, B. Van Eerdenbrugh, and L. S. Taylor, "Understanding the Tendency of Amorphous Solid Dispersions to Undergo Amorphous-Amorphous Phase Separation in the Presence of Absorbed Moisture" *AAPS PharmSciTech*, vol. 12, no. 4, pp. 1209-1219, 2011.
- [30] S. Janssens *et al.*, "Formulation and characterization of ternary solid dispersions made up of Itraconazole and two excipients, TPGS 1000 and PVPVA 64, that were selected based on a supersaturation screening study " *European Journal of Pharmaceutics and Biopharmaceutics*, vol. 69, pp. 158-166, 2008.
- [31] M. Vasanthavada, W.-Q. Tong, Y. Joshi, and M. S. Kislalioglu, "Phase Behavior of Amorphous Molecular Dispersions I: Determination of the Degree and Mechanism of Solid Solubility " *Pharmaceutical Research*, vol. 21, no. 9, pp. 1598-1606, 2004.

- [32] D. J. van Drooge , W. L. J. Hinrichs , M. R. Visser , and H. W. Frijlink , "Characterization of the molecular distribution of drugs in glassy solid dispersions at the nano-meter scale, using differential scanning calorimetry and gravimetric water vapour sorption techniques" *International Journal of Pharmaceutics* , vol. 310, pp. 220–229, 2006.
- [33] "Pharmaceutical Development, ICHQ8(R2)" International Conference on Harmonisation, Geneva, 2009.
- [34] S. Janssens *et al.*, "Influence of Preparation Methods on Solid State Supersaturation of Amorphous Solid Dispersions: A Case Study with Itraconazole and Eudragit E100" *Pharmaceutical Research*, vol. 27, no. 5, pp. 775-785, 2010.

Chapter 3

The results described in this chapter have been published total or partially in the following communications:

- I. Duarte, J. Henriques, J. F. Pinto and M. Temtem, “Predicting the *in vivo* performance of amorphous solid dispersions based on molecular descriptors and statistical analysis” (in preparation);
- 2 international conferences as a poster communication.

Authors' contribution:

I.D. was involved in the conception, design, collection and statistical analysis of data. I.D. is working on the preparation of the manuscript.

3 Predicting the *in vivo* performance of amorphous solid dispersions based on molecular descriptors and statistical analysis

3.1 Introduction

Computational tools based on molecular descriptors and statistical analysis have been used for predicting drug's oral absorption and bioavailability [1], drug's solubility in biorelevant fluids [2], drug's glass forming ability and crystallization tendency [3,4], the solubility advantage of amorphous drugs [5] or the potential to form a solid dispersion [6], to mention some applications. The strategy of using multivariate methods to correlate molecular properties with specific responses is based on quantitative structure activity/property relationships (respectively, QSAR/QSPR) methods.

With the growing interest in the development of new ASDs, there is a significant number of research papers in the literature demonstrating the improved *in vivo* bioavailability of ASDs when compared with the reference products (*e.g.* crystalline drug, drug-polymer physical mixture, current commercial product). Taking advantage of amorphous dispersions past history, the purpose of this work was to develop a statistical model, based on multivariate data analysis tools - principal components analysis (PCA) and partial least squares method (PLS) - that could help on guiding ASD formulation design to obtain the desired *in vivo* performance. The goal of this work was not to develop reliable models for the prediction of oral bioavailability of ASDs, but rather to assess if there are any trends and/or correlations between the molecular descriptors of the APIs and the polymers (POLs) and *in vivo* pharmacokinetic parameters. This work does not intend to rule out the pre-clinical *in vivo* testing in advanced stages of product development.

A database considering 37 ASDs (or observations) and 35 XY variables was constructed. The X variables included molecular descriptors that described the APIs, the POLs and interactions thereof, while the Y variables corresponded to experimental data obtained from the literature, more specifically *in vivo* pharmacokinetic (PK) parameters, such as the area under the (*in vivo*) concentration-time curve (AUC), the peak plasma drug level or maximal plasma drug concentration (C_{\max}) and the time to obtain C_{\max} (t_{\max}).

3.2 Methodology

The work developed consisted on the following steps: (1) select from the literature a reasonable number of articles with *in vivo* bioavailability data of ASDs (section 3.2.1); (2) definition of molecular descriptors that describe the API, POLs and interactions thereof (section 3.2.2); (3) creation of the database or dataset; (4) overview of the dataset and outliers identification using PCA (section 3.2.3); (5) development of PLS models between molecular descriptors (X-variables) and *in vivo* PK parameters (Y-variables) (section 3.2.3); (6) testing the PLS models on a test set of compounds and identification of correlations.

3.2.1 Database

A database with 37 observations (rows) and 35 variables (columns) was created, as schematically shown in Figure 3.1, corresponding to ASDs described in 20 scientific reports found in the literature [7-26]. The variables included simple molecular descriptors for the APIs, the polymeric excipients (POLs) and interactions thereof (see section 2.2.), together with experimental data obtained from the selected articles, namely formulation-related variables and the typically reported *in vivo* pharmacokinetic parameters.

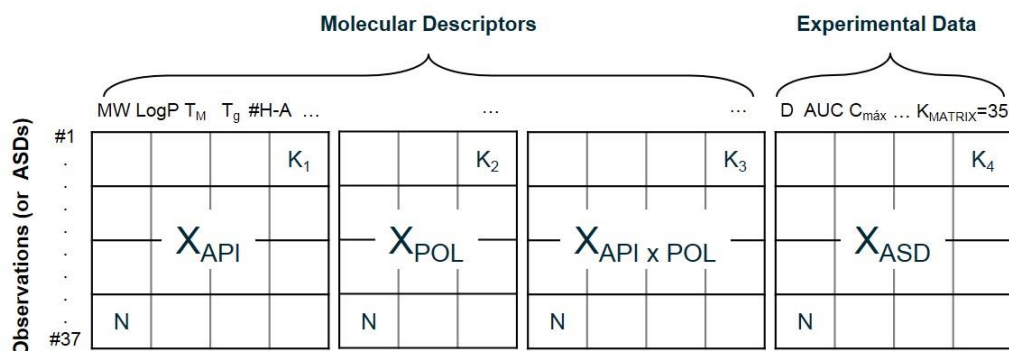


Figure 3.1. Representation of the database. A database with 37 observations (N) and 35 variables (K), in total, divided into K_1 molecular descriptors to describe the APIs, K_2 the molecular descriptors to describe the polymers (POLs), K_3 API-POL interaction variables based on the individual molecular descriptors of the APIs and POLs, and K_4 experimental variables.

The selection of data from the literature to support the creation of this database was based on the following criteria: (1) availability of *in vivo* PK data both for the ASD and a reference product (e.g. pure crystalline drug, drug-polymer physical mixture or commercial product), in order to obtain “gaining-factors” in relation to AUC, C_{max} and t_{max} ; (2) only binary

ASDs composed of an API and one excipient were considered, in order to reduce the complexity of the system and the *in vivo* phenomena involved; (3) only polymeric ASDs were considered, due to the fact that polymers are the mostly used carriers to stabilize amorphous drugs and enhance drug's dissolution; (4) the selection of the ASDs was independent from the amorphization method and the animal model selected to assess the *in vivo* performance.

Overall the database included 21 different APIs, with different ionization behaviors, and 13 different polymers across the major polymeric classes, such as those based on cellulose [*viz.* hydroxypropyl methylcellulose (HPMC), hydroxypropyl methylcellulose acetate succinate (HPMCAS), hydroxypropyl methylcellulose phthalate (HPMCP), hydroxypropyl cellulose (HPC)], polyvinylpyrrolidone (*viz.* PVP, Kollidon[®]) and polyvinylpyrrolidone/vinyl acetate (Kollidon[®] VA 64), methacrylic acid and methyl methacrylate [*e.g.* dimethylaminoethyl methacrylate, butyl methacrylate, and methyl methacrylate co-polymer or Eudragit[®] E100], and a graft copolymer composed of polyethylene glycol (PEG), polyvinylcaprolactam (PVCL), and polyvinylacetate (PVA) (*i.e.* Soluplus[®]). Table 3.1 describes the ASDs considered with the respective abbreviations used along the text and references.

3.2.2 Molecular descriptors and experimental data

To describe the APIs and the POLs, 15 and 8 molecular descriptors were considered, respectively. These were mostly molecular descriptors that could be easily computed from the molecular formula/structure, thus avoiding the dependence on complex and time-consuming computational tools.

Common structural properties to both APIs and POLs included parameters like molecular weight (MW), molar volume (MV), glass transition temperature (T_g), the total solubility parameter (SP), number of hydrogen-bond acceptor groups (#H-A), number of hydrogen-bond donor groups (#H-D), total number of hydrogen-bond groups (#H-total) and a derived parameter in an attempt to represent all possible hydrogen bonds of the API-API and the POL monomer-monomer self-association [#H-A \times #H-D, or #H(A \times D)].

Additional structural parameters used to describe the APIs included the octanol-water partition coefficient (log P, for neutral molecules), the pH-dependent octanol-water distribution coefficient (log D, at pH=5.5 and pH=7.4, for ionizable molecules), melting point (T_M), reduced glass transition temperature (T_{rg}), molecular polar surface area (PSA) and the number of rotatable bonds (#rotbonds). Whenever the molecular descriptors for the APIs were reported in the respective reference, those values were used in the database.

Table 3.1. ASDs considered as observations, with respective abbreviations and references.

# Obs.	API-Polymer Amorphous Dispersion	Abbreviation	Ref.
1	ER-34122 – HPMC (TC5RW)	ER-HPMC (TC5RW)	[7]
2	Torcetrapib – HPMCAS M	TCB-HPMCAS M	[8]
3	Torcetrapib – HPMCAS M *	TCB-HPMCAS M *	[8]
4	Compound 2 – HPMCAS M	C2-HPMCAS M	[8]
5	Compound 6 – HPMCAS L	C6-HPMCAS L	[8]
6	Tacrolimus – HPMC E5	TCL-HPMC E5	[9]
7	BMS-488043 – PVP K-29/30	BMS-K29/30	[10]
8	BMS-488043 – PVP K-29/30 *	BMS-K29/30 *	[10]
9	Danazol – PVP K-15	DNZ-K15	[11]
10	HO-221 – Kollidon® 30	HO-K30	[12]
11	HO-221 – Kollidon® VA 64	HO-KVA64	[12]
12	HO-221 – Kollidon® VA 64 *	HO-KVA64 *	[12]
13	HO-221 – HPMCP 55	HO-HPMCP 55	[12]
14	Fenofibrate – Eudragit® E100	FEN-E E100	[13]
15	AMG-517 – HPMCAS M	AMG-HPMCAS M	[14]
16	Compound I – Kollidon® 30	CI-K30	[15]
17	Compound I – Kollidon® 30 *	CI-K30 *	[15]
18	MFB-1041 – HPMC (60SH-50)	MFB-HPMC (60SH-50)	[16]
19	MFB-1041 – HPMCP 55	MFB-HPMCP 55	[16]
20	MFB-1041 – HPMCP 55 *	MFB-HPMCP 55 *	[16]
21	Nobiletin – HPC SSL	NBT-HPC SSL	[17]
22	Probucol – PVP K-30	PBC-K30	[18]
23	Probucol – PVP K-30 *	PBC-K30 *	[18]
24	Probucol – PVP K-30 *	PBC-K30 *	[18]
25	Probucol – PVP K-30 *	PBC-K30 *	[18]
26	Tolbutamide – PVP K-30	TBT-K30	[19]
27	Lonidamine – PVP K-29/32	LDM-K29/32	[20]
28	Fenofibrate – Soluplus®	FEN-SOL	[21]
29	Itraconazole – Soluplus®	ITZ-SOL	[21]
30	Raloxifene – Kollidon® 30	RXF-K30	[22]
31	Griseofulvin – HPMCAS M	GRS-HPMCAS M	[23]
32	Dutasteride – Eudragit® E100	DTT-E E100	[24]
33	Dutasteride – HPMC	DTT-HPMC	[24]
34	Dutasteride – HPC SL	DTT-HPC SL	[24]
35	Compound 1 – HPMCP 55	C1-HPMCP 55	[25]
36	Fenofibrate – HPMC E5	FEN-HPMC E5	[26]
37	Fenofibrate – HPMCAS L	FEN-HPMCAS L	[26]

The * aims to differentiate among ASDs, from the same API-POL system; means that the API load and/or the *in vivo* animal model and/or the *in vivo* dose tested was different.

Alternatively, chemical databases and software tools available online, such as ChemSpider [27] and Molinspiration [28], were used to obtain the missing molecular descriptors for the APIs. The molecular descriptors for the POLs were mostly obtained through information provided by the suppliers and from the literature. There were other parameters common to the APIs and POLs, such as the total SPs that were estimated using the Fedors group contribution [29]. The number of #H-A and #H-D for the POLs were determined per monomer unit and then normalized to 100 MW [30].

Regarding the interaction parameters, these were included to evaluate whether the combined effect of a variable of the API and the POL correlate with the *in vivo* performance of ASDs. The interaction parameters considered were:

- the ratio between the MV of the POL and MV of the API (MV_{POL}/MV_{API});
- the ratio above but considering the number of moles (#mol) of each of the components, while considering the drug load in formulation $[(MV_{POL}/MV_{API}) * (\#mol_{POL}/\#mol_{API})]$;
- the difference between the total solubility parameters of the API and the POL (Delta SP);
- the number of all possible hydrogen bonds between the #H-A of the API and #H-D of the POL ($API\#H-A * POL\#H-D$);
- the number of all possible hydrogen bonds between the #H-D of the API and #H-A of the POL ($API\#H-D * POL\#H-A$);
- the sum of the latter interactions $[(API\#H-A * POL\#H-D) + (API\#H-D * POL\#H-A)]$;
- the number of all possible hydrogen bonds between the API and the POL together with all possible hydrogen bonds of the API-API and the POL monomer-monomer self-association $[[API\#H(A*D)] * [POL\#H(A*D)]]$.

The experimental data consisted of parameters gathered from the literature on ASDs, namely the API drug load in formulation, the dose of API given to the animal model to perform the *in vivo* studies, and *in vivo* PK parameters, such as AUC, C_{max} and t_{max} . To perform the analysis with “gaining-factors” the PK parameters were normalized by calculating the ratio between AUC_{ASD} , $C_{max, ASD}$ and $t_{max, ASD}$ obtained for the ASD and AUC_{ref} , $C_{max, ref}$, $t_{max, ref}$ obtained for the reference product (*e.g.* pure crystalline drug, drug-polymer physical mixture or commercial product). These values were further converted into a logarithmic scale, due to the large variance observed among observations. In the cases where the PK parameters were not tabulated in the respective references, these had to be taken from graphical data, using the Engauge Digitizer software [31]. There were also a few cases where a graphic was not available

and only the AUC values were reported. As such C_{\max} and t_{\max} were considered as missing values.

3.2.3 Statistical analysis

In order to extract correlations from the large dataset constructed, multivariate data analysis tools were used. The principal components analysis (PCA) and the partial least squares (PLS) method enable the reduction in size of the dataset, by creating new variables, known as principal components (PCs), which consist in linear combinations of the original variables. PCA and PLS models were developed using SIMCA-P+ 13.0 software (Umetrics, Sweden). All variables from the dataset were mean centered and scaled to unit variance before the effective analysis, in order to give variables equal weight.

A PCA was first performed in order to get an overview of the dataset. This overview helps to visualize whether the observations were well distributed or grouped together, to evaluate preliminary correlations between observations and variables, and to identify potential outliers. Outliers typically show up outside the 95% confidence interval/ellipse represented in the score plot [32]. The dataset included all molecular descriptors and experimental data, as PCA does not make any differentiation between independent and dependent variables. Figure 3.1 serves as good schematic representation of the dataset considered for the PCA analysis.

As a second stage of the analysis, PLS models were developed to find correlations between the molecular descriptors (independent variables or X-variables) and the *in vivo* PK parameters, namely $\log AUC_{\text{ratio}}$, $\log C_{\max, \text{ratio}}$ and $\log t_{\max, \text{ratio}}$ (dependent variables or Y-variables). The dataset was divided in a training set and a test set. The training set was used to calibrate the model, while the test set served to validate the latter. The test set corresponded to 1/3 of the number of observations [33], and was randomly selected within the range of the dataset. To assess the performance of the PLS model, statistical parameters such as the coefficient of determination (R^2) and the cross-validation parameter (Q^2) were considered. Q^2 is obtained from the cross-validation method, specifically the leave-1/7th-out default method of SIMCA-P. The optimal number of PCs of the PLS model was determined based on the maximization of both R^2 and Q^2 . Variable selection, or the elimination of non-important descriptors, was performed to maximize model performance, minimize prediction error, and avoid overfitting.

3.3 Results and Discussion

3.3.1 Dataset overview by Principal Components Analysis (PCA)

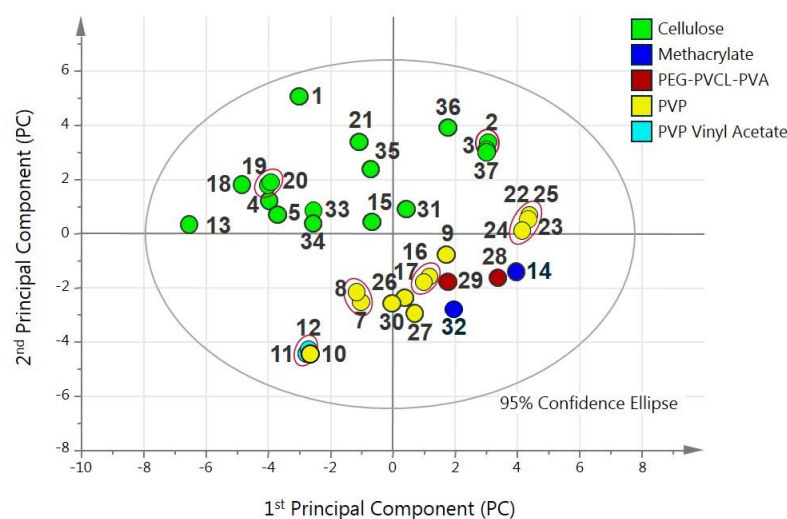
The result of a PCA is typically displayed graphically by means of two plots, *i.e.* the score and the loading plots. Both plots are complementary and should be analyzed simultaneously, in order to extract as much information as possible. While the score plot represents a summary of the correlations among observations (or ASDs), the loading plot displays the correlations among variables (*i.e.* molecular properties and experimental data) and may serve as a means to interpret the patterns in the score plot. The analysis of the score plot is also useful for the detection of outliers.

In a first PCA of the dataset, an outlier was identified. Observation #6 (*i.e.* TCL-HPMC E5) showed up outside the 95% confidence ellipse in the score plot (Figure B.1, in Supplementary Information B). The reason for this observation being an outlier was due to the API - Tacrolimus - that has certain molecular properties significantly different from the other APIs considered. This analysis was made via the contribution plot shown in Figure B.2, in Supplementary Information B. This ASD was then removed from the dataset and a new PCA generated.

The second PCA of the dataset, with two PCs, was capable of describing 44% of the total variance (R^2) in the dataset. Figure 3.2A shows the respective PCA score plot. As can be seen, no additional outliers were observed. The observations were colored according to the type of POL used to stabilize the amorphous drug. It can be observed different ASDs groups correspondent to the different POL classes. For example, ASDs that considered the methacrylate-based polymer Eudragit[®] E100 were located in the lower right quadrant, together with the ASDs based on Soluplus[®] and some based on PVP polymer. In contrast, in the lower left quadrant appeared the ASDs that used PVPVA as the polymer, while the upper left quadrant was exclusively populated with cellulose-based polymers.

Figure 3.2B shows the PCA loading plot that is complementary to the score plot. The variables were also colored, in this case according to the type of variable, *i.e.* molecular descriptors for the APIs, POLs, API-POL interactions and experimental variables.

A.



B.

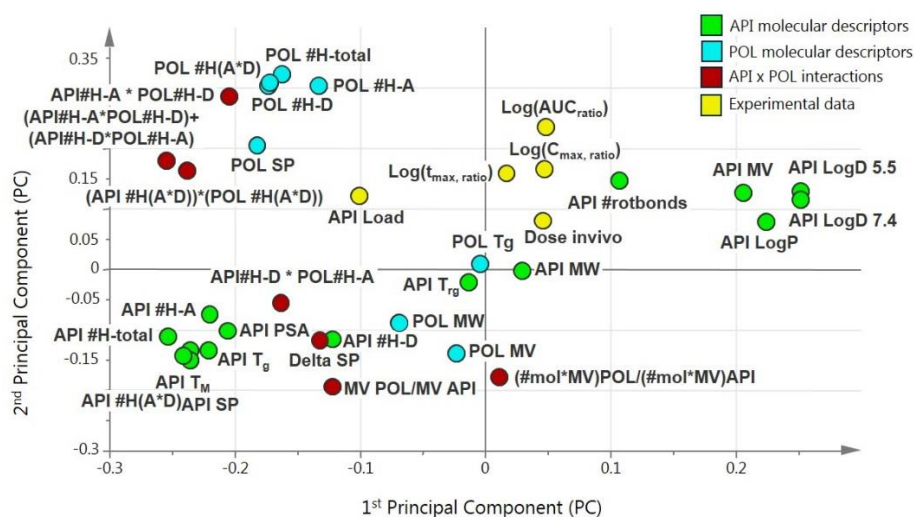


Figure 3.2. Score plot (A) and loading plot (B) of the two first PCs of the PCA dataset. In the score plot, each number identifies an ASD (Table 3.1); the color identifies the POL class, correspondent to the type of POL used to produce the ASD; observations identified with a red circle correspond to the ASDs identified with an asterisk (*) in Table 3.1. Loading plot: the color identifies the molecular descriptors correspondent to the APIs, POLs, APIxPOL interactions and experimental data taken from the literature.

Variables contributing with similar information were grouped together, which means that they were correlated. For example, the variables API log P and API log D at pH 5.5 and 7.4 that can be observed in the upper right quadrant, were grouped together for reflecting drug lipophilicity. Parameters describing the size of the APIs and POLs, such as MW and MV were also correlated. Correlated key parameters representing cohesive energy (*e.g.* API T_M , API SP and POL SP) appeared close to parameters representing the number of potential hydrogen bonds, namely API and POL #H-A, #H-D, #H-total, API PSA and interactions thereof. Among

the experimental variables, the *in vivo* PK parameters presented, as expected, higher correlation between each other, than the correlation with formulation-related parameters such as API load or *in vivo* dose. Moreover, PK parameters seem to be more correlated with API variables, than POL variables.

The distance of a variable (or group of variables) from the plot origin also provides insight on the impact of that variable on the PCA analysis. The higher the distance from the origin, the stronger the impact of that variable on the PCA. Most of the variables that were observed on the peripheral area of the plot were related with the number of possible hydrogen bonds and the API descriptors for lipophilicity.

The loading plot is also useful to understand the patterns shown in the score plot, since the position of the variables in the former links to the position of the observations in the latter. When comparing the loadings with the scores in Figure 2A, the correlation that stood out was that the number of possible hydrogen bonds was highly correlated with cellulose-based ASDs. In fact, polymers like HPMC, HPMCAS, HPMCP, are semi-synthetic macromolecules based on natural cellulose as the monomer unit, with varying degree of methyl and/or hydroxypropyl, acetate and/or succinate, and/or phthalate substitutions, respectively [34]. These groups possess high hydrogen bond acceptor and donor capability.

3.3.2 Finding correlations between molecular descriptors and ASDs *in vivo* performance using Partial Least Squares (PLS) modeling

After the preliminary analysis with PCA, from which it was possible to obtain a first overview of the dataset and identify outliers, a PLS model was developed in an attempt to establish correlations among the molecular descriptors and the *in vivo* responses (or Y-variables), namely $\log AUC_{\text{ratio}}$, $\log C_{\text{max, ratio}}$ and $\log t_{\text{max, ratio}}$. As it was observed that the Y-variables were relatively close to each other in the PCA loading plot (Figure 3.2A), meaning that a certain level of correlation exist among the latter, a PLS model with multiple responses was developed. Indeed, the strategy of modeling multiple correlated dependent variables should be considered not only because the correlations stabilize the model but also it provides a broader and simpler perspective than separate models for each response [32].

A first PLS model considering the three PK parameters (*i.e.* $\log AUC_{\text{ratio}}$, $\log C_{\text{max, ratio}}$ and $\log t_{\text{max, ratio}}$) was developed. The PLS yielded a one-component model, but with R^2 and Q^2 values significantly below the recommended guidelines for QSAR modeling, even after variable selection. In QSAR modeling, obtaining a R^2 and a Q^2 around 0.78 and 0.65

respectively is considered a good model [35]. Thus, a second PLS model considering only two PK parameters (*i.e.* $\log AUC_{\text{ratio}}$ and $\log C_{\text{max, ratio}}$) was developed. A two-component model with an R^2 of 0.7 and Q^2 of 0.5 was obtained after the variable selection. The accuracy and applicability of a predictive model is highly dependent on the quality of the dataset. Given the existing uncontrolled variability in the data - *in vivo* data obtained from disparate sources and different animal models - the PLS model obtained is considered adequate, at least, for interpretation purposes.

To further evaluate the model, Figure 3.3 shows the observed versus predicted plot obtained for each dependent variable, together with the predictions obtained for the external test set. The use of an independent test set of observations is often referred to as external validation as opposed to the internal validation, which corresponds to the method of cross-validation.

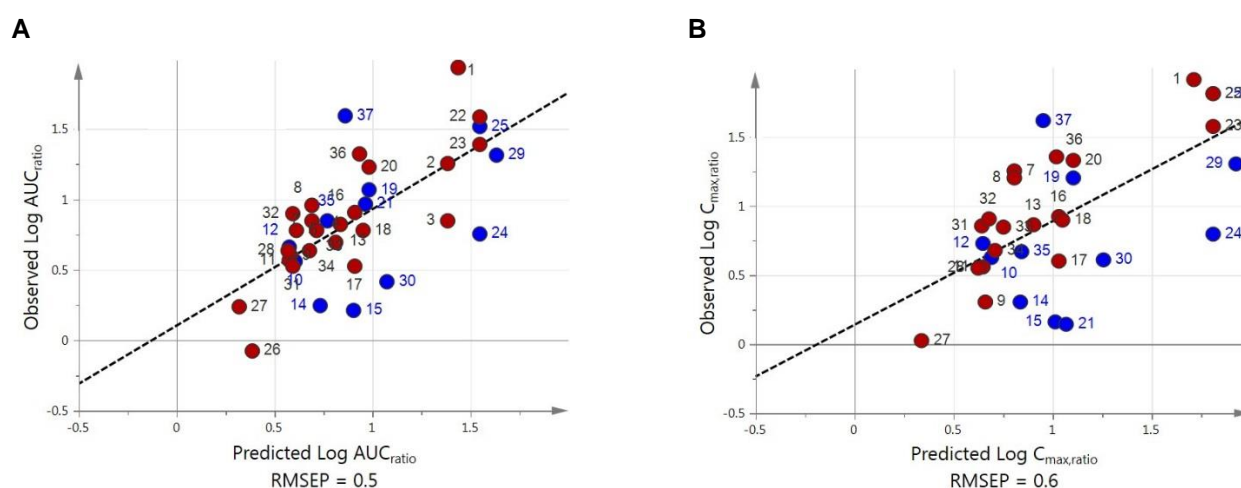


Figure 3.3. Observed data versus predicted data by the PLS model. A – $\log AUC_{\text{ratio}}$ response; B - $\log C_{\text{max, ratio}}$ response; training set (red circles); prediction set (blue circles). The numbers identify the ASDs (Table 3.1).

Ideally, the data should be close to and symmetrically distributed along the $y=x$ line. A higher correlation between the observed and predicted values was observed for the $\log AUC_{\text{ratio}}$ response when compared with $\log C_{\text{max, ratio}}$ response. In terms of the error of prediction (*i.e.* RMSEP in \log_{10} units) both models yielded similar values.

Figure 3.4A shows the loading plot for the two-component PLS model developed, and Figure 3.4B shows the variable importance plot (VIP), which shows the variables by descending order of influence in the model. The loading plot shows the relationships between the inputs and output variables simultaneously. Results from the loading plot can be interpreted as an

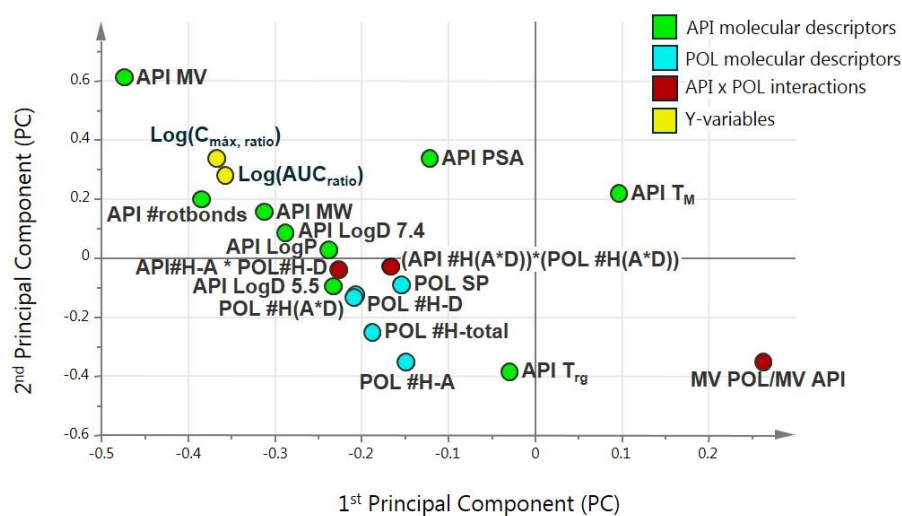
“optimization” exercise, *i.e.* we can evaluate which combination of independent variables may guide the production of an ASD with both high $\log C_{\max, \text{ratio}}$ and high $\log AUC_{\text{ratio}}$. In this respect, all variables projected on the left quadrants of the loading plot should be increased, and the ones that appeared diagonally opposite, should be decreased. According to the VIP plot in Figure 3.4B, the most important variables for the model included API-related molecular descriptors, followed by POL-related molecular descriptors and API-POL interaction variables.

This result was aligned with the fact that the global *in vivo* performance of an ASD is not only dependent on formulation-related parameters. The presence of the POL and its capacity to sustain supersaturation will only influence the drug absorption process. Besides absorption, there are other pharmacokinetic stages that highly influence the final performance, such as drug distribution and elimination. These processes are highly dependent on the drug physicochemical properties.

As can be seen in Figure 3.4B, API MV, API #rotbonds and API MW resulted as the top-3 variables with higher influence on the model. The positive strong correlation observed between these parameters and *in vivo* performance is somehow difficult to understand. On one hand, it is known that bioavailability is negatively related to molecular size, as it impacts membrane permeability, and on the other hand, reduced molecular flexibility was found to be an important predictor of oral bioavailability in rats [36]. Other API variables such as API $\log D$ and $\log P$, also presented positive influence on the model. Lipophilicity is known to be positively correlated with permeability for drugs that are absorbed by passive diffusion [37]. However, in this dataset there are certainly APIs whose absorption is not only mediated by passive diffusion, but also by active transport. API T_{rg} , API PSA and API T_{M} were the third group of API variables that were found to have a positive influence on the model. The API T_{rg} variable is related with glass stability and molecular mobility of the amorphous state. This variable may be related with *in vivo* performance in the sense that the higher the stability of the amorphous form, the lower the potential for drug precipitation and consequently higher exposure. API PSA and API T_{M} are also difficult to explain in the sense that molecules that are highly polar and with high lattice energy exhibit solubility- and permeability-limited absorption.

Among the POL variables, the ones that demonstrated higher influence on the model included POL #H-A and POL#H-total, followed by POL #H(A*D), POL #H-D, and POL SP as the polymer variable with lower influence.

A.



B.

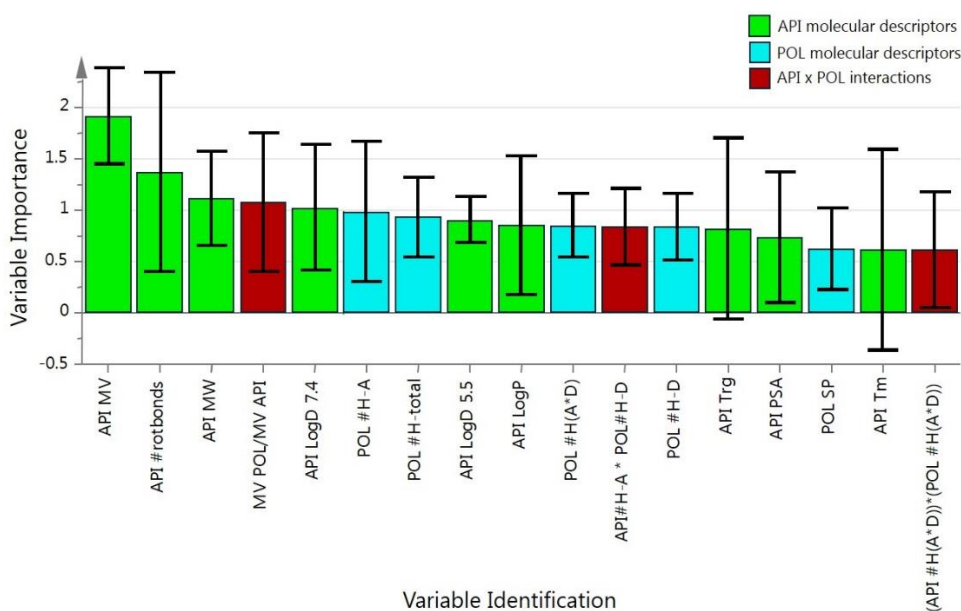


Figure 3.4. PLS loading plot (A) and correspondent variable importance plot (B). The color identifies the molecular descriptors correspondent to the APIs, POLs, API-POL interactions and dependent variables.

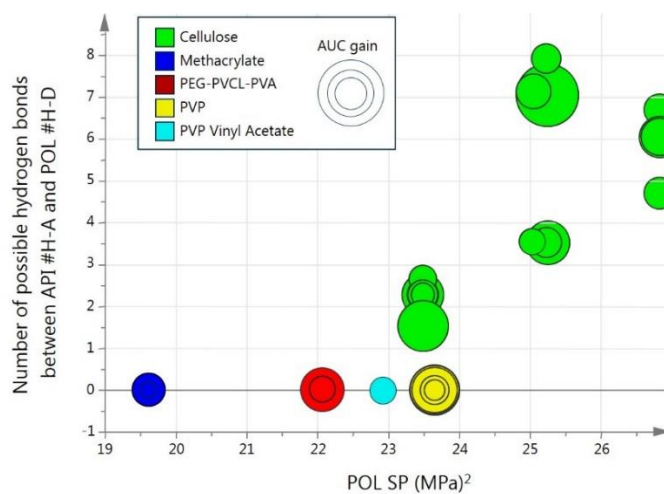
This result highlights the big influence of hydrogen bonding on ASDs performance. Still, one should not neglect the importance of other type of interactions, such as ionic interactions, that are not being captured in any of the molecular descriptors considered. Regarding the positive correlation of POL SP with *in vivo* ASDs performance. The SP gives an idea of the cohesive energy of a molecule, and according to Ilevbare *et al.*, the higher the SP of a POL the more hydrophilic it is [38]. Ilevbare *et al.* identified the POL SP as the most important variable to inhibit crystal growth of ritonavir in solution. The authors also stated that good

polymeric precipitation inhibitors should present a good hydrophilic/hydrophobic balance. POLs that are more hydrophilic (high SPs) would be expected to interact more favorably with the solvent molecules than with the API, while more hydrophobic polymers (low SPs) would have a higher tendency for self-association. This result remains to be fully elucidated.

Among the interaction variables, the one presenting the highest influence on the model was MV_{POL}/MV_{API} . The particularity of this variable was that it was the only one that appeared to negatively influence *in vivo* performance. MV_{POL}/MV_{API} was included as an interaction variable as a measure of the relative size of the POL to that of the API, and to evaluate whether this discrepancy in sizes would influence the performance. The result indicated that, the higher the MV of the POL to that of the API, the worse the *in vivo* performance. This seem to be counter-intuitive in the sense that, at a first glance, the greater the difference of API-POL size, the lower diffusion of the former in relation to the latter. Thus, the lower the diffusion of the API, higher polymeric stabilization, lower potential to recrystallize and higher *in vivo* performance. Other interaction variables such as $API \#H-A * POL \#H-D$ and $(API \#H(A*D)) * (POL \#H(A*D))$ presented a positive influence in the model. The former variable further emphasized the importance of hydrogen bonding for the optimization of performance, while the latter was an attempt to account for API and POL self-association and API-POL interaction at the same time. However, the interpretation of this variable is not straightforward.

Lastly, Figure 3.5 shows two scatter plots of two important variables for the model - $API \#H-A * POL \#H-D$ versus POL SP. The size of each point/observation corresponds to the $\log AUC_{ratio}$ and $\log C_{max, ratio}$, which can also be regarded as a “gaining-factor”. The observations were colored according to the POL class. The importance of hydrogen bonding for improving the *in vivo* performance of ASDs was in line with the observation that polymers with higher solubility parameters also tend to contribute for higher AUCs. In general, cellulose-based polymers (*i.e.* HPMCAS, HPMC, HPMCP) seem to provide better precipitation inhibition across different classes of APIs, when compared with other polymer families.

A.



B.

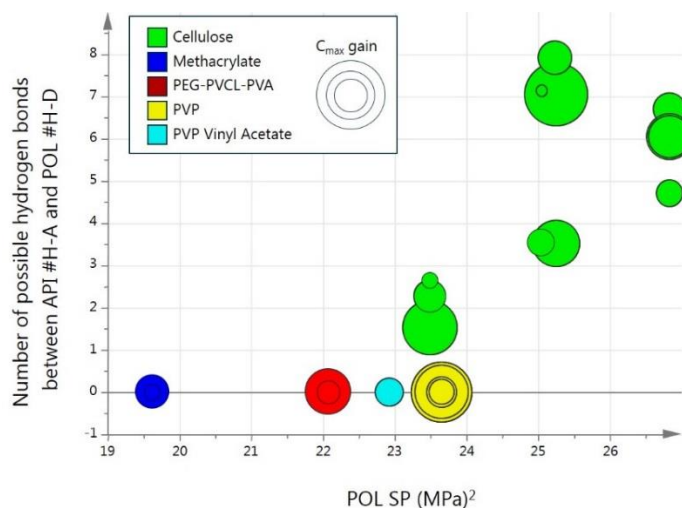


Figure 3.5. Scatter plots of two important variables for the model. The size of the points/observations represent the AUC (A) and C_{max} (B) gains. The colors represent the different POL classes.

3.4 Conclusions

In this work, multivariate data analysis was applied to assess correlations between molecular descriptors of the ASDs formulation ingredients and performance related output variables, namely AUC_{in vivo} and C_{max, in vivo}. Although the interpretation of some of the correlations obtained was not straightforward, it was possible to obtain general performance trends. It was found that hydrogen bonding capacity plays a key role in the optimization of ASDs performance and that cellulose-based polymers are general good precipitation inhibitors

among different APIs classes. Still, the accuracy of a predictive model is highly dependent of the size and diversity of the dataset and the quality of the molecular descriptors selected. By addressing some of these limitations in the future, it is believed that the model will become a useful computational tool for narrowing the polymers to be further explored, in terms of their capacity to improve amorphous dispersions *in vivo* performance. A proposed workflow demonstrating the implementation of this methodology is shown in Figure 3.6.

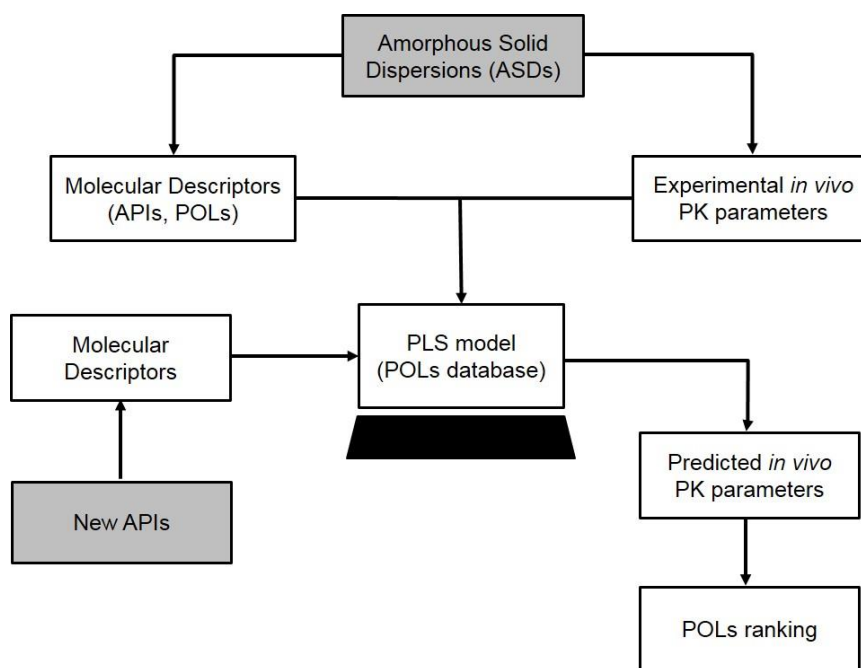


Figure 3.6. Workflow showing the application of the PLS model as a screening tool for development of amorphous systems.

3.5 References

- [1] T. Hou, Y. Li, W. Zhang, and J. Wang, "Recent Developments of In Silico Predictions of Intestinal Absorption and Oral Bioavailability" *Combinatorial Chemistry & High Throughput Screening*, vol. 12, pp. 497-506, 2009.
- [2] J. H. Fagerberg, E. Karlsson, J. Ulander, G. Hanisch, and C. A. S. Bergström, "Computational Prediction of Drug Solubility in Fasted Simulated and Aspirated Human Intestinal Fluid" *Pharmaceutical Research*, vol. 32, pp. 578–589, 2015.

- [3] D. Mahlin, S. Ponnambalam, M. H. Hockerfelt, and C. A. S. Bergstrom, "Toward In Silico Prediction of Glass-Forming Ability from Molecular Structure Alone: A Screening Tool in Early Drug Development" *Molecular Pharmaceutics*, vol. 8, pp. 498–506, 2011.
- [4] A. Alhalaweh, A. Alzghoul, W. Kaialy, D. Mahlin, and C. A. S. Bergström, "Computational Predictions of Glass-Forming Ability and Crystallization Tendency of Drug Molecules" *Molecular Pharmaceutics*, vol. 11, pp. 3123-3132, 2014.
- [5] M. Kuentz and G. Imanidis, "In silico prediction of the solubility advantage for amorphous drugs – Are there property-based rules for drug discovery and early pharmaceutical development?" *European Journal of Pharmaceutical Sciences*, vol. 48, no. 3, pp. 554-562, 2013.
- [6] M. D. Moore and P. L.D. Wildfong, "Informatics calibration of a molecular descriptors database to predict solid dispersion potential of small molecule organic solids" *International Journal of Pharmaceutics*, vol. 418, pp. 217-226, 2011.
- [7] I. Kushida, M. Ichikawa, and N. Asakawa, "Improvement of Dissolution and Oral Absorption of ER-34122, A Poorly Water-Soluble Dual 5-Lipoxygenase/Cyclooxygenase Inhibitor With Anti-Inflammatory Activity by Preparing Solid Dispersions" *Journal of Pharmaceutical Sciences*, vol. 9, no. 1, pp. 258-266, 2002.
- [8] D. T. Friesen *et al.*, "Hydroxypropyl Methylcellulose Acetate Succinate-Based Spray-Dried Dispersions: An Overview" *Molecular Pharmaceutics*, vol. 5, no. 6, pp. 1003-1019, 2008.
- [9] K. Yamashita *et al.*, "Establishment of new preparation method for solid dispersion formulation of tacrolimus" *International Journal of Pharmaceutics*, vol. 267, pp. 79-91, 2003.
- [10] G. M. Fakes *et al.*, "Enhancement of oral bioavailability of an HIV-attachment inhibitor by nanosizing and amorphous formulation approaches" *International Journal of Pharmaceutics*, vol. 370, pp. 167-174, 2009.
- [11] J. M. Vaughn, J. T. McConville, M. T. Crisp, K. P. Johnston, and R. O. Williams III, "Supersaturation Produces High Bioavailability of Amorphous Danazol Particles Formed by Evaporative Precipitation into Aqueous Solution and Spray Freezing into Liquid Technologies" *Drug Development and Industrial Pharmacy*, vol. 32, pp. 559-567, 2006.
- [12] N. Kondo *et al.*, "Improved Oral Absorption of Enteric Coprecipitates of a Poorly Soluble Drug" *Journal of Pharmaceutical Sciences*, vol. 83, no. 4, pp. 566-570, 1994.

- [13] H. He, R. Yang, and X. Tang, "In vitro and in vivo evaluation of fenofibrate solid dispersion prepared by hot-melt extrusion" *Drug Development and Industrial Pharmacy*, vol. 36, no. 6, pp. 681-687, 2010.
- [14] M. Kennedy *et al.*, "Enhanced Bioavailability of a Poorly Soluble VR1 Antagonist Using an Amorphous Solid Dispersion Approach: A Case Study" *Molecular Pharmaceutics*, vol. 5, no. 6, pp. 981-993, 2008.
- [15] J. P. Lakshman, Y. Cao, J. Kowalski, and A. T. M. Serajuddin, "Application of Melt Extrusion in the Development of a Physically and Chemically Stable High-Energy Amorphous Solid Dispersion of a Poorly Water-Soluble Drug" *Molecular Pharmaceutics*, vol. 5, no. 6, pp. 994-1002, 2008.
- [16] T. Kai, Y. Akiyama, S. Nomura, and M. Sato, "Oral Absorption Improvement of Poorly Soluble Drug Using Solid Dispersion Technique" *Chemical & Pharmaceutical Bulletin*, vol. 44, no. 3, pp. 568-571, 1996.
- [17] S. Onoue *et al.*, "Development of High-Energy Amorphous Solid Dispersion of Nanosized Nobiletin, a Citrus Polymethoxylated Flavone, with Improved Oral Bioavailability" *Journal of Pharmaceutical Sciences*, vol. 100, no. 9, pp. 3793-3801, 2011.
- [18] Y. Kubo *et al.*, "Enhanced Bioavailability of Probucof Following the Administration of Solid Dispersion Systems of Probucof–Polyvinylpyrrolidone in Rabbits" *Biological and Pharmaceutical Bulletin*, vol. 32, no. 11, pp. 1880-1884, 2009.
- [19] K. Kimura, F. Hirayama, H. Arima, and K. Uekama, "Effects of Aging on Crystallization, Dissolution and Absorption Characteristics of Amorphous Tolbutamide–2-Hydroxypropyl- β -cyclodextrin Complex" *Chemical & Pharmaceutical Bulletin*, vol. 48, no. 5, pp. 646-650, 2000.
- [20] G. F. Palmieri, F. Cantalamessa, P. Di Martino, C. Nasuti, and S. Martelli, "Lonidamine Solid Dispersions: In Vitro and In Vivo Evaluation" *Drug Development and Industrial Pharmacy*, vol. 28, no. 10, pp. 1241-1250, 2002.
- [21] H. Hardung, D. Djuric, and S. Ali "Combining HME & Solubilization: Soluplus® - The Solid Solution" *Drug Delivery Technology*, vol. 10, no. 3, pp. 20-27, 2010.
- [22] T. H. Tran *et al.*, "Development of raloxifene-solid dispersion with improved oral bioavailability via spray-drying technique" *Arch Pharmaceutical Research*, vol. 36, no. 1, pp. 86-93, 2013.

- [23] P.-C. Chiang *et al.*, "In Vitro and In Vivo Evaluation of Amorphous Solid Dispersions Generated by Different Bench-Scale Processes, Using Griseofulvin as a Model Compound" *The AAPS Journal*, vol. 15, no. 2, pp. 608-617, 2013.
- [24] I.-H. Beak and M.-S. Kim, "Improved Supersaturation and Oral Absorption of Dutasteride by Amorphous Solid Dispersions" *Chemical & Pharmaceutical Bulletin*, vol. 60, no. 11, pp. 1468-1473, 2012.
- [25] S. Lohani *et al.*, "Physicochemical Properties, Form, and Formulation Selection Strategy for a Biopharmaceutical Classification System Class II Preclinical Drug Candidate" *Journal of Pharmaceutical Sciences*, vol. 103, pp. 3007-3021, 2014.
- [26] M. Zhang *et al.*, "Formulation and delivery of improved amorphous fenofibrate solid dispersions prepared by thin film freezing" *European Journal of Pharmaceutics and Biopharmaceutics*, vol. 82, pp. 534-544, 2012.
- [27] ChemSpider Home Page. [Online]. "<http://www.chemspider.com/>"
- [28] Molinspiration Home Page. [Online]. "<http://www.molinspiration.com/>"
- [29] R. F. Fedors, "A method for estimating both the solubility parameters and molar volumes of liquids" *Polymer Engineering & Science*, vol. 14, no. 2, pp. 147-154, 1974.
- [30] D. B. Warren, C. A. S. Bergstrom, H. Benameur, C. J. H. Porter, and C. W. Pouton, "Evaluation of the Structural Determinants of Polymeric Precipitation Inhibitors Using Solvent Shift Methods and Principle Component Analysis" *Molecular Pharmaceutics*, vol. 10, no. 8, pp. 2823-2848, 2013.
- [31] Engauge Digitizer Home Page. [Online]. "<http://digitizer.sourceforge.net/>"
- [32] L. Eriksson, T. Byrne, E. Johansson, J. Trygg, and C. Vikstrom, *Multi- and Megavariate Data Analysis - Basic Principles and Applications*, 3rd edition. Malmö, Sweden, MKS Umetrics AB, 2013.
- [33] T. Næs, T. Isaksson, T. Fearn, and T. Davies, *A User-Friendly Guide to Multivariate Calibration and Classification*, Chichester, UK, NIR Publications, 2002.
- [34] A. Paudel, Z. A. Worku, J. Meeus, S. Guns, and G. Van den Mooter, "Manufacturing of solid dispersions of poorly water soluble drugs by spray drying: Formulation and process considerations" *International Journal of Pharmaceutics*, vol. 453, no. 1, pp. 253-284, 2013.

- [35] SIMCA–P and Multivariate Analysis - Frequently Asked Questions (F.A.Q.) [Online]. http://umetrics.com/sites/default/files/kb/multivariate_faq.pdf
- [36] D. F. Veber *et al.*, "Molecular Properties That Influence the Oral Bioavailability of Drug Candidates" *Journal of Medicinal Chemistry*, vol. 45, pp. 2615-2623, 2002.
- [37] C. A. S. Bergström, W. N. Charman, and C. J.H. Porter, "Computational prediction of formulation strategies for beyond-rule-of-5 compounds" *Advanced Drug Delivery Reviews*, 2016, In Press.
- [38] G. A. Ilevbare, H. Liu, K. J. Edgar, and L. S. Taylor, "Understanding Polymer Properties Important for Crystal Growth Inhibition - Impact of Chemically Diverse Polymers on Solution Crystal Growth of Ritonavir " *Crystal Growth & Design*, vol. 12, no. 6, pp. 3133-3143, 2012.

Chapter 4

The results described in this chapter have been published total or partially in the following communications:

- I. Duarte, M. L. Corvo, P. Serôdio, J. Vicente, J. F. Pinto and M. Temtem, “Production of nano-solid dispersions using a novel solvent-controlled precipitation process - benchmarking the *in vivo* with an amorphous micro-sized solid dispersion produced by spray drying” *European Journal of Pharmaceutical Sciences*, vol. 93, pp. 203-214, 2016.
- 1 international conferences as an oral communication;
- 4 international conferences as a poster communication.

Authors' contribution:

I.D. was involved in the conception, design, production and analysis of data. I.D. wrote the manuscript and is leading the revision of the article particularly on proposing the journal's reviewers questions and comments.

4 Production of nano-solid dispersions using a novel solvent-controlled precipitation process – benchmarking their *in vivo* performance with an amorphous micro-sized solid dispersion produced by spray drying.

4.1 Introduction

The focus of this work was the development of alternative, reproducible and cost-effective co-precipitation processes, suitable to produce ASDs with unique characteristics. In this regard, a novel SCP process that uses microreaction or microfluidization to fine control supersaturation and precipitation was assessed. This technology involves high shear, continuous fluid processing through a fixed geometry microreactor that provides intense and uniform micro- to nanomixing [1]. Considering that critical process parameters of the SCP process include mixing time and temperature, the micro/nano mixing provided by the micron-sized channel diameter of the microreactor, not only minimizes diffusion limitations between the solvent and anti-solvent streams, thus significantly-reducing mixing times, but also provides excellent heat exchange, due to the large surface-to-volume ratio. This system when compared with the use of high shear mixers enables the generation of nano to microparticles in a single passage through the microreactor, with a greater control over the particle size distribution, as well as a greater solid-state stability of the particles produced. The possibility of producing nanoparticles by microfluidization leads consequently to an increase of the specific surface area, which is also an advantage in terms of dissolution rate.

This work was divided in two main parts. First, a half-factorial experimental design was conducted to study the effect of formulation variables (*viz.* polymer type, drug load, and feed solids' concentration) on typical critical quality attributes (CQAs) of solid dispersions, namely particle size/morphology and drug's solid state and drug's molecular distribution within the carrier. Six different suspensions were produced using the SCP process presented, following by spray drying to isolate the particles from the liquid medium. As the second part of the work, the drug-polymer system that demonstrated higher flexibility in terms of its capacity to form both amorphous and crystalline solid dispersions, under the formulation and process conditions tested, was pursued for *in vitro* dissolution and *in vivo* bioavailability evaluation, as well as long-term stability evaluation. For benchmarking purposes, an ASD of this exact formulation was also produced by spray drying and tested. Carbamazepine (CBZ) was selected as the model drug to conduct this feasibility study. CBZ is categorized as BCS Class II or more specifically

Class IIa, according to the recent Developability Classification System (DCS) [2]. DCS Class IIa compounds present dissolution-rate limited absorption.

4.2 Materials and Methods

4.2.1 Materials

4.2.1.1 Chemicals

Crystalline carbamazepine (CBZ, anhydrous Form III, purity > 97%) was purchased from TCI Co., Ltd. (Tokyo, Japan). Two commercially available polymers with different chemical and physical properties were selected: 1:1 methacrylic acid and methyl methacrylate co-polymer (Eudragit[®] L100, Evonik Röhm GmbH, Darmstadt, Germany) and hydroxypropylmethylcellulose acetate succinate (HPMCAS grade MG, AQOAT[®], Shin-Etsu Chemical Co., Ltd., Tokyo, Japan). The solvent and anti-solvent used were methanol (MeOH) and deionized water, both of analytical grade.

4.2.1.2 Animals

Adult CD1 female mice (22-24 g) were purchased from Charles River (Barcelona, Spain). Animals were fed with standard laboratory food and water *ad libitum*. All animal experiments were carried with the permission of the local animal ethical committee, and in accordance with the Declaration of Helsinki, the EEC Directive (2010/63/UE) and Portuguese Law (DL 113/2013, Despacho n° 2880/2015), and all following legislation for usage of animals in research.

4.2.2 Methods

4.2.2.1 Design of experiments (DoE)

A half-factorial design 2^{3-1} plus 2 central points conducted to study the effect of formulation variables on critical quality attributes (CQAs) of solid dispersions produced through an alternative SCP process are described in Table 4.1 and Figure 4.1. The formulation variables and ranges studied were: the type of polymeric stabilizer (Eudragit[®] L100 or HPMCAS-MG), the drug load in the solid dispersion (20 to 60 wt.%), and the feed solids

concentration (C_{feed} , 2 to 8 wt.%). The CQAs evaluated were: solid-state and physical stability (upon preparation and 30 and 90 days under stress storage conditions), particle size and morphology, *in vitro* dissolution and *in vivo* bioavailability.

Table 4.1. Experimental design for the SCP study.

Exp. Number	Polymer Type	Drug load (wt.%)	Feed solids' concentration (C_{feed} / wt.%)
1	HPMCAS-MG	20	2
2	HPMCAS-MG	40	5
3	HPMCAS-MG	60	8
4	Eudragit® L100	20	8
5	Eudragit® L100	40	5
6	Eudragit® L100	60	2

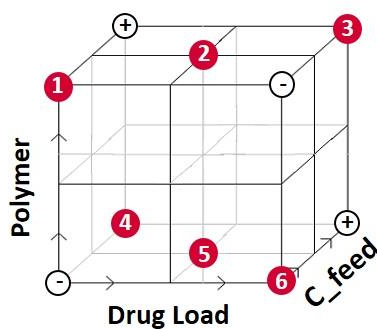


Figure 4.1. Representation of the experimental design for the SCP process study.

4.2.2.2 Solvent controlled precipitation (SCP) process

Six solutions of CBZ and each polymer were prepared in MeOH (solvent) for a total weight of solids of 3 g. The weight proportion between the components and the solids concentration in solution are described in Table 4.1. As anti-solvent, a mass of deionized water corresponding to 10 times that of the solvent was used. The water was acidified until pH=2 using a 37 wt.% hydrochloric acid solution and its temperature was maintained around 5 °C, for the lowest solubility of both components.

Solvent controlled precipitation (SCP) experiments were undertaken using PureNano™ Microfluidics Reaction Technology (MRT, CR5 Reactor model) whose setup is schematically represented in Figure 4.2. The solvent and anti-solvent streams were fed to an intensifier pump at individually controlled rates. The intensifying pump was set to impose a pressure of approximately 1379 bar (20 kPsi, maximum processing pressure). While the anti-solvent stream

was gravity fed, the peristaltic pump of the solvent reservoir was set to maintain a ratio of 1:10 of solvent and anti-solvent (~ 50 mL of solvent/min). Then, both streams were pressurized in a combined stream within the intensifier pump, and delivered to an interaction chamber with 75 μm diameter reaction channels (F20Y) followed by an auxiliary processing module with 200 μm diameter reaction channels (H30Z). After the interaction chamber, the suspension passed through a heat exchanger (ice water bath). One single passage through the processor was considered for all experiments. Following this process step, the suspensions were dried in a lab-scale spray dryer, for particle collection.

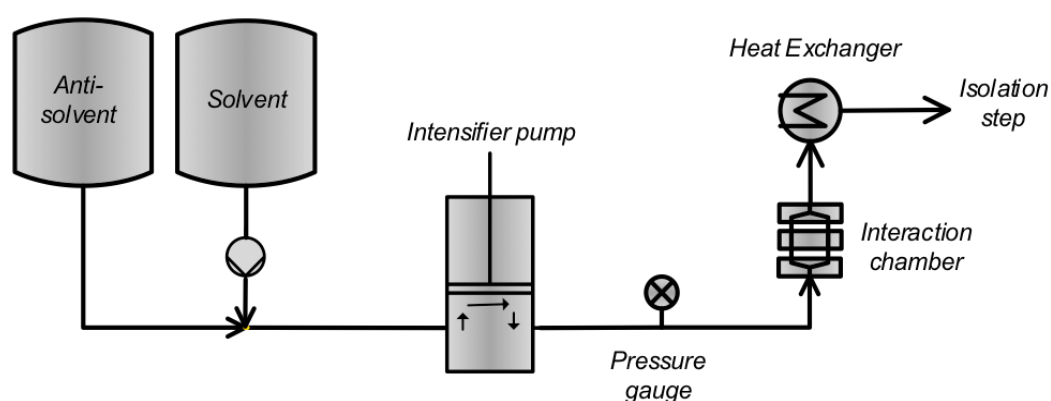


Figure 4.2. Representation of the solvent/anti-solvent controlled precipitation process, followed by the isolation step in a spray dryer.

4.2.2.3 Spray drying

A laboratory scale spray dryer (BÜCHI Mini Spray Drier B-290, Switzerland), equipped with a two fluid nozzle, was used to dry (1) all the suspensions produced by SCP and (2) a 20 wt.% CBZ: Eudragit[®] L100 homogenous solution, at 8 wt.% solids concentration. In both situations the unit was operated in open cycle mode, *i.e.* without recirculation of the drying gas. Before feeding the suspensions/solution to the nozzle, the spray dryer was stabilized with nitrogen to assure stable inlet and outlet temperatures (T_{in} and T_{out} , respectively). In the case of the suspensions produced by SCP the temperatures were optimized to dry a water suspension ($T_{\text{in}}=156$ °C, $T_{\text{out}}=80$ °C), while for the SD of the solution the temperatures were set to dry a methanolic solution ($T_{\text{in}}= 65$ °C and $T_{\text{out}}=40$ °C). After stabilization, the suspensions/solution were fed to the nozzle by means of a peristaltic pump ($F_{\text{feed}}=0.81$ kg/h), and atomized at the nozzle's tip (atomization nitrogen, $F_{\text{atom}}=1.4$ kg/h). The suspensions were kept under magnetic stirring, during spray drying. The droplets were then dried in the spray drying chamber by a co-current nitrogen stream ($F_{\text{drying}}=40$ kg/h). The stream

containing the dried particles was directed into a cyclone and collected at the bottom. The collected powders were post-dried in a tray dryer oven under vacuum at 45 °C for approximately 12 h.

4.2.2.4 Modulated differential scanning calorimetry (mDSC)

Thermal analysis experiments were performed in a TA Q1000 (TA Instruments, New Castle, Delaware, USA) equipped with a refrigerated cooling system after calibration with indium. The samples were analyzed in pinholed DSC aluminum pans and under continuous dry nitrogen purge (50 mL/min). Samples, weighing between 5 to 10 mg, were analyzed using a modulated heating ramp from -10 °C to 250 °C at a heating rate of 2 °C/min using a period of 60 s and an amplitude of 0.32 °C.

Data was analyzed and processed using the TA Universal Analysis 2000 Software (TA Instruments, New Castle, Delaware, USA). The glass transition temperature (T_g) was taken as the inflection point in the heat capacity change (ΔC_p) observed in the reversible heat flow, while exothermic and endothermic peaks were identified in the non-reversible and total heat flows.

4.2.2.5 X-ray powder diffraction (XRPD)

XRPD experiments were performed in a D8 Advance Bruker AXS $\theta/2\theta$ diffractometer with a copper radiation source (Cu $K\alpha$, wavelength = 1.5406 Å), voltage 40 kV, and filament emission 35 mA. The samples were measured over a 2θ interval from 3 to 70° with a step size of 0.017° and step time of 50 s.

4.2.2.6 Scanning Electron microscopy (SEM)

To obtain the micrographs, samples were attached to adhesive carbon tapes (Ted Pella Inc., CA, USA), previously fixed to aluminum stubs where the powder in excess was removed by a jet of pressurized air. The samples were left in vacuum for 2 hours and then coated with gold/palladium (South Bay Technologies, model E5100, San Clement, CA). A JEOL JSM-7001F/Oxford INCA Energy 250/HKL scanning electron microscope (JEOL, Tokyo, Japan) in high vacuum operated at a typical accelerating voltage of 15 – 20kV. Micrographs were taken at various magnifications, ranging from 1500x up to 40,000x.

4.2.2.7 Particle size

The particle size of the dried powders, expressed as the mean circular diameter, was determined by image analysis using the ImageJ software (National Institute of Health, Bethesda, MD, USA) from around 200 randomly selected particles, which demonstrated a normal distribution of sizes. The parameter “circular diameter” is the diameter of a circle having the same area of the manually selected particle in the SEM image.

4.2.2.8 Surface area determination

The specific surface area of the samples was determined using an ASAP 2000 equipment (One Micromeritics Drive, Norcross, GA, USA). A six-point Brunauer-Emmett-Teller (BET) method from the nitrogen adsorption analysis was performed after degassing the samples with helium (purity >99,5%) until a stabilized absolute vacuum below 15 μm of mercury at 25°C was reached. Sample weight after degassing was around 200 mg. The adsorbate used was nitrogen (purity >99.9%) and the specific surface area was determined in the relative pressure (P/P_0) range of 0.05 to 0.30, with an equilibration time of 5 sec, allowing the determination of pore diameters between 300 nm to 1.7 nm.

4.2.2.9 Evaluation of the stability of the amorphous powders

Samples were placed in open Petri dishes at 25°C/60% RH and 40°C/75% RH. To create these storage conditions, glass desiccators with oversaturated salt solutions were prepared and conditioned at the desired temperatures (tray dryer oven and room temperature). Samples were removed and analyzed by XRPD after 30 and 90 days after storage.

4.2.2.10 High performance liquid chromatography (HPLC)

The quantification of CBZ was performed using a Waters HPLC system (model 2695) with a dual wavelength absorbance detector (model 2487) (Waters, Milford, MA, USA). The column used was a Zorbax[®] XDB - C18 (4.6 mm \times 150 mm, 3.5 μm) and the mobile phase was a 60:40 vol.% of methanol and water. The injection volume was 10 μL and the isocratic flow rate was maintained constant at 1 mL/min. The CBZ UV absorbance was measured at $\lambda=285$ nm. The temperature of the column was maintained at 25°C. The chromatographs were collected and the areas under the peaks integrated using Empower Version 2.0 (Waters, Milford, MA, USA).

4.2.2.11 Drug content in solid dispersions

The drug content in the solid dispersions that were considered for *in vitro* dissolution and *in vivo* bioavailability were assayed according to the HPLC method described in Section 4.2.2.10. Concentrated stock solutions of the respective solid dispersions in MeOH were prepared. Standard solutions with a target CBZ concentration of 10 µg/mL were prepared by diluting an aliquot of each concentrated stock solution in MeOH prior to analysis. The quantification was performed against a single-point external standard of pure CBZ in MeOH (10 µg/mL).

4.2.2.12 *In vitro* dissolution studies

Powder dissolution profiles were obtained using a microcentrifuge dissolution method [3,4]. The experiments were conducted in 2 mL microcentrifuge tubes in a 37°C temperature water bath. The simulated gastric phase consisted of 0.9 mL of 0.01 N HCl (pH=2) and the simulated intestinal phase consisted of an additional volume of 0.9 mL of FaSSIF biorelevant media (pH=6.5) (Biorelevant.com, Croydon, Surrey, UK). Both media were degassed and preheated to 37 °C prior to use. The dissolution experiments were performed with a target drug load of 850 µg of CBZ, which corresponded to approximately 5 and 2 times the concentration at equilibrium of CBZ in the gastric and intestinal phases, respectively. Samples were taken at various time points (10, 20, 35, 60, 90, 150 and 180 min) with no dissolution medium replacement. The pH-shift occurred at the 50-min time point. The preparation of the test tubes for sampling consisted of removing the latter from the water bath and centrifuged using a Himac Microcentrifuge CT15RE (Hitachi Koki Co, Ltd, Tokyo, Japan) for 1 min at 13,000 rpm. Then, 25 µL of the supernatant was aliquoted, but only 10 µL was diluted 15-fold in methanol in a HPLC vial with low volume insert (150 µL). The solutions remaining in the test tubes were vortexed for a few seconds until total redispersion of the sediments was observed. The test tubes were placed back in the water bath until the next time point.

The amount of drug in the samples was measured by HPLC according to the method described in Section 4.2.2.10, against a single-point external standard of pure CBZ in 1:15 v/v FaSSIF:MeOH (20 µg/mL).

The area under the dissolution curves (AUCs) for the total dissolution tests was calculated by the linear trapezoidal method.

4.2.2.13 *In vivo* pharmacokinetic studies

On the day of administration, the animals were fasted for approximately 6 h before the beginning of the experiments. This period was considered sufficient for the emptying of the stomach of mice [5]. The mice were dosed by oral gavage with an equivalent amount of each formulation to provide 7.4 mg/kg body weight of CBZ (n=3, except otherwise stated). The vehicle was acidified water (0,01N HCl, pH~2) and the concentration of the suspension was adjusted in such way that an appropriate dose was present in 0.35 mL of the suspension. By an appropriate dose means a dose not too low which will then impact with drug detection, but not excessively high in order to have a homogenous suspension for administration. Moreover, being the stomach capacity of a mouse approximately 0.4 mL, 0.35 mL was considered an ideal oral dosage volume to not overload the stomach capacity and/or avoid reflux into the esophagus [6]. The time interval between suspension preparation and dose administration was around 30 s. After administration, mice were kept in restraining cages, with free access to water.

Blood samples (~ 1 mL) were collected from the orbital sinus at 2, 5, 10, 15, 30, 45, 60, 120 and 180 min post administration. The blood samples were centrifuged, and the serum samples were refrigerated until the assay.

4.2.2.14 Bioanalytical method

The concentration of CBZ in the serum was assayed using an IMMULITE 2000[®] XPi Immunoassay System (Siemens Healthcare Diagnostics, Erlangen, Germany). This system combines chemiluminescence and immunoassay reactions (*i.e.* solid-phase, competitive chemiluminescence enzyme immunoassay). The assay is based on the measurement of light emission produced by dephosphorylation of a substrate, which is directly conjugated to the drug in the sample. Thus, the light produced by the reaction is proportional to the amount of drug in the sample. The lower limit of quantification (LOQ) of the immunoassay method was 1.25 µg/mL.

4.2.2.15 CBZ extraction of serum samples

Pre-selected serum samples with an amount of drug below the LOQ of the bioanalytical method described above were treated by a liquid-liquid extraction method and assayed by HPLC (Section 4.2.2.10).

Aliquots of serum were transferred to 2 mL microcentrifuge tubes. Methanol in a ratio of 1:4 v/v was then added to each tube and vortex mixed for 5 min. White-opaque solutions

were formed due to precipitation of water-soluble proteins. The samples were then centrifuged using a Himac Microcentrifuge CT15RE (Hitachi Koki Co, Japan) at 2,000 rpm for 5 min. The supernatants were extracted and directly transferred to HPLC vials with low volume inserts (150 μ L). The quantification was performed against a single-point external standard of pure CBZ in MeOH (1 μ g/mL) that was prepared from dilution of a more concentrated stock standard (1 mg/mL of CBZ).

The average yield of extraction when applying the extraction method to samples with CBZ, *i.e.* samples that were above the LOQ of the immunoassay method, was around 60%.

4.3 Results and Discussion

4.3.1 Part I - Experimental Design

This study proposes an alternative SCP process (Figure 4.2) based on microfluidization to produce solid dispersions.

In the first part of this work, six spray-dried co-precipitated powders were obtained and were characterized in terms of particle size and morphology as well as the drug's solid state and molecular distribution within the carrier.

4.3.1.1 Particle size and morphology of the spray-dried co-precipitated particles

The SEM results obtained for the different spray-dried co-precipitated products according to the DoE conducted (Figure 4.1) are present in Figure 4.3.

Spherical particles were generally obtained among all the formulations tested. These results were expected as spray drying was the technology chosen to isolate the particles in suspension, after co-precipitation [7,8].

When analyzing the particles at higher magnifications, the observation of the surface of the particles revealed that the latter were aggregates of individual particles, most of them within the submicron range and with a mean circular diameter around 100 nm. These results lead us to two important conclusions: first, the final suspensions obtained after the SCP process were nanosuspensions, that following drying aggregated as nano-composite particles; second, these nanoparticles were compact, while *e.g.* the microparticles of vemurafenib produced via SCP using high shear mixing were highly porous, meaning that the thermodynamics of mixing

between the components (*i.e.* drug-polymer-solvent-anti-solvent) and the kinetics of precipitation played a major role in the type of particulate structure obtained.

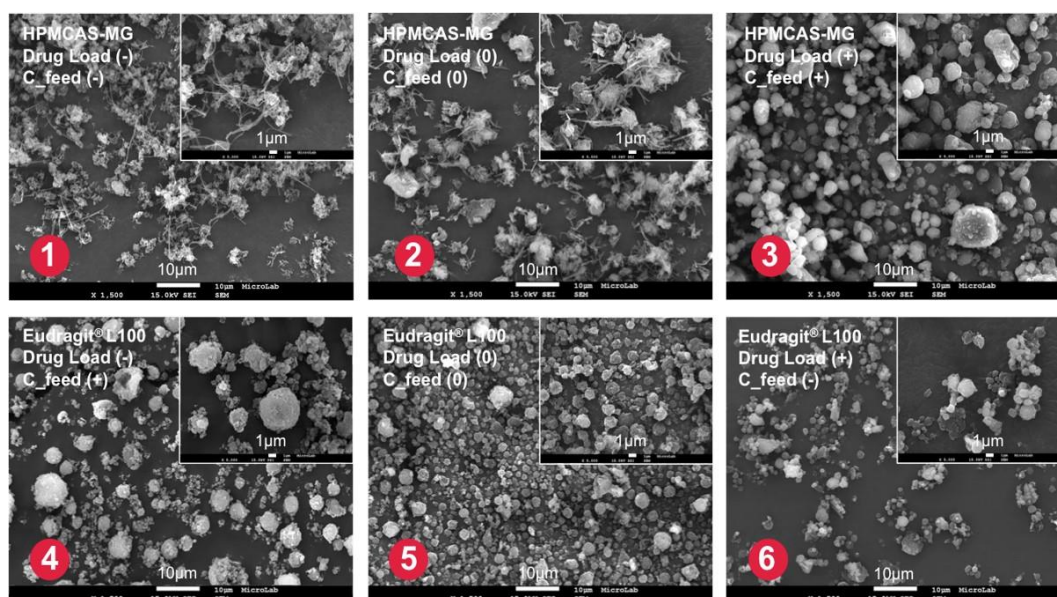


Figure 4.3. SEM micrographs corresponding to Tests 1, 2, 3 and Tests 4, 5, 6 of the DoE conducted. The micrographs on the back were taken at 1500x magnification, while the inserts were taken at 5000x magnification.

In fact, and as far as liquid-liquid demixing of polymeric solutions is concerned, whether precipitation occurs via nucleation and growth or spinodal decomposition, different co-precipitated structures can be obtained [9,10]. For example, precipitation path A typically results in porous structures (Figure 4.4), due to the nucleation and growth of droplets of polymer-poor phase in a polymer-rich phase. By opposition, in case of precipitation path B, nucleation and growth of droplets of the polymer-rich phase in a polymer-poor phase occurs. Particulate structures are typically obtained when following this path.

It was also interesting to observe that these submicron particles obtained from the two CBZ-based formulations tested presented different shapes which were more pronounced for lower drug loads. For instance, when comparing the images of Tests 1 and 4, the former demonstrated more filamentous-like particles entangled with spherical particles, while the latter showed a higher number of spherical aggregates composed of easily distinguishable nanoparticles. Possible reasons for these differences may be related with the different precipitation paths followed in the ternary diagram as previously explained and/or the presence of crystalline material in the CBZ: HPMCAS-MG samples, according to the solid-state and physical stability results, demonstrated in the following Section 4.3.1.2.

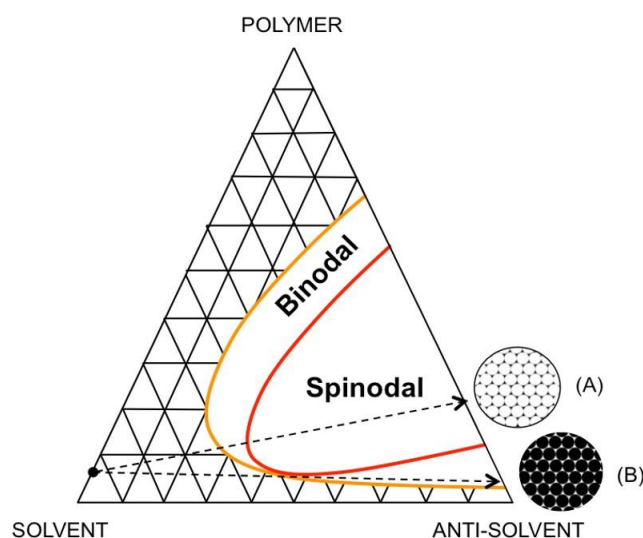


Figure 4.4. Representation of a hypothetical ternary phase diagram for the system polymer-solvent-anti-solvent, indicating two possible precipitation paths (A and B) and respective polymeric structures obtained.

When increasing the drug load of both formulations, *i.e.* from 20% to 40% and then 60% of CBZ, it was observed that particle aggregation between nanoparticles increased from Tests 2 and 5 and then Tests 3 and 6, leading to the overall reduction of the surface area-to-volume ratio of the co-precipitated particles produced. Indeed, aggregation of nanoparticles during the isolation step, either using spray drying or freeze-drying, is a major concern reflected in the literature [7,11,12]. If nanoparticles form aggregates, this may compromise the redispersibility of these powders upon contact with the aqueous medium, thus neglecting the dissolution-rate gain and ultimately the enhancement of the bioavailability. The results obtained suggested that the level of aggregation was mainly dependent on the drug load in formulation or, in other words, in the amount of polymeric stabilizer presented. This again links with the mechanisms of nucleation and growth of polymer-poor and polymer-rich phases, as explained above. Moreover, this result is aligned with the findings in the literature, which describe as important formulation variables to overcome drying induced aggregation the addition of one or more stabilizers to the suspension before the drying step [7,13], the type of stabilizer selected (*i.e.* ionic *versus* non-ionic, leading to electrostatic *versus* steric stabilization) [7,14], the distribution of the stabilizer in the formulation (*i.e.* surface adsorption *versus* matrix distribution) [15,16], and the concentration of the stabilizers [17,18].

In this work, no significant differences in the aggregation level were observed among the polymers tested, apart from the observation of the filamentous-like particles in the CBZ: HPMCAS-MG co-precipitated powders. Both HPMCAS-MG and Eudragit® L100 are ionic polymers, so can be suggested that electrostatics contributed to the stabilization of the

nanoparticles while in the liquid medium. According to Thorat and Dalvi, in the electrostatic stabilization mechanism, charged stabilizers cause repulsion between particles due to similar charges on particle surface, thus leading to the prevention of aggregation [19].

Feed solids' concentration (C_{feed}) in solution demonstrated to have no effect on the level of aggregation, as when analyzing the results of Tests 1 and 6 and Tests 4 and 3, which represent the extreme cases in terms of aggregation, these were run at the same C_{feed} .

The mean circular diameter results obtained for the different spray-dried co-precipitated products are present in Figure 4.5. The mean circular diameter of the aggregated particles ranged between 1.14 and 4.58 μm for all the tests performed. However, differences in particle size were observed between Tests 1, 2, 3 and Tests 4, 5, 6. In general, from Test 1 to Test 3 an increasing number of particles with a larger diameter was observed, while from Test 4 to Test 6 it was observed a progressive increase in the number of particles with a reduced diameter. The tendencies of the results obtained demonstrated that the particle size of the spray dried co-precipitated powders was mainly dependent on the feed solids' concentration in solution, as from Test 1 to Test 3 the C_{feed} increased from 2% to 8%, and from Test 4 to Test 6 the C_{feed} decreased from 8% to 2%. To our best knowledge, no correlations between the C_{feed} of the initial solution prepared for the co-precipitation process and the particle size of the final spray dried aggregates have been made in previous research described in the literature.

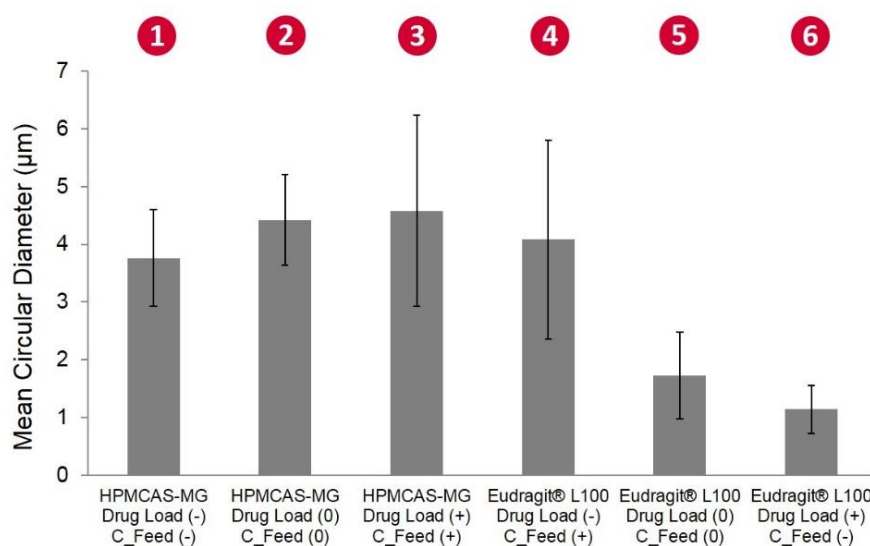


Figure 4.5. Mean circular diameter results correspondent to Tests 1, 2, 3 and Tests 4, 5, 6 of the DoE conducted. The bars represent the standard deviation.

4.3.1.2 Drug's solid-state and molecular distribution within the co-precipitated particles

Regarding the drug's solid-state and molecular arrangement of the six spray-dried co-precipitated materials produced, these were characterized by XRPD analysis, to evaluate the presence of crystalline material, and by mDSC, to evaluate the glass transition temperature (T_g) and phase separation phenomena. Amorphous phase separation was defined based on the detection of two T_g 's corresponding to the pure components, whereas the detection of a single T_g value between the T_g 's of the pure components corresponded to the formation of an amorphous and homogeneously mixed system (*i.e.* glass solution). Figure 4.6 shows the XRPD diffractograms obtained for the different spray dried co-precipitated products. The data associated with the mDSC analysis is available as Supplementary Information C (Table C.1).

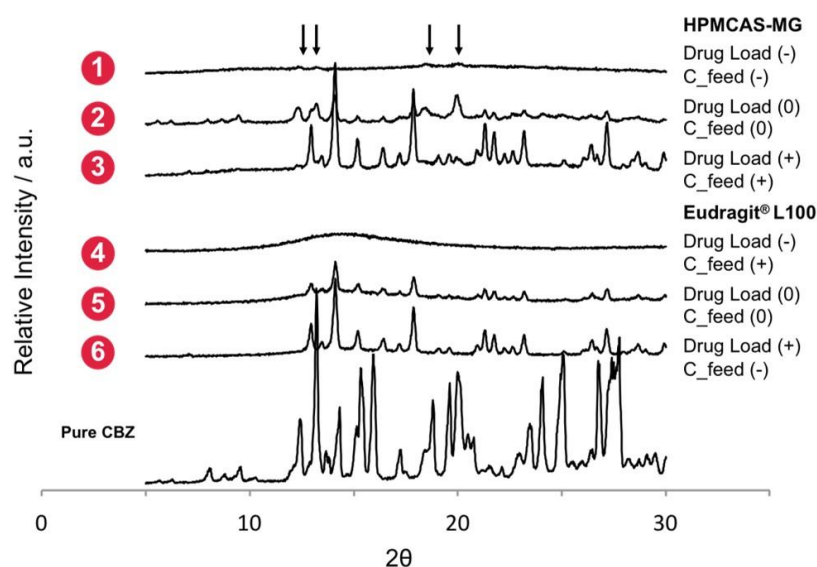


Figure 4.6. Powder diffractograms correspondent to Tests 1, 2, 3 and Tests 4, 5, 6 of the DoE conducted. The arrows indicate crystalline peaks with reduced intensity.

Differences in the drug's solid state and drug's molecular arrangement were observed between the groups of Tests 1, 2, 3 and Tests 4, 5, 6 correspondent to the two CBZ-based systems evaluated, *i.e.* CBZ:HPMCAS-MG and CBZ:Eudragit® L100, respectively, and within each group correspondent to the increase of drug load in the formulation, *i.e.* from 20%, to 40% and 60% of CBZ. Regarding the CBZ:HPMCAS-MG formulations, it was observed a gradual increase in the relative intensity of the characteristic peaks of crystalline CBZ from Test 1 up to Test 3, indicating the formation of crystalline solid dispersions. Consequently, and

as expected, it was also observed a gradual decrease in the drug amorphous halo's intensity from Test 1 to Test 3.

A good alignment was observed by comparing these results with the ones obtained from the mDSC analysis. Only the 20% CBZ: HPMCAS-MG formulation presented a single T_g around 102°C, a value that was consistent with the mixed T_g obtained using the Gordon-Taylor equation (*i.e.* 106°C) [21]. In fact, a significant percentage of this product was still amorphous and homogeneously mixed, as indicated by the absence of any additional or secondary glass transition temperature. The thermal evidence of crystalline material in the CBZ: HPMCAS-MG formulations was related with the detection of endothermic events within the temperature ranges ~150-16°C and ~188°C that were coincident with two endothermic peaks characteristic of pure CBZ. Pure CBZ, when heated, first presents a polymorphic transformation at 150°C, followed by the melting of the new phase formed at 186°C [22].

Comparing the CBZ: HPMCAS-MG co-precipitated products with the CBZ: Eudragit® L100 counterparts, the latter demonstrated to be capable of forming both amorphous and crystalline solid dispersions under the formulations and process conditions tested in the DoE. According to the XRPD results, Test 4 showed a halo characteristic of the amorphous form with no characteristic peaks of the XRPD profile of pure crystalline CBZ being observed in this co-precipitated product. In terms of thermal behavior only one single T_g was detected, and no signs of amorphous-amorphous phase separation were observed. Similarly to Test 1, the T_g value obtained for Test 4 was also in agreement with the respective Gordon-Taylor equation (*i.e.* 167°C versus 166°C, respectively). Eudragit® L100 apart from providing sufficient stabilization of CBZ at 20% drug load, and thus enabling the formation of a true glass solution, its high T_g (190°C) also leveraged the T_g of the final mixture to values well above 75°C, which is an ideal situation from a product shelf-life perspective, but also in terms of processability. Test 5 and Test 6, correspondent to the 40% and 60% CBZ:Eudragit® L100 formulations, showed identical results to Test 2 and Test 3. These co-precipitated products also resulted in crystalline solid dispersions of the drug within the polymer, indicated by the presence of the CBZ characteristic peaks either in the XRPD diffractograms and mDSC thermal profiles. During thermal analysis, it was also detected a single T_g in the reversible heat flow profile of Test 5, which was not observed in Test 6.

From the results obtained it was concluded that different types of solid dispersions, with different levels of drug's molecular arrangement, were capable of being produced using the novel SCP process presented in this work. The possibility of producing nano-sized glass solutions is of utmost importance due to the potential dual benefit of the high energy amorphous

state, which provides an increase on saturation solubility, together with the particle size reduction up to the nanoscale, that it is known for having a greater positive impact on the dissolution rate. By opposition, producing crystalline nanoencapsulated particles as crystalline nano-solid dispersions/solutions offer the advantage of higher drug loadings in the formulation, enabling the possibility of decreasing the number of administrations to patients, which can be an advantage, namely on increasing patient compliance. Moreover, working with the crystalline state can be an advantage in terms of stability during scale-up and downstream processing.

As the results in this section showed, the selection of the polymeric carrier or stabilizer as well as the drug load in formulation are critical formulation variables that will impact the type of solid dispersion obtained. The feed solids' concentration had no effect on this matter, as both amorphous and crystalline nano-solid dispersions were obtained from solutions at low- and high-level of C_{feed} (Tests 1 and 6 and Tests 4 and 3, respectively).

Regarding the polymer type, when considering the production of crystalline solid dispersions, the drug's physical stability aspect is not a major concern and thus both polymers evaluated - HPMCAS-MG or Eudragit® L100 - showed to be a viable option to nanoencapsulate crystalline CBZ up to high drug loads (60% minimum). In contrast, if the objective is to obtain a glass solution, the maintenance of its physical stability either during processing and long-term storage are critical factors that must be taken into consideration when choosing the polymer or optimizing the drug load, in order to avoid recrystallization. In this case Eudragit® L100 was suggested to be a better stabilizing polymeric agent for CBZ to produce glass solutions, when compared to HPMCAS-MG. Possible explanations for this difference might be related, among others, with the type and strength of interactions that can be established between the hydrogen bond acceptor and donors of CBZ and each of the polymers [16] and/or the different T_g 's of the polymers that help to increase the overall stability of the amorphous mixture as explained above for the case with Eudragit® L100. On the top of these formulation variables, one should not neglect the effect of process variables, namely temperature, working pressure and the type of interaction chamber that will define the homogenization conditions, the time between the production of the suspensions and the isolation step. These are some critical process variables that were maintained constant in this work but are known to affect the incorporation of drug within the carrier. For example, according to Sertsou *et al.* although intense mixing and faster precipitation is favorable for the creation of the amorphous, increasing mass transfer may also lead to a greater polymer's plasticization and loss of drug as part of the solid dispersion [23].

In terms of the influence of the drug load in formulation, obtaining an amorphous or crystalline solid solution/dispersion will depend on the equilibrium crystalline drug solubility

in the polymer and the maximum drug-polymer amorphous miscibility. These limits are typically evaluated by means of the construction of the thermodynamic phase diagrams of the drug and the polymer, which include the plot of the binodal and spinodal curves, as schematically shown in Figure 4.7. These curves help to define the maximum limits of drug that the polymer can “incorporate”, before nucleation and growth or spinodal decomposition takes place. The formulator by knowing in which point of the phase diagram is, can define *a priori* a potential range of drug loads to be further evaluated in advanced stages of product development, whether their intention is to obtain an amorphous or crystalline solid dispersion.

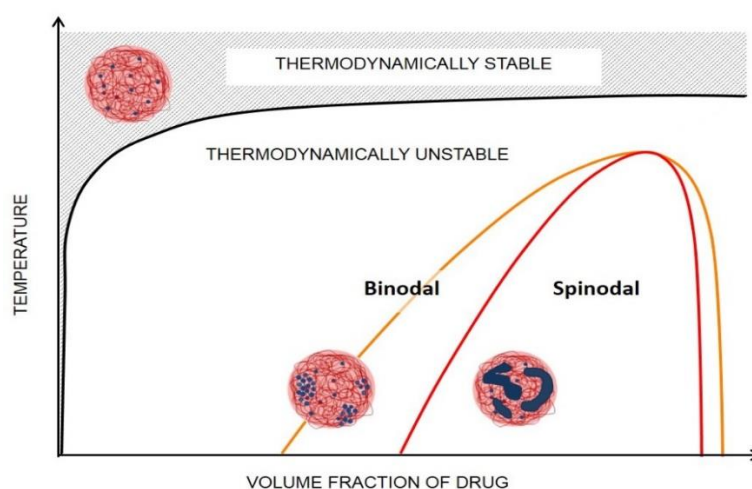


Figure 4.7. Representation of a hypothetical temperature-composition phase diagram for a general drug-polymer binary system.

4.3.2 Part II - Benchmarking solid dispersions obtained through SCP and SD processes

Following the experimental design, it was defined that the CBZ-based system that demonstrated higher flexibility in terms of its capacity to form both amorphous and crystalline nano-solid dispersions, under the formulations and process conditions tested in the DoE, would follow to part II of this work. According to the results obtained in Section 4.3.1.2, a comparative study was then performed using different formulations of CBZ: Eudragit[®] L100. For the *in vitro* and *in vivo* performance evaluation, one of the formulations tested was the nano-sized amorphous solid dispersion formulation produced by the SCP process (Test 4), hereafter defined as *NanoAmorphous*. In order to study the effect of different surface area-to-volume ratios in the dissolution rate of CBZ, a second formulation of 20% CBZ: Eudragit[®] L100 micro-sized amorphous solid dispersion formulation was produced by spray drying (*MicroAmorphous*, Supplementary Information C, Figure C.1). Finally, in order to assess the

solubility-gain of the amorphous *versus* the crystalline drug maintaining identical submicron particle size and high surface area, a third system consisting of 60% CBZ: Eudragit® L100 nano-crystalline solid dispersion formulation was produced by the SCP process (Supplementary Information C, Figure C.2). This *NanoCrystalline* formulation was obtained under the same experimental conditions of Test 6, but at 8% feed solids concentration to maintain the particle size of the spray-dried aggregates. Pure crystalline CBZ was also used, without further processing, in the *in vitro* and *in vivo* studies. For the powder stability study, only the *NanoAmorphous* and *MicroAmorphous* powders were considered, in order to assess their resistance to recrystallization under temperature and humidity stress conditions.

4.3.2.1 *In vitro* dissolution

In the literature a significant number of research papers exist demonstrating the higher dissolution rate of nano-composite aggregates obtained from spray-dried nanosuspensions when compared with their micro-sized counterparts [7,11,13,23]. Figure 4.8 shows the powder pH-shift dissolution profiles, over 180 minutes, for the different CBZ: Eudragit® L100 formulations, as described above.

As can be seen from Figure 4.8, powders showed significantly different CBZ release profiles once placed in contact with the acidic aqueous medium. As expected, the crystalline CBZ reference product was the one that demonstrated a lower dissolution rate. The drug dissolved in the medium from pure CBZ crystalline particles was only around 15% in the first 10 min of testing, reaching its maximum of 20%, after 35 min. This crystalline powder was tested unprocessed, thus presenting the largest particle size among all the formulations tested, and was used as received, which means no additional wetting agents were added. When comparing this dissolution profile with the ones obtained for the *NanoAmorphous*, *NanoCrystalline* and *MicroAmorphous* formulations, these powders demonstrated a 2 to 3-fold increase in the dissolution rate for the first 10 min of testing.

There are two important reasons for this difference. The first is related with the fact that these latter powders are all solid dispersions, *i.e.* regardless the drug's solid state and molecular arrangement, the polymeric carrier, in this case Eudragit® L100, is present in the formulation and polymers are known for providing an *a priori* improvement in the wettability of the drug.

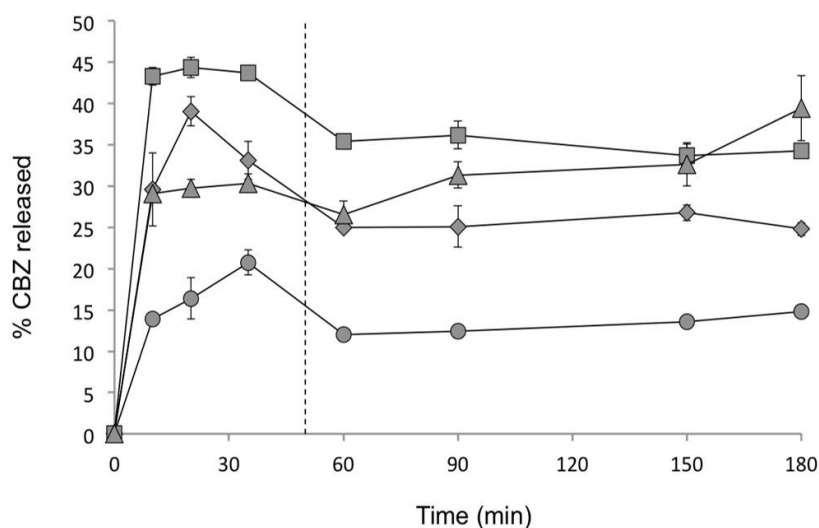


Figure 4.8. Powder dissolution profiles correspondent to the formulations *NanoAmorphous* (20% CBZ: Eudragit® L100, squares), *NanoCrystalline* (60% CBZ: Eudragit® L100 diamonds), *MicroAmorphous* (20% CBZ: Eudragit® L100, triangles), pure crystalline CBZ (circles). The vertical dashed line at the 50-min time point corresponds to the pH-shift. The bars correspond to the standard deviation from triplicates.

The second reason, probably the most relevant, is related with the reduced particle size of these powders, in the order of a few microns, when compared with pure crystalline CBZ particles, which promotes a dissolution boost as soon as they contact the liquid medium. When comparing the *in vitro* releases and performances among the *NanoAmorphous*, *NanoCrystalline* and *MicroAmorphous* formulations, these showed differences among each other. The *NanoAmorphous* powder was the one that exhibited the higher dissolution rate, with almost 45% of CBZ dissolved within the first 10 minutes of test. At the 10 min timepoint, the *MicroAmorphous* and *NanoCrystalline* powders were only able to reach 30% of drug dissolved in the medium. After 20 min, a 10% increase in the amount of drug dissolved was observed for the *NanoCrystalline* formulation.

To complement this analysis, Figure 4.9 and Table 4.2 show the SEM images and surface area measurements, respectively, for the *NanoAmorphous*, *NanoCrystalline* and *MicroAmorphous* powders. The *NanoAmorphous* powder is noticeable for having a significantly larger specific surface area, with a value around 4 and 9 times higher than the surface area of the *NanoCrystalline* and *MicroAmorphous* powders, respectively. The surface area of the *NanoCrystalline* powder with respect to the *NanoAmorphous* was lower due to the higher level of aggregation between nanoparticles promoted by the lower concentration of polymeric stabilizer present in the formulation, as explained in the Section 4.3.1.1.

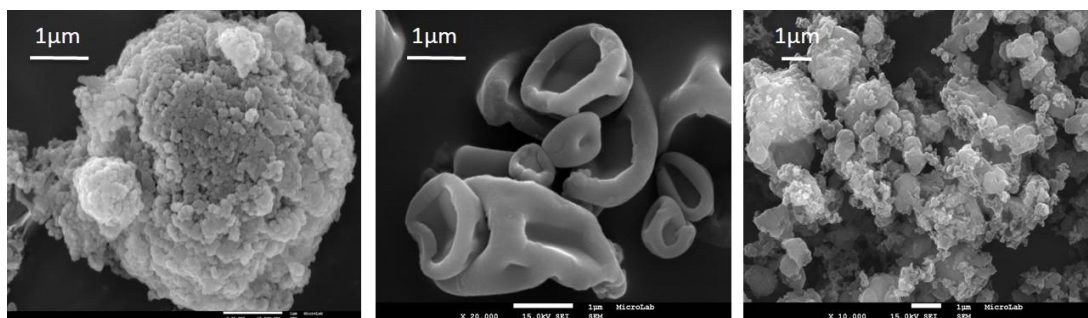


Figure 4.9. SEM micrographs corresponding to the *NanoAmorphous*, *MicroAmorphous* and *NanoCrystalline* powders, from left to right.

Table 4.2. Results for the surface area for the *NanoAmorphous*, *MicroAmorphous* and *NanoCrystalline* powders.

	<i>NanoAmorphous</i>	<i>MicroAmorphous</i>	<i>NanoCrystalline</i>
Surface Area (m ² /g)	81.7	9.1	19.7

Still, the surface area of this crystalline nano-sized formulation is around 2 times higher the surface area of the *MicroAmorphous* powder. The surface area enhancement factor obtained when comparing the *NanoAmorphous* with the *MicroAmorphous* powder was aligned with the general observed 10-fold increase in surface area when reducing from micron to nanoparticles, as reported by Shah *et al.* [24]. However, when comparing with the highly porous amorphous microparticles of vemurafenib produced by SCP using high shear mixing, the surface area enhancement factor of the *NanoAmorphous* powder reduces to about 4 times, a similar gain relatively to the *NanoCrystalline* powder [25].

When analyzing the SEM micrographs in Figure 4.9, both nano-composite particles obtained by the SCP process – the *NanoAmorphous* and *NanoCrystalline* – presented a completely different structure when compared with a spray-dried powder. The spray-dried particles showed similar particle size in the micron range when compared with the co-precipitated aggregates, but in terms of particle shape corresponded to the typically one-phased composite and hollow particles with smooth surface, and in this case with a shriveled morphology. The spray dried co-precipitated powders obtained by SCP for presenting a much more reticular structure consequently present a significantly higher specific surface area.

As described by the Noyes-Whitney equation, the dissolution rate is directly proportional to the diffusion coefficient of the drug, the surface area of the particle and the difference between the saturation solubility of the drug in the boundary layer and its concentration in the bulk liquid medium, and is inversely proportional to the thickness of the

diffusion layer [26]. Therefore, as the particle size decreases, the surface area increases, which results in the enhancement of the dissolution rate of the drug. Moreover, particles with reduced size also present reduced diffusion layers, which further contributes for a positive effect on the dissolution rate. Another factor that can ultimately increase the dissolution rate is the increase of the saturation solubility of the drug if the particle size is reduced below 100 nm [24]. The surface area results were completely aligned with the differences in the dissolution rate observed for the different powders. The *NanoAmorphous* powder for being the one that presented a lower level of aggregation, and thus the highest specific surface area, was the one that presented a higher dissolution rate, followed by the *NanoCrystalline* and the *MicroAmorphous* powders that presented almost identical dissolution profiles. The *NanoCrystalline* powder for being more aggregated, presented a reduced surface area and a slower dissolution rate at the 10 min timepoint, when compared with the *NanoAmorphous* powder that was less aggregated. Kumar *et al.* observed the same results when evaluating the impact of particle's aggregation on the dissolution rate of spray dried crystalline nanoparticles obtained from nanosuspensions [17]. These results also suggested that, in fact, a synergistic effect from the amorphous state together with the particle size reduction may promote a significant increase in the dissolution rate and absorption of BCS/DCS Class IIa compounds.

The rationale of performing a pH-shift dissolution test was to evaluate the capacity of the formulations to maintain CBZ supersaturation in solution after changing from acid to basic conditions, and to enable better *in vitro-in vivo* correlations. Supersaturation is a thermodynamically unstable state, and if the drug is not sufficiently stabilized in solution, it will tend to recrystallize, eventually losing the solubility advantages generated. As long as supersaturation is maintained in the gastro-intestinal tract more time is given for drug absorption to occur, thereby promoting an increase in the bioavailability. The presence of the polymeric stabilizer has a key role in the prevention of drug's recrystallization and maintenance of the drug's supersaturation *e.g.* by interacting with the drug via hydrogen bonding and other ionic interactions and/or by creating nano and micellar structures where the drug is incorporated and safe from recrystallization. Ionic polymers, for example, such as methacrylate copolymers (*i.e.* Eudragit® L100) can create complexes with the drug and thus maintain its supersaturation [27].

As expected, pure crystalline CBZ presented the lower area under the dissolution curve (AUC_d) over the 180 min period of testing (433 mg.h/L). Both the *NanoAmorphous* and *MicroAmorphous* formulations were capable of maintaining their levels of CBZ supersaturation in acid conditions until medium transfer. The *NanoCrystalline* formulation, in turn, precipitated

from the 20 min timepoint onwards and CBZ concentration decreased gradually, and after 60 min, the dissolution profile of the *NanoCrystalline* formulation intersected the dissolution profile of the *MicroAmorphous* powder, leading to the second lowest AUC observed (844 mg.h/L). Upon medium transfer, a slight decrease in the CBZ release was observed for the *NanoAmorphous* and *MicroAmorphous* formulations, but this was maintained constant until the end of the test. The *MicroAmorphous* powder showed a progressive increase in the percentage of CBZ dissolved as approaching the 180 min timepoint, which should be related with the successive centrifuge cycles of the dissolution test method developed that promoted further hydration/wetting of the powder. Non-formulated amorphous spray dried powders typically present poor wetting properties and often need additional dispersion steps to allow a good hydration of the powder. Spray dried co-precipitated aggregates, by opposition, readily disintegrated and formed fine suspensions.

Therefore, the formulation performance ranking by ascending order of potential to improve CBZ *in vivo* exposure was the following: pure crystalline CBZ < *NanoCrystalline* < *MicroAmorphous* (AUC_d ~962 mg.h/L) < *NanoAmorphous* (AUC_d ~ 1.1 g.h/L).

4.3.2.2 *In vivo* pharmacokinetics

In order to provide a deeper understanding of the particle size effect in the absorption and bioavailability of BCS/DCS Class IIa drugs, pharmacokinetic (PK) studies with the *NanoAmorphous*, *NanoCrystalline* and *MicroAmorphous* formulations, as well as pure crystalline CBZ particles, were performed in mice in the fasted state. The fasted state was selected because in certain cases the presence of food may interact (either increasing or decreasing) the dissolution performance, especially of micro-sized formulations [24]. Figure 4.10 shows the pharmacokinetic profiles, obtained over 180 min, for the different CBZ: Eudragit[®] L100 formulations.

The *NanoAmorphous* and the *NanoCrystalline* formulations were the ones that exhibited higher *in vivo* dissolution rates. When compared with the *MicroAmorphous* powder or pure crystalline CBZ particles, drug levels in serum samples of mice dosed with the nano-solid dispersions were distinctively superior. The amount of drug dissolved, and consequently absorbed, from both the *MicroAmorphous* and pure crystalline formulations was well below 1.25 mg/L, and even when assuming a yield of 60% for the liquid-liquid extraction process, drug levels would still be well below the LOQ of the method, and consequently far away from the performance of the nano-sized systems.

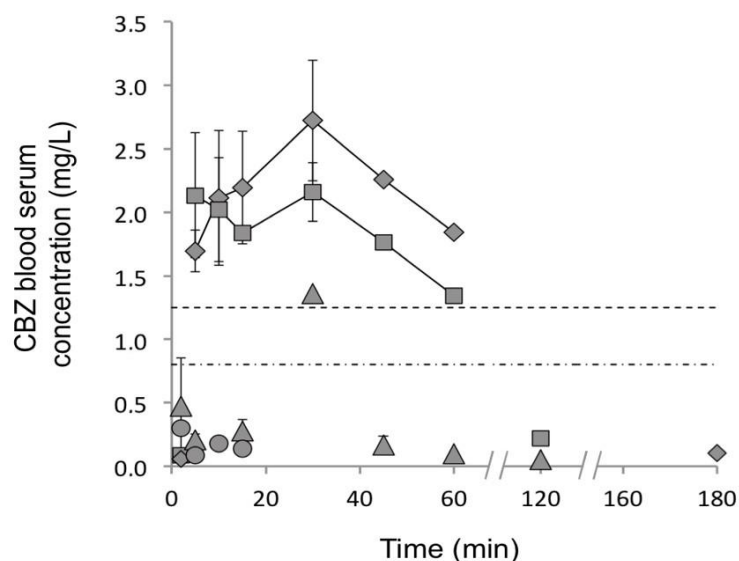


Figure 4.10. Pharmacokinetic profiles, correspondent to the formulations *NanoAmorphous* (20% CBZ:Eudragit[®] L100, squares), *NanoCrystalline* (60% CBZ:Eudragit[®] L100, diamonds), *MicroAmorphous* (20% CBZ:Eudragit[®] L100, triangles), pure crystalline CBZ (circles). The dashed line corresponds to the limit of quantification (LOQ) of the immunoassay method, which is 1.25 mg/L. The broken-dashed line corresponds to the maximum of drug concentration obtainable in the serum samples, if a 60% yield is considered for the extraction process. The bars correspond to the standard deviation from $n=3$. When no bars are shown data points are from $n \leq 2$ animals.

From the results obtained it can be concluded that the observed differences are clearly related to the difference in particle sizes and surface areas between the formulations. The high specific surface area of the nano-solid dispersions, both the *NanoAmorphous* and the *NanoCrystalline*, when exposed to the gastro-intestinal fluids led to very rapid dissolution rates, which in turn contributed to a greater amount of CBZ in solution. Since the absorption of CBZ is not limited by permeability, if more drug is present in solution, a higher amount can potentially be absorbed both by passive and/or active mechanisms and can reach the systemic circulation. The concentration of CBZ that reaches the blood will consequently be quantified in the blood serum. Neither the *MicroAmorphous* nor the pure crystalline powders were able to dissolve sufficiently fast in the gastro-intestinal fluids, due to their larger particle size and lower surface area. A lower quantity of drug in solution, led to lower absorption resulting in a lower bioavailability, as observed. The results obtained were in line with the works reported by Kumar *et al.* [13] and Angi *et al.* [18], who also evaluated the *in vivo* dissolution rate and bioavailability of nano-sized amorphous formulations obtained by co-precipitation followed by spray drying, against the respective micro-sized formulations. According to Shah *et al.* [24], apart from particle size reduction, other factors that may contribute for the increase in

bioavailability is the mucoadhesion behavior of nanoparticles in the gastric and intestinal mucosa, similarly to an extended-release formulation.

In terms of the total drug exposure or AUC both *NanoAmorphous* and *NanoCrystalline* formulations were considered identical. No clear distinction or ranking could be established between these two systems due to the high variability observed between mice of the same group. The same issue was encountered when attempting to obtain other pharmacokinetic parameters, such as the time and the value of the maximum concentration (*i.e.* t_{\max} and C_{\max}). These results somehow contradicted our initial expectations, in the sense that, the *a priori* dual benefit for bioavailability of having the drug in the amorphous state and the particle size of the solid dispersion reduced to the nano-range was not clearly verified. Indeed, the results suggested that for CBZ the effect of the reduction of particle size is more important than having the drug in its amorphous state. Further research and validation would be needed to verify whether this hypothesis could be extended to all BCS/DCS Class IIa compounds. Nevertheless, and taking into consideration that amorphization apparently does not bring any additional advantage to this system, formulation development can focus on the optimization of crystalline nano-solid dispersions. As already mentioned in Section 4.3.1.2, crystalline nanoparticles offer not only the stability advantage (storage and processability stability) but also the possibility of obtaining formulations with higher drug loads. A final-dosage form with a higher drug load can be delivered at a lower dose to maintain the same therapeutic effect.

From the PK profiles shown in Figure 4.10, the information gained for the *NanoAmorphous* and *NanoCrystalline* systems, was that t_{\max} was most likely achieved within the first 30 min, and C_{\max} had a value between a minimum and a maximum of 1.73-2.38 mg/L and 1.42-3.47 mg/L, for the former and latter formulations respectively. When comparing these values with the PK parameters obtained after administration of rats, the closest animal model to mice, with an oral solution of CBZ in PEG-400 at 25 mg/kg ($t_{\max}=90$ min, $C_{\max}=2.29$ mg/L) it can be concluded that nano-solid dispersions presented a significant reduction in t_{\max} , and for a lower dose (7.4 mg/kg in this work) the C_{\max} was identical [28]. This further confirms that the high dissolution rate of the nanoparticles led to the supersaturation of the drug in the GI fluids promoting the absorption of CBZ, thus improving its bioavailability.

Comparing the AUCs of the nano-sized formulations with those obtained for the *MicroAmorphous* and pure crystalline CBZ samples, these were approximately 5 and 50 times higher, respectively. According to Shah *et al.*, the overall bioavailability of nanoparticles was reported to be a 3-fold increase when compared with micronized particles and a 9-fold increase

when compared with coarse powder [24]. Thus, the results obtained in this work are in agreement with the data found in the literature.

Finally, in what regards the PK parameters obtained for the *MicroAmorphous* formulation, there was one mouse that presented a concentration marginally above 1.25 mg/L in its serum, at the 30 min timepoint. Similarly, and despite the mice variability observed, when comparing this result with the *in vivo* profiles of the nano-sized samples, these values were most likely related with the C_{\max} and t_{\max} achieved for this formulation.

Comparing the *in vivo* with the *in vitro* results, these were generally aligned with each other, although a change in the ranking between the *NanoCrystalline* and *MicroAmorphous* formulations was observed. One should not neglect the fact that *in vivo* powder dissolution and absorption are much more complex and dynamic processes when compared with what happen *in vitro*.

4.3.2.3 Amorphous powder stability

For the powder stability study, only the amorphous powders, either produced by SCP and SD, were considered in order to assess their potential for recrystallization under temperature and humidity stress conditions. Figure 4.11 shows the XRPD diffractograms of the *NanoAmorphous* and *MicroAmorphous* powders obtained after 90 days in open Petri dishes conditioned inside glass dessicators at 25 °C/65% RH and 40 °C/75% RH conditions. It should be pointed out, that although the results obtained after 30 days of storage were omitted for simplicity, but the conclusions remained the same.

As can be seen, both powders exhibited the typical halo characteristic of the amorphous state and no peaks of pure CBZ were detected under both stress conditions and up to 90 days of storage. Both amorphous powders showed identical long-term storage physical stability, and acceptable resistance to recrystallization.

The assurance of long-term storage physical stability is the ultimate goal when developing an amorphous formulation. The formulation should be capable of maintaining its solid state and physical stability during the shelf life of the product. In this respect, (1) the selection of the right polymeric stabilizer, (2) the respective drug-polymer miscibility and (3) the method of amorphization or method of production are fundamental variables that may affect the physical stability of an amorphous formulation.

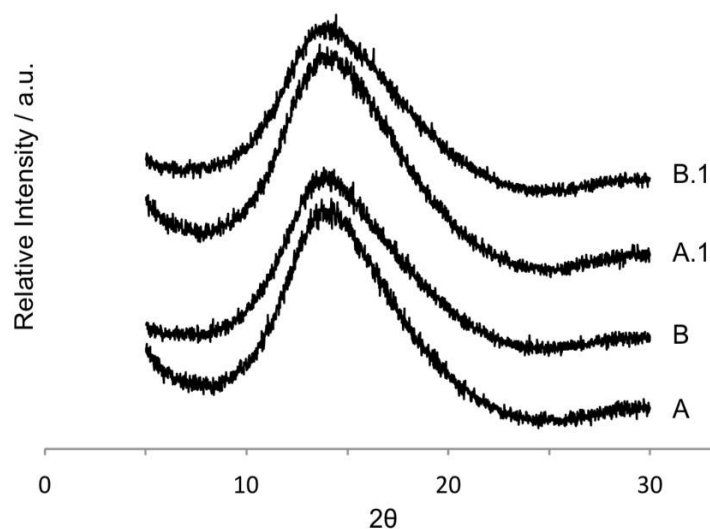


Figure 4.11. Powder diffractograms correspondent to the *NanoAmorphous* and *MicroAmorphous* formulations after 90 days of storage at 25°C/65% RH (A and B, respectively) and 45°C/75% RH (A.1 and B.1, respectively).

In the case of this work, and as regards to the polymeric stabilizer, Eudragit® L100 possess certain characteristics that most probably contributed for the high physical stability of these powders. As already explained in Sections 4.3.1.2 and 4.3.2.1 Eudragit® L100 has a relatively high T_g by comparison to other polymeric carriers and it is an ionic polymer. In what concerns drug-polymer miscibility, as the drug load in formulation increases the propensity for phase separation and recrystallization also increases. Indeed, the miscibility of the amorphous drug within the carrier was limited. The amorphous formulations produced in this work and tested for long-term storage stability have a 20% CBZ load. This is a relatively low drug fraction that typically provides completely amorphous and homogenous ASDs. Finally, both the SCP and SD allowed sufficiently fast precipitation to form homogenous and physically stable amorphous formulations up to 20% CBZ load.

4.4 Conclusions

In this work, an alternative SCP process based on microfluidization was evaluated to produce solid dispersions. Six different suspensions were produced by co-precipitation and were dried using spray drying. Spray-dried nano-composite microparticles were obtained, meaning that the final suspensions produced by co-precipitation were in fact nanosuspensions. The nano solid dispersions were non-porous and presented a mean circular diameter around 100

nm. The level of aggregation of the nanoparticles was shown to be dependent on the drug-polymer ratio, while the feed solids' concentration in solution defined the particle size of the micro-sized aggregates. Both amorphous and crystalline nano-solid dispersions were produced, which showed to be dependent on the type of stabilizing polymer used and drug load in formulation.

The nano-solid dispersions (either amorphous or crystalline) presented faster dissolution rates and improved bioavailability when compared with a spray dried amorphous solid dispersion. The effect of particle size and surface area showed to be more important than the amorphization of the drug, for improving the bioavailability of CBZ, a BCS/DCS Class IIa compound. Further validation is needed to evaluate whether this result can be extrapolated to other compounds that present dissolution-rate limited absorption. In case this hypothesis is verified means that formulation development can focus on the optimization of crystalline nano-solid dispersions, which offer stability advantages and higher drug loads in formulation.

Still, the long-term storage physical stability of the amorphous nano-solid dispersion produced by SCP was comparable to the amorphous micro-solid dispersion produced by SD.

4.5 References

- [1] T. Panagiotou, S. V. Mesite, and R. J. Fisher, "Production of Norfloxacin Nanosuspensions Using Microfluidics Reaction Technology through Solvent/Antisolvent Crystallization" *Industrial & Engineering Chemistry Research*, vol. 48, pp. 1761-1771, 2009.
- [2] J. M. Butler and J. B. Dressman, "The Developability Classification System: Application of Biopharmaceutics Concepts to Formulation Development" *Journal of Pharmaceutical Sciences*, vol. 99, no. 12, pp. 4940-4954, 2012.
- [3] D. T. Friesen *et al.*, "Hydroxypropyl Methylcellulose Acetate Succinate-Based Spray-Dried Dispersions: An Overview" *Molecular Pharmaceutics*, vol. 5, no. 6, pp. 1003-1019, 2008.
- [4] W. Curatolo, J. A. Nightingale, and S. M. Herbig, "Utility of Hydroxypropylmethylcellulose Acetate Succinate (HPMCAS) for Initiation and Maintenance of Drug Supersaturation in the GI Milieu" *Pharmaceutical Research*, vol. 26, no. 6, pp. 1419-1431, 2009.
- [5] T. L. Jensen, M. K. Kiersgaard, D. B. Sørensen, and L. F. Mikkelsen, "Fasting of mice: a review." *Laboratory Animals*, vol. 47, no. 4, pp. 225-240, 2013.

- [6] E. L. McConnell, A. W. Basit, and S. Murdan, "Measurements of rat and mouse gastrointestinal pH, fluid and lymphoid tissue, and implications for in-vivo experiments" *Journal of Pharmacy and Pharmacology.*, vol. 60, no. 1, pp. 63-70, 2008.
- [7] M. V. Chaubal and C. Popescu, "Conversion of Nanosuspensions into Dry Powders by Spray Drying: A Case Study" *Pharmaceutical Research*, vol. 25, no. 10, pp. 2302-2308, 2008.
- [8] J. Lee, "Drug Nano- and Microparticles Processed into Solid Dosage Forms: Physical Properties" *Journal of Pharmaceutical Sciences*, vol. 92, no. 10, pp. 2057-2068, 2003.
- [9] S. P. Nunes and T. Inoue, "Evidence for spinodal decomposition and nucleation and growth mechanisms during membrane formation" *Journal of Membrane Science*, vol. 111, pp. 93-103, 1996.
- [10] M. Temtem *et al.*, "Supercritical CO₂ generating chitosan devices with controlled morphology. Potential application for drug delivery and mesenchymal stem cell culture" *Journal of Supercritical Fluids*, vol. 48, no. 3, pp. 269-277, 2009.
- [11] J. Hu, W. Kiong Ng, Y. Dong, S. Shen, and R. B.H. Tan , "Continuous and scalable process for water-redispersible nanoformulation of poorly aqueous soluble APIs by antisolvent precipitation and spray-drying" *International Journal of Pharmaceutics*, vol. 404, pp. 198-204, 2011.
- [12] M. Azad, C. Arteaga, B. Abdelmalek, R. Davé, and E. Bilgili , "Spray drying of drug–swellable dispersant suspensions for preparation of fast-dissolving, high drug-loaded, surfactant-free nanocomposites" *Drug Dev Ind Pharm.*, vol. 41, no. 10, pp. 1617-31, 2015.
- [13] S. Kumar, J. Shen, and D. J. Burgess, "Nano-amorphous spray dried powder to improve oral bioavailability of itraconazole" *Journal of Controlled Release*, vol. 192, pp. 95-102, 2014.
- [14] S. V. Dalvi and R. N. Dave, "Controlling Particle Size of a Poorly Water-Soluble Drug Using Ultrasound and Stabilizers in Antisolvent Precipitation" *Ind. Eng. Chem. Res.*, vol. 48, no. 16, pp. 7581-7593, 2009.
- [15] L. Lindfors, S. Forssén, J. Westergren, and U. Olsson, "Nucleation and crystal growth in supersaturated solutions of a model drug" *Journal of Colloid and Interface Science*, vol. 325, no. 2, pp. 404-413, 2008.
- [16] D. Douroumis and A. Fahr, "Stable carbamazepine colloidal systems using the cosolvent technique" *European Journal of Pharmaceutical Sciences*, vol. 30, no. 5, pp. 367–374, 2007.

- [17] S. Kumar, X. Xu, R. Gokhale, and D. J. Burgess , "Formulation parameters of crystalline nanosuspensions on spray drying processing: A DoE approach" *International Journal of Pharmaceutics*, vol. 464, no. 1-2, pp. 34-45, 2014.
- [18] R. Angi *et al.*, "Novel continuous flow technology for the development of a nanostructured Aprepitant formulation with improved pharmacokinetic properties" *European Journal of Pharmaceutics and Biopharmaceutics*, vol. 86, pp. 361-368, 2014.
- [19] A. A. Thorat and S. V. Dalvi, "Liquid antisolvent precipitation and stabilization of nanoparticles of poorly water soluble drugs in aqueous suspensions: Recent developments and future perspective" *Chemical Engineering Journal*, vol. 181-182, pp. 1-34, 2012.
- [20] K. Six, G. Verreck, J. Peeters, M. Brewster, and G. Van den Mooter, "Increased Physical Stability and Improved Dissolution Properties of Itraconazole, a Class II Drug, by Solid Dispersions that Combine Fast- and Slow-Dissolving Polymers" *Journal of Pharmaceutical Sciences*, vol. 93, no. 1, pp. 124-131, 2004.
- [21] A. L. Grzesiakg, M. Lang, K. Kim, and A. J. Matzger, "Comparison of the Four Anhydrous Polymorphs of Carbamazepine and the Crystal Structure of Form I" *Journal of Pharmaceutical Sciences*, vol. 92, no. 11, pp. 2260-2271, 2003.
- [22] G. Sertsou, J. Butler, A. Scott, J. Hempenstall, and T. Rades, "Factors affecting incorporation of drug into solid solution with HPMCP during solvent change co-precipitation" *International Journal of Pharmaceutics*, vol. 245, pp. 99-108, 2002.
- [23] Y. Dong, W. K. Ng, J. Hu, S. Shen, and R. B.H. Tan , "Continuous production of redispersible and rapidly-dissolved fenofibrate nanoformulation by combination of microfluidics and spray drying" *Powder Technology*, vol. 268, pp. 424-428, 2014.
- [24] D. A. Shah, S. B. Murdande, and R. H. Dave, "A Review: Pharmaceutical and Pharmacokinetic Aspect of Nanocrystalline Suspensions" *Journal of Pharmaceutical Sciences*, vol. 105, no. 1, pp. 10-24, 2016.
- [25] N. Shah *et al.*, "Improved Human Bioavailability of Vemurafenib, a Practically Insoluble Drug, Using an Amorphous Polymer-Stabilized Solid Dispersion Prepared by a Solvent-Controlled Coprecipitation Process" *Journal of Pharmaceutical Sciences*, vol. 102, no. 3, pp. 967-981, 2013.
- [26] A. A. Noyes and W. R. Whitney, "The rate of solution of solid substances in their own solutions" *Journal of the American Chemical Society*, vol. 19, no. 12, pp. 930-934, 1897.

- [27] S. R. K. Vaka *et al.*, "Excipients for Amorphous Solid Dispersions" in *Amorphous Solid Dispersions: Theory and Practice*, Navnit Shah *et al.*, Springer, 2014.
- [28] A. Beig and A. Dahan, "Quantification of carbamazepine and its 10,11- epoxide metabolite in rat plasma by UPLC-UV and application to pharmacokinetic study" *Biomedical Chromatography*, vol. 28, pp. 934-938, 2014.

Chapter 5

The results described in this chapter have been published total or partially in the following communications:

- I. Duarte, M. J. Pereira, L. Padrela and M. Temtem, “Synthesis and particle engineering of cocrystals” WO 2015/036799 A1, filed September 16, 2014, and issued March 19, 2015;
- I. Duarte, R. Andrade, J. F. Pinto and M. Temtem, “Green Production of cocrystals using a solvent-free by spray congealing” *International Journal of Pharmaceutics*, vol. 506, no. 1-2, pp. 68-78, 2016;
- 1 international conferences as a poster communication;
- 3 international conferences as an oral communication.

Authors' contribution:

I.D. was involved in the conception, design, production and analysis of data. I.D. wrote the manuscript and led the revision of the article particularly on proposing the journal's reviewers questions and comments.

5 Green production of cocrystals using a new solvent-free approach by spray congealing

5.1 Introduction

Despite the potential of cocrystals, their application in the pharmaceutical field is still limited due, in part, to the scarcity of suitable large-scale production methods and lack of robust and cost-effective processes. In order to address some of these challenges a novel solvent-free approach by spray-congealing (SCG) was evaluated in this work to produce pharmaceutical cocrystals.

SCG is a well-established manufacturing technology in the food and pharmaceutical industries for the production of microencapsulates, taste masked and controlled release products [1-3]. SCG can be described as a hybrid technology between SD and HME, comprising the best of particle's engineering and green chemistry/pharmacy fields.

As schematically presented in Figure 5.1, SCG consists of feeding a molten mixture to an atomizer (1), which then breaks the liquid feed into small droplets (2), and those droplets are cooled and solidified in a co-current stream of cooling gas that removes thermal energy from the droplets (3). The particles are then separated from the cooling gas in a cyclone (4) and collected in a container.

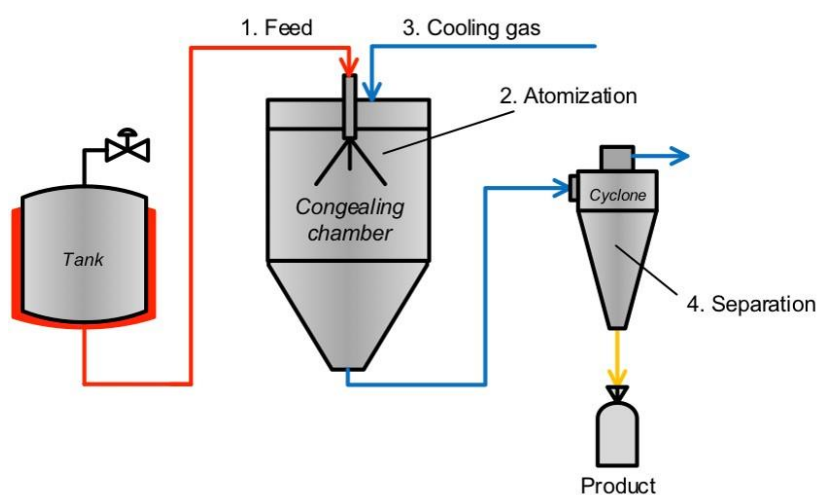


Figure 5.1. Representation of the spray congealing process.

The major advantage of cocrystallization by SCG when compared with traditional solvent-based methods, such as HPH or SD, is the fact that it is a solvent-free technique. Cocrystallization via SCG complies with green chemistry and sustainable pharmacy principles, allows cost reduction and avoids the formation of solvates. Moreover, when compared with similar processes such as HME the major asset of SCG is that it allows the particle engineering of cocrystals *in situ*, avoiding additional downstream processing steps. Because the unit operation can be conducted in a modified spray drying apparatus the scale-up is relatively straightforward [4]. This can be considered as an advantage over the SCF-based methods that require more specific equipment design. Finally, because SCG only implies the melting of the pharmaceutical components, additional concerns such as limited solubility in organic solvents or supercritical fluids, are discarded.

The main limitation of the SCG process is the heating of the pharmaceutical components to obtain the molten mixture, which according to the physicochemical properties of the API and coformers, can occur at high temperatures and thus attention should be paid with heat labile compounds in order to avoid degradation.

This work was divided in two main parts. In the first part, a feasibility study of SCG applied to cocrystallization was conducted. This was performed with two cocrystals that were already characterized in the literature - Caffeine:Salicylic Acid (CAF:SAL, Figure 5.2A) and Carbamazepine:Nicotinamide (CBZ:NIC, Figure 5.2B), both at 1:1 molar ratio.

Both caffeine (CAF) and carbamazepine (CBZ) are typical API model compounds in pharmaceutical cocrystallization studies. CAF is considered a BCS Class I compound (high solubility/high permeability), whereas CBZ belongs to Class II (low solubility/high permeability). Both are low molecular weight organic molecules, easily crystallizable from the undercooled melt according to Baird *et al.* [5].

The 1:1 CAF:SAL cocrystal was first obtained by Lu *et al.* [6] presumably using the slurry method according to Zhang *et al.* [7,8]. The 1:1 CBZ:NIC cocrystal has already been obtained from solution and slurry crystallization [6,9,10], neat grinding [11] and melt method [12]. At least two polymorphic forms of 1:1 CBZ:NIC cocrystal are known in the literature, form I and II, being the latter identified from the melt during a calorimetric study [13,14].

In the second part of this work, a design of experiments (DoE) with 2 parameters at 2 levels plus 1 central point was conducted with another CAF-based cocrystal also well described in the literature, to further evaluate the applicability of SCG. The cocrystal selected was the 1:1 Caffeine:Glutaric Acid (CAF:GLU, Figure 5.2C) that was previously produced using liquid-assisted grinding [15], slurry conversion [7], spray-drying [16], cooling crystallization [17].

Similarly to the 1:1 CBZ:NIC cocrystal, the 1:1 CAF:GLU also presents two polymorphic forms, form I and II, both structurally characterized in the literature [15,18].

The goal of performing an experimental design was to assess the effect of two critical process variables of the SCG process on cocrystal formation, purity, particle size, shape and powder flow properties. The parameters evaluated were atomization and cooling-related parameters.

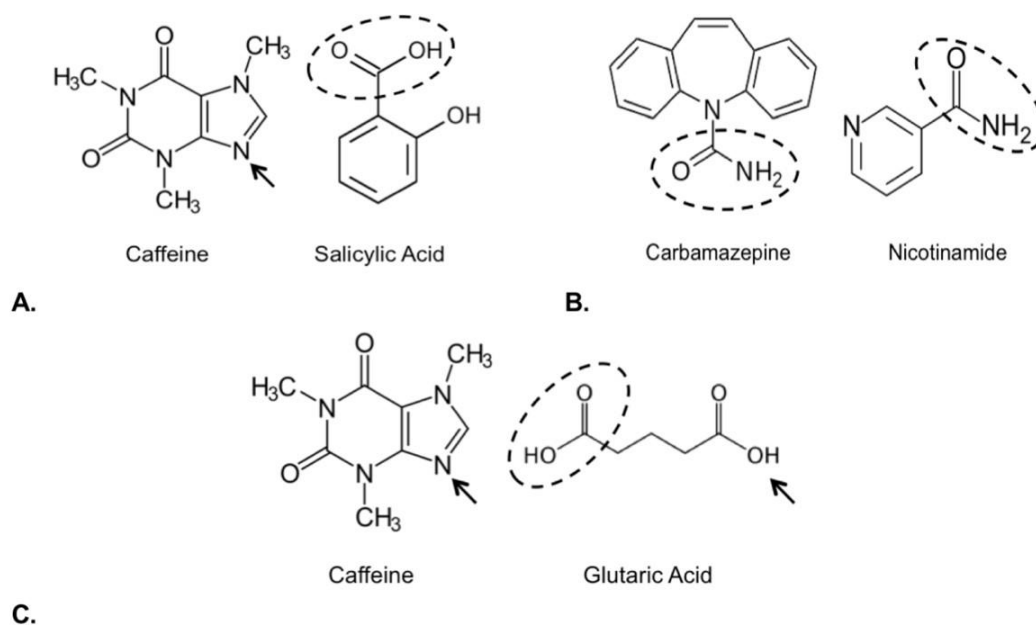


Figure 5.2. Chemical structures of the APIs and coformers considered in the study. The chemical functionalities with potential to form H-bond interactions are identified.

5.2 Materials and Methods

5.2.1 Materials

Caffeine (CAF, β -caffeine anhydrous, purity 99%), glutaric acid (GLU, purity 99%), salicylic acid (SAL, purity $\geq 99\%$) and nicotinamide (NIC, purity $\geq 99\%$) were purchased from Sigma-Aldrich Quimica SA (Alcobendas, Spain). Carbamazepine (CBZ, anhydrous Form III, purity $> 97\%$) was purchased from TCI Co., Ltd. (Tokyo, Japan).

5.2.2 Methods

5.2.2.1 Cocrystallization by spray congealing

Stoichiometric mixtures of each API and respective coformers (total mass of ~30 g) were physically blended in a laboratory turbula mixer for 10 min. The physical mixture was slowly fed into a jacketed beaker and agitated with a magnetic stirrer. A silicone-based heat transfer fluid (SYLTHERM XLT, Dow Chemical Co.) circulated inside the jacket of the beaker, feed line, and nozzle in order to keep the mixture in a molten state until the atomization point. The physical mixture was heated, through small temperature increments, until total melting of both API and coformer was observed ($T_{M, \text{mix}}$).

Spray congealing (SCG) was conducted using a modified lab scale spray dryer (4M8-TriX ProCepT, Zelzate, Belgium), adapted for spray congealing and operated in open cycle mode. The cooling chamber height was set to its maximum (180 cm). Atomization was conducted with a jacketed two fluid nozzle (orifice size of 1.20 mm) that was used to atomize the melt. Co-current nitrogen was used to promote the solidification of the melt after atomization. The congealing gas flow rate (F_{gas}) was kept constant in all tests at 0.35 m³/min. Before feeding the melt to the nozzle, the SCG unit was stabilized with nitrogen to assure stable inlet (T_{in}) and outlet (T_{out}) temperatures. After stabilization, the liquid/melt was fed by pressurizing the beaker using a pressure regulator. The liquid feed rate (F_{feed}) was kept constant and was approximately 5 g/min. The droplets were then cooled and solidified in the SCG chamber by the co-current nitrogen stream. The stream containing the product was directed to a cyclone to separate the solids from the gas.

Table 5.1 compiles the formulation and process variables tested in both phases of this work (feasibility study and DoE), complementing the above description.

For the DoE, the two process variables studied were the F_{atom} and the T_{in} of the congealing gas, represented as ΔT . These two process variables are directly related with the atomization and cooling phases of the spray congealing process, which are fundamental steps for spray-congealed particle formation. The low-level chosen for the F_{atom} (11 L/min) was related to the “minimum atomization gas volume” to “feed rate” ratio necessary to create a homogenous and continuous spray inside the congealing chamber. The high-level of 20 L/min was then selected to decrease the droplet size. Varying the ΔT value enabled modulation of the cooling efficiency. At $\Delta T=0^{\circ}\text{C}$ the cooling kinetics will be slower, because the molten droplets will be cooled and solidified only by means of the decreasing temperature gradient observed

inside the congealing chamber, while at $\Delta T=50^{\circ}\text{C}$ the cooling efficiency will theoretically improve.

Table 5.1. API/coformer systems tested and process variables defined for each test.

	API/Coformer system	Molar ratio	Exp. number	Spray Congealing Process Variables				
				$T_{M, \text{mix}}$ ($^{\circ}\text{C}$)	T_{in} ($^{\circ}\text{C}$)	T_{out} ($^{\circ}\text{C}$)	$\Delta T=T_{M, \text{mix}}-T_{\text{in}}$ ($^{\circ}\text{C}$)	F_{atom} (L/min)
Feasibility study	Caffeine:Salicylic acid (CAF:SAL)	1:1	-	150	100	58	50	9
	Carbamazepine: Nicotinamide (CBZ:NIC)	1:1	-	175	50	36	125	12
2^{2+1} Design of Experiments (DoE)	Caffeine:Glutaric acid (CAF:GLU)	1:1	#1		140	85	0	11
			#2		90	57	50	11
			#3	140	140	85	0	20
			#4		90	57	50	20
			#5		115	70	25	16

5.2.2.2 Modulated Differential Scanning Calorimetry (mDSC)

Modulated differential scanning calorimetry experiments were performed in a TA Q1000 (TA Instruments, New Castle, Delaware, USA) equipped with a Refrigerated Cooling System (RCS). The enthalpy response was calibrated using indium. The raw materials, physical mixtures and spray-congealed samples were analyzed in pinholed DSC aluminum pans and under continuous dry nitrogen purge (50 mL/min). 1:1 CAF:SAL and 1:1 CBZ:NIC samples were analyzed using a modulated heating ramp from 25°C to 300°C at a heating rate of $5^{\circ}\text{C}/\text{min}$ using a period of 60 s and amplitude of 0.8°C . Respective raw materials and physical mixtures were analyzed using the same method. The 1:1 CAF:GLU samples and respective physical mixture were analyzed using a heating ramp, from 25°C to 250°C at a heating rate of $10^{\circ}\text{C}/\text{min}$. All samples weighed between 5 to 10 mg.

Data was analyzed and processed using the TA Universal Analysis 2000 Software (TA Instruments, New Castle, Delaware, USA).

5.2.2.3 X-Ray Powder Diffraction (XRPD)

X-ray powder diffractograms were obtained in a D8 Advance Bruker AXS $\theta/2\theta$ diffractometer with a copper radiation source ($\text{Cu K}\alpha$, $\lambda=1.5406 \text{ \AA}$), voltage of 40 kV, and

filament emission of 35 mA. For the total scan, the samples were measured over a 2θ interval from 3 to 70° with a step size of 0.017° and step time of 50 s. For the slow scan, the samples were measured over a 2θ interval from 10 to 14° with a step size of 0.017° and step time of 1500 s.

5.2.2.4 Scanning Electron Microscopy (SEM)

The samples were attached to adhesive carbon tapes (Ted Pella Inc., CA, USA), previously fixed to aluminum stubs where the powder in excess was removed by a jet of pressurized air. The samples were left under vacuum for 2 h and then coated with gold/palladium (South Bay Technologies, model E5100, San Clement, CA). A JEOL JSM-7001F/Oxford INCA Energy 250/HKL scanning electron microscope (JEOL, Japan) operated in high vacuum at an accelerating voltage of 15 kV was used. Micrographs were taken at different magnifications from 50x up to 5000x.

5.2.2.5 Particle size analysis

The particle size of the 1:1 CAF:SAL and 1:1 CBZ:NIC samples, expressed as the mean circular diameter, was determined by image analysis using the ImageJ software (National Institute of Health, Bethesda, MD, USA) from 400 randomly selected particles, which demonstrated a normal distribution of sizes.

In the case of the 1:1 CAF:GLU samples, the particle size was expressed as the circular equivalent diameter (CED) and was analyzed in a Morphologi G2 particle characterization system (Malvern Instruments, Worcestershire, UK). CED is the diameter of a circle having the same area of the projected particle image. Approximately 10 mg of each sample was dry dispersed onto a glass slide using the system sample preparation device ($n=3$). Sample preparation settings were as follows: injection pressure: 2.0 bar; injection time: 200 ms; delay time: 2 s. Image analysis was conducted using 10x and 20x magnification lens, with the plate tilt compensation enabled. The resolution ranges covered were $3.5\ \mu\text{m}$ to $210\ \mu\text{m}$ and $1.8\ \mu\text{m}$ to $100\ \mu\text{m}$, respectively. The scanning area was a square with approximately $56\ \text{mm}^2$, centered in the center of the glass slide. Diascopic illumination was used to visualize the particles, and light intensity was automatically calibrated prior to the analysis of each sample ($80.00 \pm 0.20\%$). The number of particles counted in each glass slide ($n=3$, per test) was combined in a single result giving a total count of approximately 1000 particles. Number-based CED distributions ($D_{n,50}$) were obtained and then compared.

5.2.2.6 Characterization of powder flowability

The powder flow characteristics of the different 1:1 CAF:GLU samples was analyzed using a FT4 powder rheometer (Freeman Technology Ltd., Tewkesbury, UK). Powder compressibility and permeability data of the different materials produced were measured according to the respective standard test programs. The compressibility and permeability tests were performed using the 23.5 mm blade and the 25 mm vessel.

In the compressibility test, each powder was compressed at different normal stresses, from 1 to 15 kPa, with a vented piston to enable release of entrained air. In the permeability test, each powder was subjected to the same program sequence of the compressibility test, though with the difference that a stream of air at constant velocity (2 mm/s) was continuously injected below the powder bed while being compressed. The permeability tests were performed first, with fresh samples, followed by the compressibility tests re-using the same materials.

5.3 Results and Discussion

The first two case-studies that are described in the following section were part of the feasibility study of using SCG to produce pharmaceutical cocrystals.

5.3.1 Feasibility study: cocrystals of 1:1 CAF:SAL and 1:1 CBZ:NIC using spray congealing

Figure 5.3A and Figure 5.3B show the total heat flow curves corresponding to the thermal analysis of the 1:1 CAF:SAL and 1:1 CBZ:NIC cocrystals, respectively. The pure APIs, coformers and respective physical mixtures (same molar proportion) were also analyzed by thermal analysis and are also represented in the respective thermal profiles. Table 5.2 summarizes the onset temperatures and enthalpy data associated to the principal endothermic events detected in the thermal profiles.

The endothermic events, namely phase transformations and melting peaks, observed for the pure components were in agreement with those reported in the literature [6,12]. Pure CAF presented two endothermic peaks, one at 139°C correspondent to the transition of β -caffeine to α -caffeine, and the other at 233°C correspondent to the formation of an isotropic liquid when heating the α -anhydrous form. The DSC profile of pure SAL presented a sharp endothermic peak at 156°C attributed to the melting of the material followed by a broad endothermic peak that may correspond to degradation.

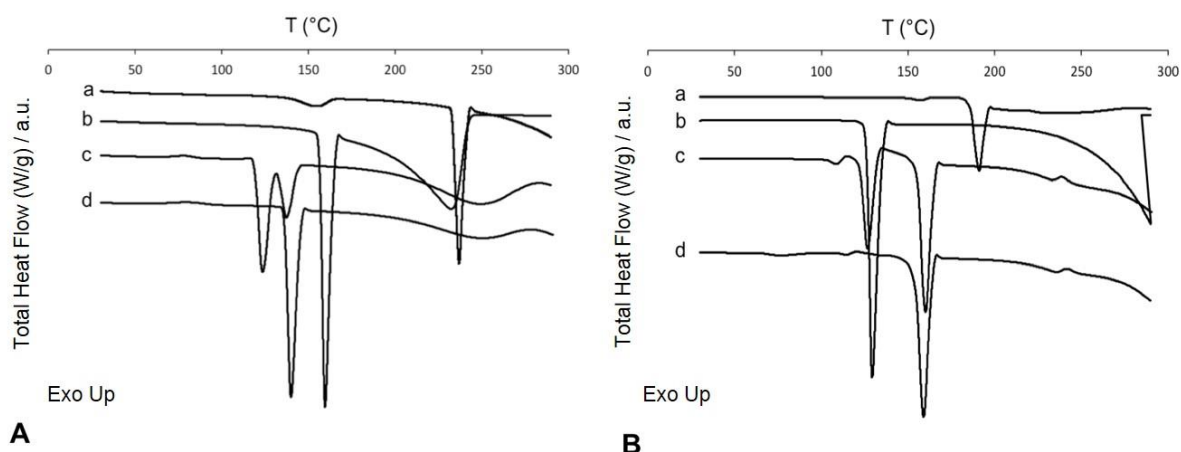


Figure 5.3. Total heat flow profiles of 1:1 CAF:SAL (A) and 1:1 CBZ:NIC (B): a – pure API, b – pure coformer, c – respective physical mixture in the same molar proportion, d – cocrystal obtained by spray congealing. CAF and CBZ are considered the APIs and the SAL and NIC the cofomers.

Pure CBZ first underwent a polymorphic transformation at 150°C, followed by the melting of the new phase formed at 186°C. Finally, the thermogram of pure NIC presented a single endothermic peak at 126°C attributed to the thermodynamic melting of the material, also followed by a broad endothermic peak that may correspond to degradation.

Starting with the comparison of the thermal profiles of the pure APIs and cofomers with the respective spray-congealed materials, it was observed that any of the endothermic events characteristic of the pure components were present in the thermal profiles of the final products produced by SCG. These results were indicative that new crystalline forms were produced and thus presented a different thermal behavior when compared with the pure precursors. The thermal profiles obtained for the physical mixtures also serve as a confirmatory analysis for cocrystal formation. When heating a physical mixture of an API and a coformer in a preferred stoichiometric ratio both components typically undergo two different stages, in which the first is correspondent to the formation of a eutectic phase and the second to the cocrystal melting [6]. This can be confirmed *e.g.* when analyzing curve c of Figure 5.3A. The physical mixture of 1:1 CBZ:NIC (curve c, Figure 5.3B), in this regard, presented another endothermic event at 103°C with a much smaller associated enthalpy (4.0 J/g) preceding the eutectic and cocrystal melting peaks.

Table 5.2. Onset temperatures and enthalpy values of the endothermic events detected in the thermal profiles of the pure components, respective physical mixtures and spray-congealed products.

	Sample (profile ID)	1 st Endothermic Event		2 nd Endothermic Event	
		T (°C)	ΔH (J/g)	T (°C)	ΔH (J/g)
Figure 3A	CAF (a)	139.1	17.3	232.8	109.8
	SAL (b)	156.4	202.1	-	-
	Phy. Mix. (c)	119.4	68.6	132.7	30.4
	Cocrystal (d)	136.32	167.4	N.D.	N.D.
Figure 3B	CBZ (a)	149.6	5.1	186.0	94.12
	NIC (b)	126.3	264.9	-	-
	Phy. Mix. (c)*	122.0	64.5	155.6	99.6
	Cocrystal (d)*	154.2	137.3	N.D.	N.D.

N.D. – not detected;

* Two small thermal events, one before and the other after, the major peak(s) were detected.

According to Chieng *et al.*, this small peak may correspond to an endo-exothermic event associated with a phase transformation [11]. Still, the temperature at which the cocrystal melting occurs can be used as a reference of cocrystal formation. In this work, when comparing the thermal profiles of the physical mixtures and the respective cocrystals, it was observed that the eutectic peaks were absent in the latter but the cocrystal melting peaks appeared within the same temperature range - 133-136°C and 154-156°C for the 1:1 CAF:SAL and 1:1 CBZ:NIC cocrystals, respectively. These results further suggest the high purity of the materials produced by spray congealing.

As mentioned in the Introduction section the 1:1 CBZ:NIC cocrystal presents two polymorphic forms, termed as form I and II. According with Seefeldt *et al.* [13] the thermal profile of the form I cocrystal shows a single endothermic event around 158°C, while form II shows an additional first exothermic peak around 83-90°C correspondent to the phase transformation of form II to form I. Given the results obtained, one can concluded that form I of the 1:1 CBZ:NIC cocrystal was obtained by SCG. Another event was detected in the thermal profiles of the 1:1 CBZ:NIC physical mixture and cocrystal at 227°C (~3.0 J/g). Similarly to the thermal event observed at 103°C (4.0 J/g), this peak may be an endo-exothermic event, which may be related with a phase transformation or even a small recrystallization. However, this event has not been reported by Chieng and co-workers [11].

Finally, the cocrystal melting temperatures were in agreement with the temperatures observed for the same cocrystal systems prepared by different techniques [6,11,12].

XRPD analyses were conducted to further characterize the materials. Figure 5.4A and Figure 5.4B show the XRPD patterns correspondent to the 1:1 CAF:SAL and 1:1 CBZ:NIC cocrystals, respectively. The diffractograms of the pure APIs, coformers, physical mixtures and respective cocrystals obtained from the Cambridge Structural Database (CSD) are also represented [19]. Similarly to the thermal analysis, the XRPD diffractograms for the pure components were equivalent to the ones reported in the literature [6,11,12].

The XRPD diffractograms obtained for the physical mixtures were, as expected, equivalent to the patterns of the pure crystalline starting components. In contrast, when comparing the latter results with the diffractograms of the materials produced by SCG the appearance of new crystalline peaks and an overall decrease in the peak intensities of the characteristic peaks of the pure components was observed. These results corroborated the thermal analysis and confirmed that new crystalline forms were produced by SCG. Moreover, these diffractograms were in agreement with previously reported as well as with the existing data in the CSD.

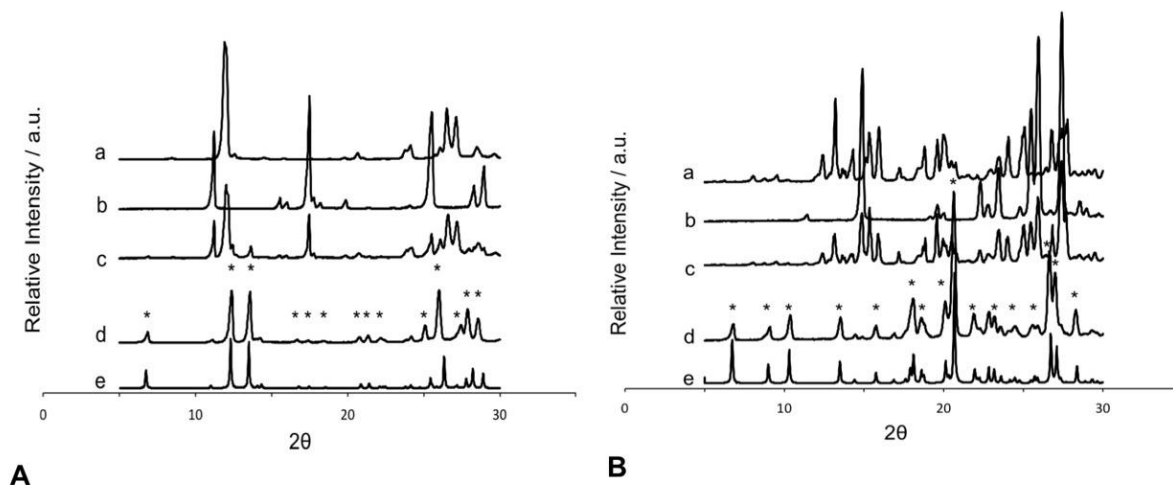


Figure 5.4. Powder diffractograms correspondent of 1:1 CAF:SAL (A) and 1:1 CBZ:NIC (B): a – pure API, b – pure coformer, c – respective physical mixture in the same molar proportion, d – cocrystal obtained by spray congealing, e – cocrystal data obtained from CSD (1:1 CAF:SAL – XOBCAT and 1:1 CBZ:NIC (form I) – UNEZES). CAF and CBZ are considered the APIs and SAL and NIC the coformers.

In relation to particle size and morphology Figure 5.5, A and B, shows the SEM micrographs correspondent to the 1:1 CAF:SAL and 1:1 CBZ:NIC cocrystals, respectively. For both systems, compact and spherical particles were obtained, with a mean circular diameter of

$13.59 \pm 7.85 \mu\text{m}$ for the 1:1 CAF:SAL cocrystal system, and $31.56 \pm 8.08 \mu\text{m}$ for the 1:1 CBZ:NIC. The observation of particles' surface under high magnification (Figure 5.5, A.2 and B.2) revealed that the particles were aggregates of individual cocrystals entangled with or adhered to each other. Both crystalline systems presented a needle-shaped habit, however the 1:1 CAF:SAL cocrystals were more elongated when compared with the 1:1 CBZ:NIC cocrystals.

In order to evaluate the influence of particle morphology on the dissolution kinetics, a simple dissolution test was carried out in acidic medium with the 1:1 CBZ:NIC cocrystal and pure CBZ (data not shown). It was observed that particle morphology did not influence CBZ release into the medium, and similarly to the results obtained by other groups [20,21], the cocrystal showed an enhanced resistance to hydrate formation when compared with pure CBZ, which is an advantage in terms of stability.

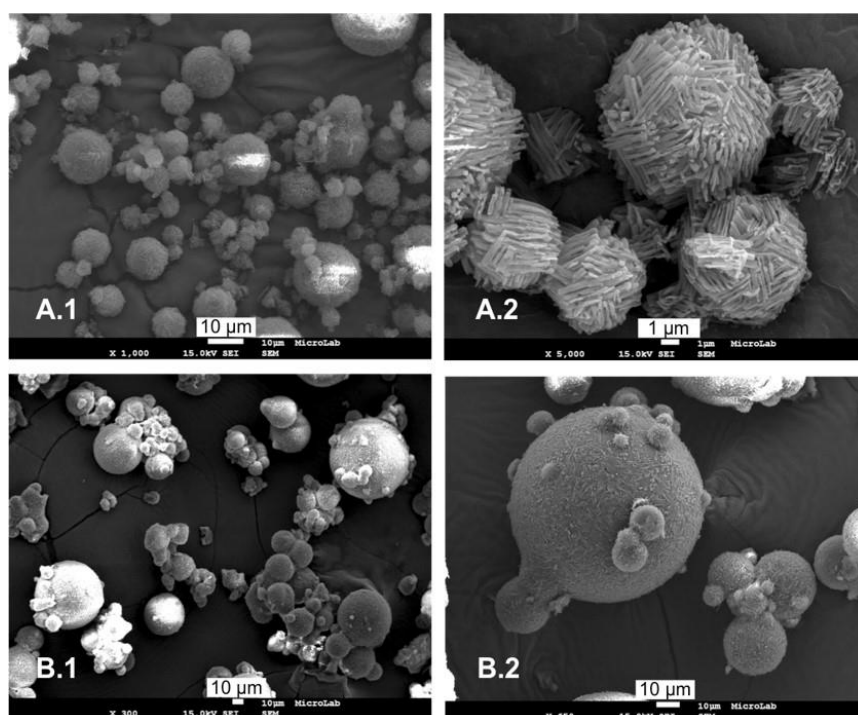


Figure 5.5. Micrographs correspondent of 1:1 CAF:SAL (A) and 1:1 CBZ:NIC (B).

5.3.2 2²+1 Experimental design: particle engineering of 1:1 CAF:GLU cocrystals

Critical process variables associated with SCG include the congealing gas flow rate (F_{gas}), the feed flow rate (F_{feed}), the inlet and outlet temperatures of the congealing gas (T_{in} and T_{out} , respectively) and atomization parameters, such as the nozzle type and orifice diameter and gas flow rate (F_{atom}). In this work the F_{gas} , F_{feed} , nozzle type and orifice diameter were maintained constant, while F_{atom} and the T_{in} of the congealing gas, represented as ΔT , were varied according to the ranges shown in Table 5.1. The F_{atom} and the T_{in} of the congealing gas are two of the most important critical process variables. The former influences the droplet size/particle size, while the latter has direct impact of the cooling stage.

5.3.2.1 Effect of process variables on cocrystal formation and cocrystal purity

Figure 5.6 shows the total heat flow profiles of the 1:1 CAF:GLU physical mixture and the different tests performed.

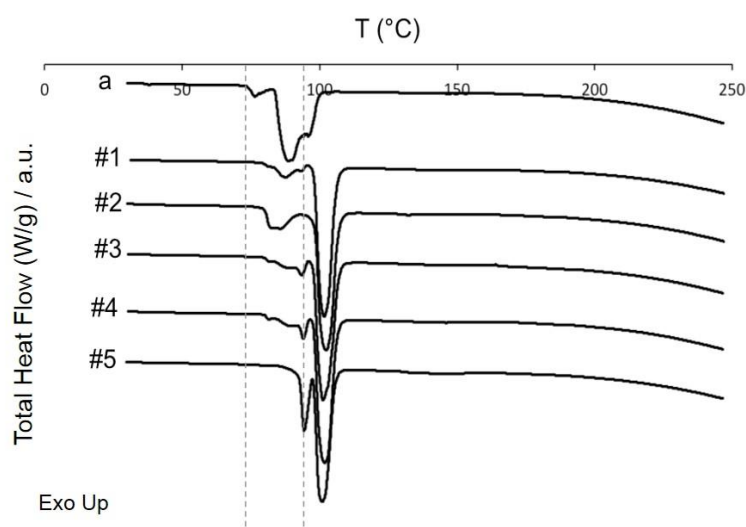


Figure 5.6. Total heat flow profiles correspondent of 1:1 CAF:GLU: a – 1:1 CAF:GLU physical mixture, #1 to #5 –experimental design.

The total heat flow profiles of pure CAF and GLU are represented in Figure 5.3A (curve a) and Supplementary Information D (Figure D.1), respectively. While the thermal analysis correspondent to the pure CAF presented two endothermic peaks, one at 139°C and the other at 233°C (see Section 5.3.1), the endothermic peaks correspondent to pure GLU were observed at

lower temperatures, *i.e.* 70°C and 95°C, which, according to the literature, corresponded to a solid-solid phase transformation followed by melting, respectively [22]. Analyzing the thermal profile of the 1:1 CAF:GLU physical mixture (Figure 5.6, curve a) this showed a first peak at 70°C, most likely correspondent to the phase transformation of pure GLU, the second at 82°C corresponded to the melting of the CAF:GLU eutectic, and the third peak at 94°C to the melting of the cocrystal formed, which agrees with the data reported by Lu *et al.* [6].

Now, when analyzing the thermal analysis of the different spray-congealed materials produced (Figure 5.6, curves #1 to #5) these showed a set of minor endothermic events within the temperature range of 81-93°, followed by a major endothermic peak observed at 98.0 ± 0.3 °C and with an average enthalpy value of 115.0 ± 12.5 J/g. The agreement between the onset temperatures of these major peaks and the onset temperature of the cocrystal melting obtained from the physical mixture, was a first good indicator that cocrystals were formed, and varying the F_{atom} or ΔT during the SCG process had no impact on the formation of 1:1 CAF:GLU cocrystals. The minor endothermic events observed in the thermograms are related with a polymorphic phase transformation characteristic of this cocrystal, as previously mentioned in the Introduction section. The thermal analysis of both polymorphic forms of the 1:1 CAF:GLU cocrystal was recently reported by Vangala *et al.* [23]. They observed that form I of the cocrystal only exhibited a single endothermic peak correspondent to its melting at 99°C, while form II presented two endothermic events – the first around 79-94°C correspondent to the phase transformation of form II to form I, and the second at 99°C correspondent to the melting of form I. Thus, according to the results obtained, one concluded that form II of the 1:1 CAF:GLU cocrystal was consistently produced among tests. The existence of polymorphic cocrystals has increased in the last few years, and the results obtained raised another potential advantage of the SCG process, which is the capacity of achieving polymorphic selectivity from the cooled melt by controlling the kinetics of crystallization.

In what regards the purity of these cocrystals, from the DSC analysis, one believe that high conversion percentages were obtained, since the characteristic peaks of pure CAF were absent in all thermograms. This suggested that most of the CAF was combined with the GLU, forming the cocrystal.

In order to complement the thermal analysis results, Figure 5.7 shows the XRPD diffractograms obtained for the different tests performed (Test 1 to 5) together with the diffractograms of the two polymorphic forms of the 1:1 CAF:GLU cocrystal obtained from the CSD. The XRPD diffractograms of pure CAF and GLU are represented in Figure 5.4A (spectrum a) and Supplementary Information D (Figure D.2), respectively. As can be observed,

the reflections of the different spray-congealed products matched with those already reported for polymorph form II of the 1:1 CAF:GLU cocrystal. These results were aligned with the thermal analysis not only further confirming that cocrystals were formed, but also that the endothermic peaks observed before the cocrystal melting were related to the phase transformation of form II to form I. However, when going into detail in the analysis of the spectra, it was also observed a small reflection at ~ 11.8 2θ in all patterns, with exception of Test 5. When comparing with the diffractograms of the pure components and physical mixture, it was concluded that this reflection corresponded to pure CAF, as its most intense reflection appears at 11.8 2θ . These results were indicative that, in fact, traces of unconverted pure components that were not detected from the thermal analysis existed in the final cocrystal particles obtained from Tests 1 to 4.

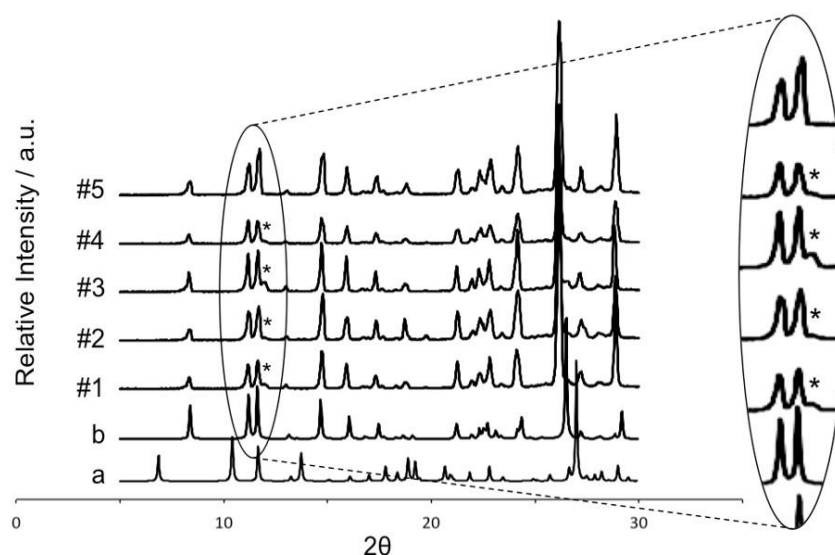


Figure 5.7. XRPD diffractograms correspondent of 1:1 CAF:GLU: a– 1:1 CAF:GLU cocrystal data obtained from CSD, EXUQUJ01 (form I), b– EXUQUJ (form II), #1 to #5 – different tests performed according to the experimental design. The stars in the insert indicate the impurity peaks.

In order to estimate cocrystal purity, a limit test for the CAF “impurity” was developed using XRPD. This method consisted in the comparison of the reflection area at 11.8 2θ either present in (1) a pure cocrystal sample spiked with a known and low concentration of CAF, and (2) the spray-congealed cocrystal samples. The pure form II of 1:1 CAF:GLU cocrystal was obtained from cooling crystallization according to the method reported by Yu *et al.* [17] (see Supplementary Information D), and the limit of quantification of CAF considered was 5 wt.%. The development of this limit test is further explained in detail in the Supplementary Information D (Figure D.5 to D.7).

Table 5.3 summarizes the reflection areas at $11.8\ 2\theta$ measured for the 5 wt.% CAF:standard cocrystal physical mixture, considered as the reference, and for Test 1 to 5, using a slow scan over the 2θ interval from 10° to 14° , in order to improve peak detection. According to the results obtained, the following ranking by descending order of reflection area can be set: Reference>Test 3>Test 1>Test 4>Test 2>Test 5. Taking into account that the reflection area of the reference sample corresponded to 5 wt.% CAF, the results indicated that all the spray-congealed cocrystals showed an amount of unconverted CAF below 5 wt.%, with Tests 3 and 5 presenting the highest and the lowest level of unconverted CAF, respectively. Test 3 presented approximately 5 wt.% of unconverted CAF, while Test 5 was a pure cocrystal comparable with the standard produced by cooling crystallization.

Table 5.3. Reflection areas measured at $11.8\ 2\theta$ for the 5 wt.% CAF:standard cocrystal physical mixture and for the different tests performed.

	Reference	Test 1	Test 2	Test 3	Test 4	Test 5
Reflection area (counts)	14986.1	7914.9	2501.6	14932.9	4238.2	N.D.
wt.% CAF	5	< 5	< 5	< 5	< 5	N.D.

N.D. – not detected

In order to understand the causes behind the different cocrystal purity levels observed, the process variables applied in each test were compared. In this respect, while the ΔT suggested to be a parameter with a positive influence on cocrystal purity, the F_{atom} appears to have had a negative effect. In what regards the effect of ΔT , the results were aligned with our expectations. In Tests 1 and 3, ΔT was set to 0°C , while in Tests 2, 4 and 5, ΔT was set from 25°C to 50°C . At $\Delta T=0^\circ\text{C}$ the molten droplets are cooled and solidified only by means of the decreasing temperature gradient observed inside the congealing chamber, thus slowing down the cooling kinetics. Delayed solidification and/or insufficient cooling may have contributed to the incomplete conversion of pure components in cocrystal, leading to the detection of an “impurity” peak with a higher area in the diffractograms of Tests 1 and 3, when compared with those detected in Tests 2 and 4 or even Test 5. The conversion of the cocrystal into its pure components, due to the loss of residual heat upon storage may also be a possibility as pointed out by Qiyun G [24]. Regarding the possible negative effect of F_{atom} on cocrystal purity, the results did not agree with the expected. The F_{atom} correlates with cocrystal purity since it determines the particle size, and said particle size consequently impacts the droplet/particle

cooling kinetics. In theory, the smaller the particle size of the molten droplet, the higher the cooling efficiency due to the enhanced surface area, and higher the purity of the cocrystal produced. However, when comparing the “impurity” peak areas observed for Tests 3 and 4, run at $F_{\text{atom}}=20$ L/min, with Tests 1 and 2 or even Test 5, run at $F_{\text{atom}}= 11$ and 16 L/min, respectively, the former were indicative of lower cocrystal purity levels. Further discussion regarding the particle size of the cocrystals will be presented in the following section. The generation of a pure cocrystal from Test 5, the central point, was another unexpected result that warrants further study. Nevertheless, this is a good example that pure cocrystals can be obtained by using spray congealing, and cocrystal purity can be optimized by tuning the process variables.

5.3.2.2 Effect of process variables on cocrystal particle size, shape and flowability

Figure 5.8 shows the SEM micrographs correspondent to the different 1:1 CAF:GLU cocrystals produced. To complement, Table 5.4 summarizes the number-based circular equivalent diameter (CED) distributions for the different tests performed, as well as, the compressibility and permeability results.

As can be observed, solid particles were obtained among the different tests performed with $D_{n,50}$ values for CED ranging between 3.8 μm for Test 2 and 6.6 μm for Test 4. Being the particle size mostly determined by the atomization conditions, it was expected to be inversely proportional to F_{atom} , for the same ΔT conditions. However, this was not observed when comparing the CED ($D_{n,50}$) values of Tests 1 - 2 with Tests 3 - 4. In turn, these results may explain the negative correlation obtained between F_{atom} and cocrystal purity as mentioned in Section 5.3.2.1. The cocrystals obtained from Tests 3 - 4 were apparently less pure than the ones obtained from Tests 1 - 2 due to their larger particle size associated with a less efficient cooling.

In terms of circularity all 1:1 CAF:GLU cocrystals produced were identical, however a certain degree of agglomeration between particles was also observed among tests. When evaluating the surface of the particles under higher magnification plate-shaped individual cocrystals, adhered with each other, were observed. The standard 1:1 CAF:GLU cocrystals produced by cooling crystallization were similar in terms of shape (see Figure D.4). Cocrystal particles obtained from Test 3 were an exception in this respect, presenting a spikier surface, with sharp-needle form individual cocrystals.

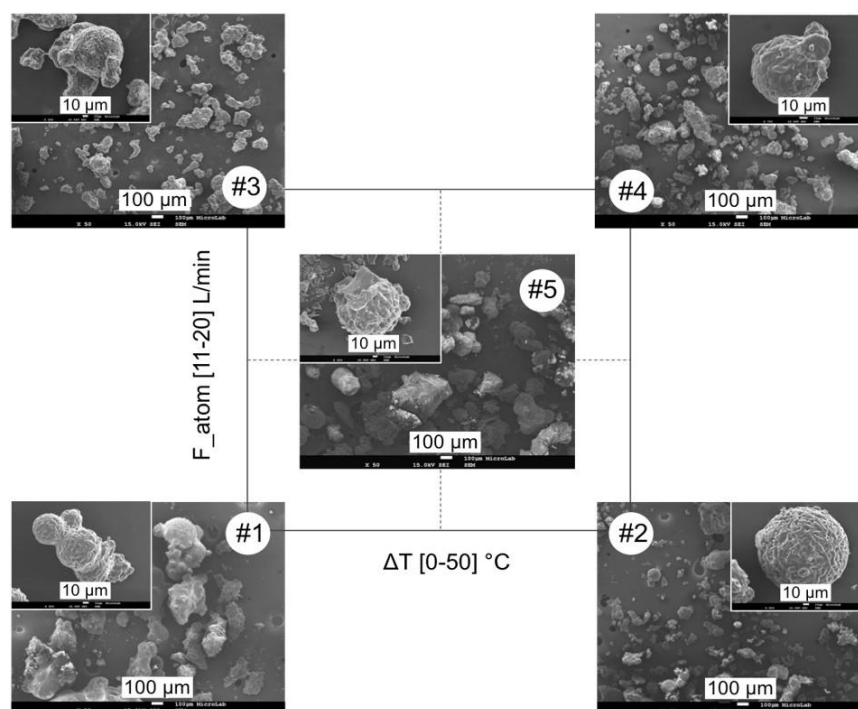


Figure 5.8. SEM micrographs correspondent to the 1:1 CAF:GLU cocrystals obtained.

A possible explanation for the unexpected particle size results obtained may be related with the insufficient cooling power for this specific 1:1 CAF:GLU cocrystal system. Insufficient cooling of the droplets during the spray congealing process itself may have promoted the observed agglomeration between particles, which consequently increased the particle size. Each API-coformer system is unique, and presents its own physicochemical properties while in the molten (*e.g.* viscosity, solidification behavior) and solid states (*e.g.* level of crystallinity, crystal shape). For example, when comparing these results with the ones obtained for the system 1:1 CAF:SAL - same API, but different coformer - a ΔT equal to 50°C showed to be sufficient to cool and solidify single and perfectly spherical particles with a high purity level. Probably the minimum cooling requirements for the 1:1 CAF:GLU system should be above $\Delta T=50^{\circ}\text{C}$.

The compressibility and permeability tests provided information on the powder's level of cohesiveness and flowability behavior, with relevance *e.g.* in processes of gravity feeding in tableting machines. The powder from Test 5 stands out for being the less compressible and also appears to have the lowest pressure drop. Powders presenting low compressibility and low-pressure drop are generally non-cohesive or free flowing, due to the large particle size, and are linked to good tableting performance. Thus, when compared with the powders from Test 1 and Tests 2, 3 and 4, the powder from Test 5 was suggested to have superior downstream processing

properties, namely in tableting, thus presenting less potential for weight variability issues during filling, but also potentially lower probability of capping and lamination during compression.

Table 5.4. Number-based circular equivalent diameter distribution ($D_{n,50}$), compressibility and pressure drop across the powder bed for Test 1 to Test 5.

	Test 1	Test 2	Test 3	Test 4	Test 5
Circular equivalent diameter, $D_{n,50}$ (μm)	4.10	3.82	4.66	6.61	5.93
Compressibility @ 15 kPa (%) *	19.60	28.94	25.94	31.37	6.53
Pressure drop across the powder bed @ 15 kPa and 2 mm/s (mbar) **	0.17	0.42	0.37	0.34	0.04

* The compressibility percentage represents the increase in bulk density at a specified normal stress, in this case at 15 kPa; ** The pressure drop across the powder bed is a measure of how easily a powder can transmit air through its bulk at a specified normal stress, in this case at 15 kPa.

5.4 Conclusions

The results obtained with 1:1 CAF:SAL and 1:1 CBZ:NIC successfully demonstrated the feasibility of spray congealing to produce pharmaceutical cocrystals. The DSC and XRPD results of the spray-congealed products were different from the pure components or physical mixtures and were aligned with those reported for the same cocrystals systems produced by other techniques. Cocrystal particles were compact and spherical consisting of aggregates of individual cocrystals entangled or adhered with each other. From the DoE study, it was concluded that cocrystal formation was independent from ΔT and F_{atom} , but varying both parameters suggested to influence cocrystal purity. Moreover, it was demonstrated that cocrystal particle properties (*i.e.* purity, size, shape, flow properties) can be adjusted, *in situ*, by varying ΔT and F_{atom} .

When compared with typical solvent- or mechanochemical-based processes (*e.g.* reaction crystallization, neat or liquid-assisted grinding, spray drying) to produce cocrystals, spray congealing is a “green” and cost-effective method, easy scalable, compatible with continuous pharmaceutical processes and, most importantly, it allows particle engineering of pharmaceutical cocrystals in a single stage operation without the need for any downstream

processing. Particle properties can be fine-tuned, allowing for optimization of powder properties, which in turn results in more efficient pharmaceutical processes.

5.5 References

- [1] I. Ilić *et al.*, "Microparticle size control and glimepiride microencapsulation using spray congealing technology" *International Journal of Pharmaceutics*, vol. 381, pp. 176-183, 2009.
- [2] T. Yajima *et al.*, "Particle Design for Taste-Masking Using a Spray-Congealing Technique" *Chemical Pharmaceutical Bulletin*, vol. 44, no. 1, pp. 187-191, 1996.
- [3] N. Passerini *et al.*, "Controlled release of verapamil hydrochloride from waxy microparticles prepared by spray congealing" *Journal of Controlled Release*, vol. 88, pp. 263–275, 2003.
- [4] P. Cordeiro, M. Temtem, and C. Winters, "Spray congealing: applications in the pharmaceutical industry" *Chimica Oggi - Chemistry Today*, vol. 31, no. 5, pp. 69-72, 2013.
- [5] J. A. Baird, B. Van Eerdbernard, and L. S. Taylor, "A Classification System to Assess the Crystallization Tendency of Organic Molecules from Undercooled Melts" *Journal of Pharmaceutical Sciences*, vol. 99, no. 9, pp. 3787-3806, 2010.
- [6] E. Lu, N. Rodríguez-Hornedo, and R. Suryanarayanan, "A rapid thermal method for cocrystal screening" *CrystEngComm*, vol. 10, pp. 665–668, 2008.
- [7] G. G. Z. Zhang, R. F. Henry, T. B. Borchardt, and X. Lou, "Efficient Co-crystal Screening Using Solution-Mediated Phase Transformation" *Journal of Pharmaceutical Sciences*, vol. 96, no. 5, pp. 990-995, 2007.
- [8] D.-K. Bučar *et al.*, "Cocrystals of Caffeine and Hydroxybenzoic Acids Composed of Multiple Supramolecular Heterosynthons: Screening via Solution-Mediated Phase Transformation and Structural Characterization" *Crystal Growth & Design*, vol. 9, no. 4, pp. 1932–1943, 2009.
- [9] S. G. Fleischman *et al.*, "Crystal Engineering of the Composition of Pharmaceutical Phases: Multiple-Component Crystalline Solids Involving Carbamazepine" *Crystal Growth & Design*, vol. 3, no. 6, pp. 909-919, 2003.

- [10] N. Rodríguez-Hornedo, S. J. Nehm, K. F. Seefeldt, Y. Pagán-Torres, and C. J. Falkiewicz, "Reaction Crystallization of Pharmaceutical Molecular Complexes" *Molecular Pharmaceutics*, vol. 3, no. 3, pp. 362-367, 2005.
- [11] N. Chieng, M. Hubert, D. Saville, T. Rades, and J. Aaltonen, "Formation Kinetics and Stability of Carbamazepine-Nicotinamide Cocrystals Prepared by Mechanical Activation" *Crystal Growth & Design*, vol. 9, no. 5, pp. 2377-2386, 2009.
- [12] X. Liu *et al.*, "Improving the Chemical Stability of Amorphous Solid Dispersion with Cocrystal Technique by Hot Melt Extrusion" *Pharmaceutical Research*, vol. 29, pp. 806-817, 2012.
- [13] K. Seefeldt, J. Miller, F. Alvarez-Núñez, and N. Rodríguez-Hornedo, "Crystallization Pathways and Kinetics of Carbamazepine–Nicotinamide Cocrystals From the Amorphous State by In Situ Thermomicroscopy, Spectroscopy and Calorimetry Studies" *Journal of Pharmaceutical Sciences*, vol. 96, no. 5, pp. 1147-1158, 2007.
- [14] W. W. Porter III, S. C. Elie, and A. J. Matzger, "Polymorphism in Carbamazepine Cocrystals" *Crystal Growth & Design*, vol. 8, no. 1, pp. 14-16, 2008.
- [15] A. V. Trask, W. D. Samuel Motherwell, and W. Jones, "Solvent-drop grinding: green polymorph control of cocrystallisation" *Chemical Communications*, pp. 890-891, 2004.
- [16] A. Alhalaweh and S. P. Velaga, "Formation of Cocrystals from Stoichiometric Solutions of Incongruently Saturating Systems by Spray Drying" *Crystal Growth & Design*, vol. 10, no. 8, pp. 3302-3305, 2010.
- [17] Z. Q. Yu, P. S. Chow, and R. B. H. Tan, "Operating Regions in Cooling Cocrystallization of Caffeine and Glutaric Acid in Acetonitrile" *Crystal Growth & Design*, vol. 10, no. 5, pp. 2382-2387, 2010.
- [18] A. V. Trask, W. D. Samuel Motherwell, and W. Jones, "Pharmaceutical Cocrystallization: Engineering a Remedy for Caffeine Hydration" *Crystal Growth & Design*, vol. 5, no. 3, pp. 1013-1021, 2005.
- [19] F. H. Allen, "The Cambridge Structural Database: a quarter of a million crystal structures and rising" *Acta Crystallographica B*, vol. 58, pp. 380-388, 2002.
- [20] S. P. Patil, S. R. Modi, and A. K. Bansal, "Generation of 1:1 Carbamazepine:Nicotinamide cocrystals by spray drying" *European Journal of Pharmaceutical Sciences*, vol. 62, no. 1, pp. 251-257, October 2014.

- [21] Z. Rahman, C. Agarabi, A. S. Zidan, S. R. Khan, and M. A. Khan, "Physico-mechanical and Stability Evaluation of Carbamazepine Cocrystal with Nicotinamide" *AAPS PharmSciTech*, vol. 12, no. 2, pp. 693-704, June 2011.
- [22] D. P. McNamara *et al.*, "Use of a Glutaric Acid Cocrystal to Improve Oral Bioavailability of a Low Solubility API" *Pharmaceutical Research*, vol. 23, no. 8, pp. 1888-1897, 2006.
- [23] V. R. Vangala, P. S. Chow, M. Schreyer, G. Lau, and R. B. H. Tan, "Thermal and in Situ X-ray Diffraction Analysis of a Dimorphic Co-Crystal, 1:1 Caffeine-Glutaric Acid" *Crystal Growth & Design*, 2015, DOI: 10.1021/acs.cgd.5b00798.
- [24] G. Qiyun, "A Study of Factors Affecting Spray-Congeaed Micropellets for Drug Delivery", PhD Thesis, Department of Pharmacy, National University of Singapore, 2007.

Chapter 6

6 Conclusions and future work

On the development of ASDs, both the drug's chemical/physical stability and the *in vivo* performance are among the most important critical quality attributes (CQAs). Critical formulation variables that may impact these parameters include the selection of the right polymeric carrier and the definition of the drug load in formulation. This is reason why the early selection of critical formulation and process variables is of utmost importance to prevent late-stage development failures due to drug-polymer incompatibility or drug recrystallization.

In this work, two computational screening tools, one to predict amorphous physical stability and the other to predict *in vivo* performance were developed. The computational tool for predicting drug-polymer physical stability was reported to support the development of spray-dried dispersions and considers drug-polymer miscibility thermodynamics, solid-liquid and solid-solid diffusion and solvent evaporation. The model allowed to challenge both formulation and drying process variables simultaneously - an advantage over commonly applied approaches that allow an evaluation of drug-polymer miscibility thermodynamics as a function of temperature. The model showed to be useful for obtaining a preliminary physical stability or drug-polymer miscibility assessment, indicating the lower/higher propensity for amorphous phase separation of a drug with different stabilizing carriers at different drug loadings. Still, the predictions obtained should be evaluated in the light of the limitations of the model. In order to improve the predictive capacity of this tool, advanced (sub) models to describe the drug-polymer thermodynamics of mixing, the component's diffusion and the evaporation rate during particle formation should be considered. For example, the Flory-Huggins (F-H) thermodynamic lattice model does not account for important specific molecular interactions, such as hydrogen bonding or ionic interactions that are known for having a significant impact on the thermodynamics of mixing and miscibility. The F-H interaction parameter (χ) itself, apart from depending on the structure of the molecular components, also depends on temperature, component's composition, and polymer molecular weight. The implementation of more advanced models to describe the thermodynamics of mixing [*e.g.* Perturbed-chain statistical associating fluid theory (PS-SAFT)] should also be evaluated. In the case of the kinetics of diffusion, a more complex formalism should be implemented to account for component's precipitation, particle's external shell formation, and the increasing viscosity of the solution/solid as this is being dried. The diffusivity of the drug-polymer-solvent system is a relevant physical attribute for controlling phase homogeneity. Finally, and in what accounts

the evaporation model, an upgrade should be made in order to consider the use of binary solvent mixtures and the relative evaporation rate of the solvents with different vapor pressures. By combining such complex (sub) models, the computational processing capacity and simulation time can significantly increase. The benefit-cost ratio should be evaluated according to the stage of process development, as *e.g.* during the screening phase quick estimates are preferred.

Regarding the computational tool to guide polymer selection aiming the optimization of the *in vivo* performance of an ASD, this consisted on the development of a statistical model using multivariate data analysis tools, and based on ASDs past history. The input variables were general molecular descriptors of the drugs, polymers and drug-polymer interactions. These simple molecular descriptors can be simply computed based on the molecular structure of the components and have been used/identified in the literature as important variables for describing *e.g.* drug's bioavailability and polymer precipitation inhibition capacity. As output variables, typical *in vivo* pharmacokinetic parameters obtained from the literature were considered. The model allowed to identify some interesting correlations between the molecular descriptors of the formulation components and performance related output variables. Polymers presenting higher hydrogen bonding capacity and higher solubility parameters seem to contribute for higher *in vivo* performances. Moreover, cellulose-based polymers seem to provide better precipitation inhibition across different classes of APIs, when compared with other polymer families. Correlations obtained between the molecular descriptors of the drug and the output variables were more difficult to interpret. Among the drug-polymer interaction variables considered, the ones that appeared as having most influence on the model, were similarly difficult to interpret. Indeed, the accuracy of the correlations obtained from a statistical model is highly dependent on the quality, size and diversity of the input dataset and the complexity of the molecular descriptors selected. The fact that the model was developed based on data obtained from the literature, adds a certain degree of uncontrolled variability into the system that may impact the accuracy of the model developed.

All in all, and despite the identified limitations of the screening methodologies developed, combining the information obtained from both models, it is possible to successfully rank the best polymers for amorphous drug stabilization, both in the solid-state and in solution, as well as to narrow down the drug load range for an optimal concentration window to be tested in the following stages of formulation development, using *e.g.* miniaturized/bench screening methodologies.

Another objective of this thesis, was the development of alternative preparation methods for the production of amorphous solid dispersions and pharmaceutical cocrystals with unique

particle properties. A solvent controlled precipitation technology based on microfluidization with potential to produce amorphous dispersions in the nano-range was assessed. The feasibility study was successfully demonstrated and nano-solid dispersions (both amorphous and crystalline) showed to be an advantage for drugs presenting dissolution-rate limited absorption, when compared with spray dried dispersions. Additionally, an evaluation focused on the impact of certain formulation variables on the final ASD was performed. For example, it was observed that level of aggregation between nanoparticles, after the isolation step, was dependent on the drug load in formulation, while the feed solids' concentration in solution influenced the particle size of the nanocomposite aggregates. However, there are other formulation and process variables that are also known to affect the final product. Thus, as future work, other formulation variables such as the type of solvent and anti-solvent and the solvent-anti-solvent ratio, as well as process variables such as working pressure and mixing conditions should be evaluated in order to get an improved understanding of the factors affecting the final critical quality attributes of co-precipitated ASDs. The possibility of extending the co-precipitation process to non-ionic or immediate release polymers should also be evaluated, as in this work only enteric polymers were evaluated. This would also enable to reduce the constraints of solubility compatibility between the drug and the polymer in the same solvent system and the possibility to increase the solid's concentration in the feed solution.

On the solubility enhancement field, the use of pharmaceutical cocrystals has been drawing the attention of formulators in the last years. In this work, spray congealing was assessed as an alternative preparation method to produce cocrystals. Spherical cocrystals particles with high purity were obtained, and by varying the process conditions, particle properties can be fine-tuned in order to facilitate their incorporation into the final-dosage forms. Still, the improved understanding of the thermodynamics and kinetics of crystallization from the undercooled melt would be beneficial to extend the applicability of the technology for any drug compound. For example, there are APIs with a greater tendency to turn amorphous during the cooling step. Difficult to crystallize APIs are more easily cocrystallized via solution-based methods due to the presence of solvents/moisture that may enhance chemical reactivity and promote cocrystallization. The manipulation of the spray congealing process variables in order to produce cocrystals from difficult to crystallize molecules should be further explored. Similarly, the capacity of achieving polymorphic selectivity from the undercooled melt via spray congealing is another potential advantage of the process that should be further evaluated.

In conclusion, it can be said that all the objectives proposed were successfully achieved, namely on contributing for the development of novel screening methodologies and alternative

production methods for the production of ASDs and pharmaceutical cocrystals, thus demonstrating the Thesis Hypothesis formulated at the beginning of the work.

Supplementary Information

Supplementary Information

A. Chapter 2

- Melting point depression studies to determine χ_{dp} at T_M of ITZ:

Crystalline ITZ and the polymers were dried in a tray dryer oven at 40°C under vacuum during 24h before use. Physical mixtures of ITZ and each polymer were prepared by co-grinding via mortar pestle, during 5 min to obtain a fine and homogenous powder. The concentration range of the physical mixtures produced varied from 15% to 35% (w/w) of polymer (total weight of 0.2 g). Physical mixtures with a concentration of polymer below 15% (w/w) were not tested, because it is usually observed a nonlinear relationship between χ and $1/T$ in such range [1, 2]. Triplicates were prepared at each concentration. Powders were sieved using a 220 μm mesh screen and solids collected analyzed through conventional differential scanning calorimetry (DSC Q1000, TA Instruments, New Castle, Delaware, USA) for ITZ melting temperature measurement. The scan rate used was 1°C/min and the end points of melting were obtained from the DSC thermograms [1, 2]. Figure A.1, Figure A.2 and Figure A.3 show the melting temperature of ITZ as a function of decreasing ITZ composition for the different physical mixtures prepared.

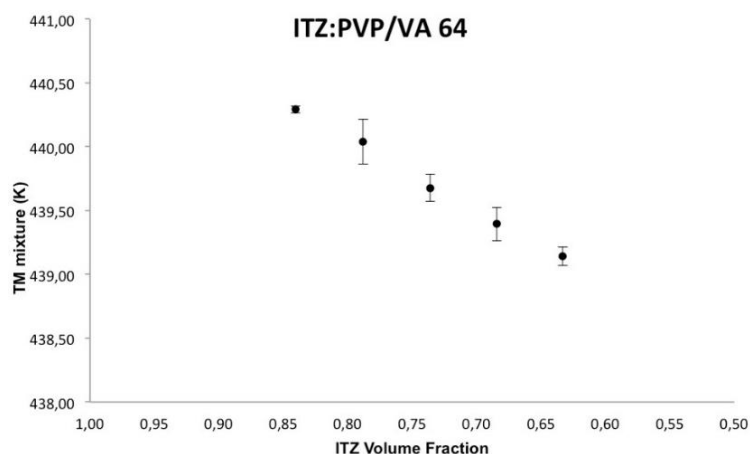


Figure A.1. Offset of the melting point temperature of ITZ and PVP/VA 64 physical mixture. Bars represent the standard deviation ($n=3$).

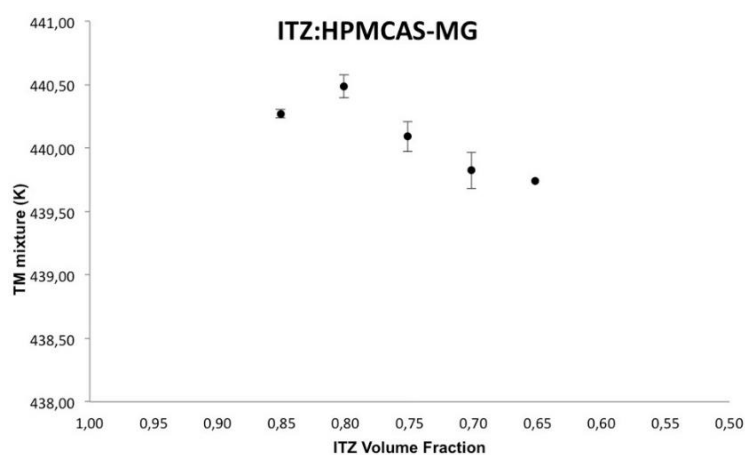


Figure A.2. Offset of the melting point temperature of ITZ and HPMCAS-MG physical mixture. Bars represent the standard deviation (n=3).

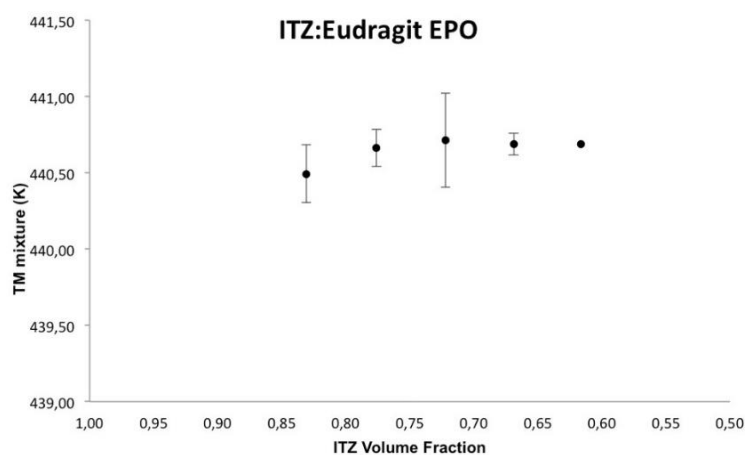


Figure A.3. Offset of the melting point temperature of ITZ and Eudragit[®] EPO physical mixture. Bars represent the standard deviation (n=3).

- Analytical characterization of ITZ-based cast films:

Cast films were analyzed by modulated differential scanning calorimetry (mDSC), using a heating ramp from -10°C to 250°C at a heating rate of $5^{\circ}\text{C}/\text{min}$ using a period of 60s and amplitude of 1.592°C .

The results given by thermal analysis of the cast films are presented in Table A.1.

Table A.1. Glass transition temperature values (T_g) and indicators of phase-separation observed after analysis of the solvent casted films.

Composition/ % ITZ (w/w)	Key Indicators of Miscibility/Phase-separation			
	$T_g \pm$ s.d (°C)	Mesophase?	Crystallization \pm s.d (°C)	Melting \pm s.d (°C)
ITZ:HPMCAS-MG				
10	91.0 \pm 8.0	No	-	-
15	95.1 \pm 5.5	No	-	-
35	57.9 \pm 7.5	No	-	-
45	56.0 \pm 5.3	No	-	-
65	N.D.	No	-	151.6 \pm 1.2
85	62.1 \pm 3.2	No	111.2 \pm 8.4	156.2 \pm 1.5
ITZ:PVP/VA 64				
10	N.D.	N.D.	N.D.	N.D.
15	N.D.	N.D.	N.D.	N.D.
35	N.D.	N.D.	N.D.	N.D.
45	82.3 \pm 5.4	No	-	-
65	69.8 \pm 0.5	No	119.1 \pm 10.2	152.4 \pm 2.0
85	62.5 \pm 0.7	No	120.6 \pm 2.4	159.1 \pm 0.2
ITZ:Eudragit [®] EPO				
10	47.0 \pm 1.2	No	-	-
15	48.6 \pm 2.6	No	-	-
35	51.1 \pm 1.5/60.7 \pm 0.5	Yes	-	-
45	54.5 \pm 5.8/63.4 \pm 5.0	Yes	122.2 \pm 3.0 ^a	161.8 \pm 5.5
65	59.2 \pm 2.2	Yes	118.5 \pm 2.8	160.2 \pm 0.8
85	61.8 \pm 0.7	Yes	112.0 \pm 3.5	161.1 \pm 0.7

s.d: standard deviation (n=3); N.D: not detected

^a n=2;

- Analytical characterization of ITZ-based spray dried dispersions:

Spray dried amorphous dispersions were also analyzed by mDSC, using a heating ramp from -10°C to 250°C at a heating rate of 5°C/min using a period of 60s and amplitude of 0.8°C. In addition, PLM was used to infer about the presence of starting crystalline material in the freshly prepared powders. The absence of interference colors is indicative of an amorphous material. The results given by thermal analysis and microscopy of the spray-dried powders are summarized in Table A.2 and Table A.3.

Table A.2. Glass transition temperature values (T_g), indicators of phase-separation and indication of birefringence between crossed polarizers after analytical characterization of the spray-dried powders.




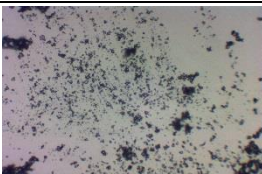
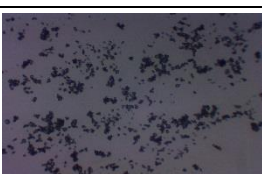
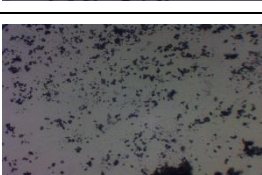
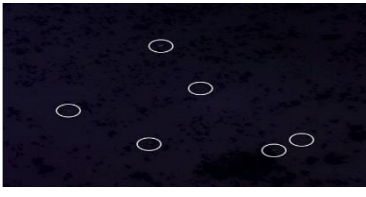
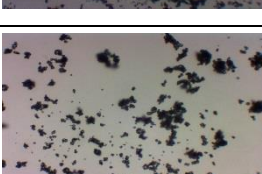
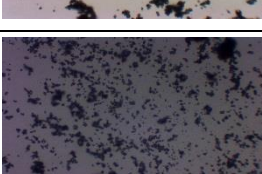
Composition/ % ITZ (w/w)	Key Indicators of Miscibility/Phase-separation				
	$T_g \pm$ s.d (°C)	Mesophase?	Crystallization \pm s.d (°C)	Melting \pm s.d (°C)	Birefringence?
ITZ:HPMCAS-MG					
45	80.9±1.8	No	-	-	No
65	72.1±0.2	No	123.5±1.4	155.4±0.3	No
ITZ:PVP/VA 64					
45	87.1±1.7	No	-	-	No
65	75.4±1.1	No	-	-	No
85	64.7±0.7	No	113.4±0.2	163.1±2.8	Yes
ITZ:Eudragit® EPO					
15	52.1±0.7	No	-	-	No
35	52.5±0.7	Yes	117.7±1.1	154.6±0.3	No

s.d: standard deviation (n=3);

References

- [1] Y. Tian, J. Booth, E. Meehan, D. S. Jones, S. Li, and G. P. Andrews, “Construction of Drug-Polymer Thermodynamic Phase Diagrams Using Flory-Huggins Interaction Theory: Identifying the Relevance of Temperature and Drug Weight Fraction to Phase Separation within Solid Dispersions” *Molecular Pharmaceutics*, vol. 10, pp. 236-248, 2013.
- [2] D. Lin and Y. Huang, “A thermal analysis method to predict the complete phase diagram of drug-polymer solid dispersions” *International Journal of Pharmaceutics*, vol. 399, no. 1-2, pp. 109-115, 2010.

Table A.3. Pure ITZ and respective spray-dried powders analyzed through PLM.

Composition	wt.% ITZ	Bright Field (10x)	Polarized Light	Comment
Pure ITZ	100	-		Crystalline
ITZ:HPMCAS-MG	45		Completely Dark Field	Amorphous
ITZ:HPMCAS-MG	65		Completely Dark Field	Amorphous
ITZ:PVP/VA 64	45		Completely Dark Field	Amorphous
ITZ:PVP/VA 64	65		Completely Dark Field	Amorphous
ITZ:PVP/VA 64	85			Crystalline
ITZ:Eudragit® EPO	15		Completely Dark Field	Amorphous
ITZ:Eudragit® EPO	35		Completely Dark Field	Amorphous

B. Chapter 3

- Score plot of the 1st PCA - outliers identification:

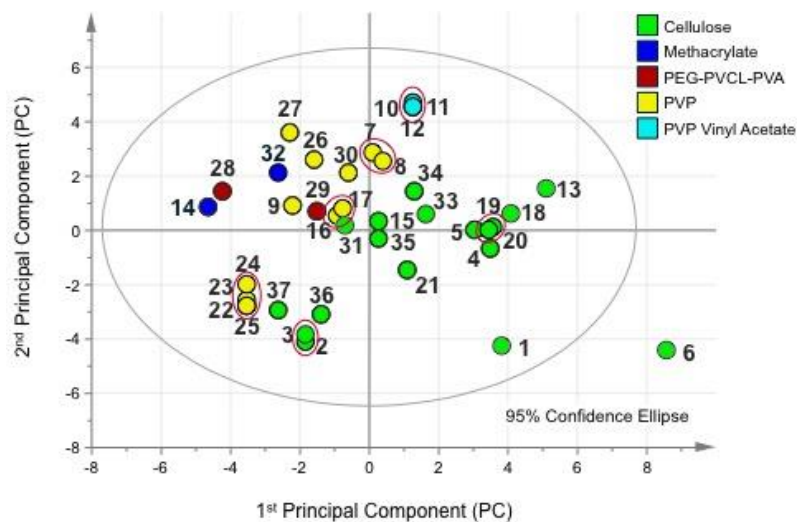


Figure B.1. Score plot of the first PCA performed.

- Contribution Plot – Observation 6:

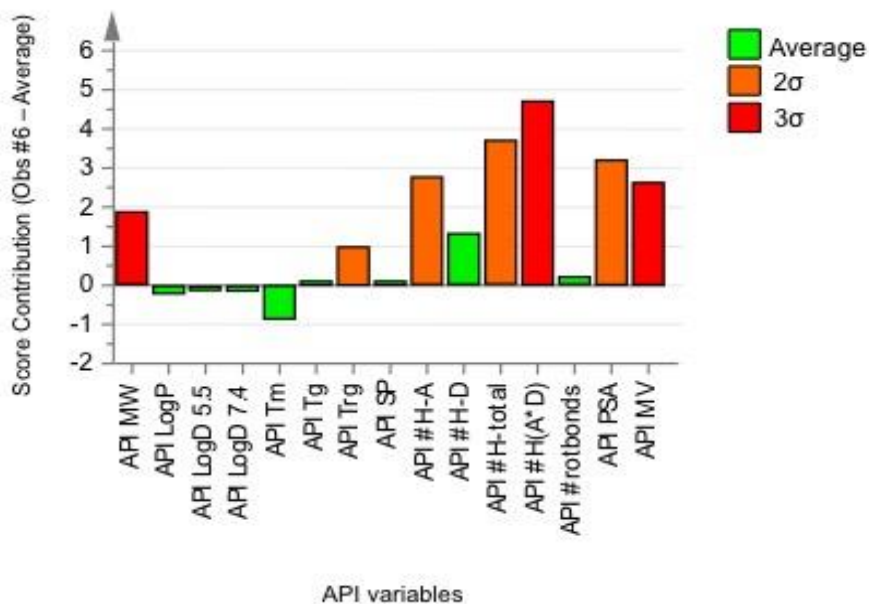


Figure B.2. Contribution plot: API – Tacrolimus.

C. Chapter 4

- Thermal analysis of the CBZ-based co-precipitated products (Tests 1 to 6):

Regarding the thermal analysis of the CBZ-based co-precipitated products, Table C.1 summarizes the results obtained.

Table C.1. Thermal analysis of the different co-precipitated products (Tests 1 to 6): glass transition temperature (T_g) and change in heat capacity (ΔC_p) during glass transition, temperature (T) and enthalpy (ΔH) of other endothermic events detected.

Exp. Number	Glass Transition		Other Endo. Peaks	
	T_g (°C)	ΔC_p (J/g °C)	T (°C)	ΔH (J/g)
1	101,73	0,11	144,98	25,43
2	N.D.	N.D.	167,31	69,96
			187,59	132,80
3	N.D.	N.D.	148,60	38,31
			187,39	53,99
4	166,80	0,20	198,20	0,54
5	136,44	0,21	150,45	1,25
			164,10	60,03
6	N.D.	N.D.	139,76	24,20
			182,02	50,49

N.D. – not detected.

Starting with the 20% (w/w) drug load formulations, both CBZ:HPMCAS and CBZ:Eudragit[®] L100 systems presented a single T_g value which was consistent with the averaged mixed T_g obtained using the Gordon-Taylor equation (~106 and ~167 °C for Test 1 and 4, respectively). These results suggested that amorphous dispersions or amorphous solutions were formed. No signs of phase-separation or drug recrystallization were detected during heating, but different endothermic events were observed. For example, in the thermal profile of 20% CBZ: HPMCAS, an endothermic peak at 145°C was observed. The existence of an endothermic event without the observation of a prior exothermic recrystallization may indicate the presence of starting crystalline material in the sample.

For the 20% CBZ:Eudragit® L100 an endothermic peak around 190°C was also detected, but this was most probably related with the cyclic anhydride formation between Eudragit® L100 polymer chains [1].

Moving forward with the thermal analysis of the 40% CBZ:HPMCAS and CBZ:Eudragit® L100 systems, while for the former any glass transition events were detected, the latter presented a T_g value at 136,44°C, which by comparison with the value obtained by the Gordon-Taylor equation (~141°C), it may correspond to a mixed T_g .

The endothermic peaks that appeared in both thermal profiles and within the temperature ranges ~150-167°C and ~164 to 188°C were coincident with two endothermic peaks characteristic of pure CBZ. Pure CBZ first presents a polymorphic transformation at 150°C, followed by the melting of the new phase formed at 186°C [2]. Temperature fluctuations are normal to happen due to the presence of the polymers. These results were indicative that both Tests 2 and 5 resulted in crystalline suspensions of CBZ within the respective polymers, still with the possibility of Test 5 to present a certain percentage of amorphous CBZ.

When the drug load of both CBZ-based formulations was increased to up 60%, no glass transition events were observed. Moreover, the endothermic events associated with the phase transformation and/or melting of crystalline CBZ were still presented in the respective non-reversible heat flow curves. Similarly to the results obtained for Test 2 and 5, Test 3 and 6 also corresponded to crystalline suspensions.

- Spray-dried amorphous dispersion, equivalent to Test 4:

Figure C.1 shows the XRPD results obtained for the co-precipitated product and respective spray-dried formulation.

As can be observed, both diffractograms were equivalent. The spray-dried formulation also exhibited the typical halo characteristic of the amorphous state, and no signs of crystalline material were detected. In terms of drug molecular distribution within the polymeric matrix, the thermal analysis of the spray-dried product only revealed a single glass transition at 160°C, which also agreed with the thermal behavior of its co-precipitated counterpart. These results indicated that the 20% CBZ:Eudragit® L100 spray-dried product was also an amorphous solid solution.

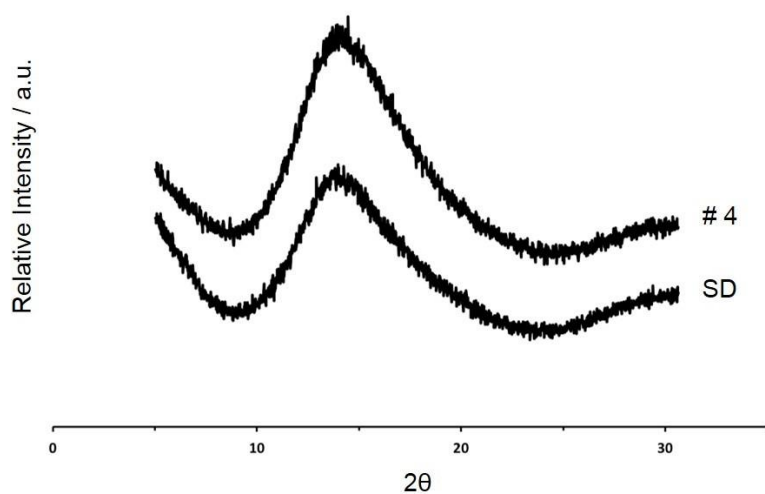


Figure C.1. Powder diffractograms correspondent to the 20% CBZ:Eudragit[®] L100 co-precipitated product (Test 4) and the 20% CBZ:Eudragit[®] L100 spray-dried product, at C_{feed} 8% (w/w).

- *NanoCrystalline* solid dispersion by solvent controlled precipitation:

Figure C.2 shows the XRPD result for the 60% CBZ:Eudragit[®] L100 at 8% C_{feed}, produced by co-precipitation. The XRPD correspondent to Test 6 (60% CBZ:Eudragit[®] L100, at 2% C_{feed}) is also represented for comparison purposes.

As can be observed, the XRPD diffractogram of the *NanoCrystalline* formulation was equivalent to Test 6. The characteristic peaks of crystalline CBZ were detected, indicating the formation of a crystalline solid dispersion.

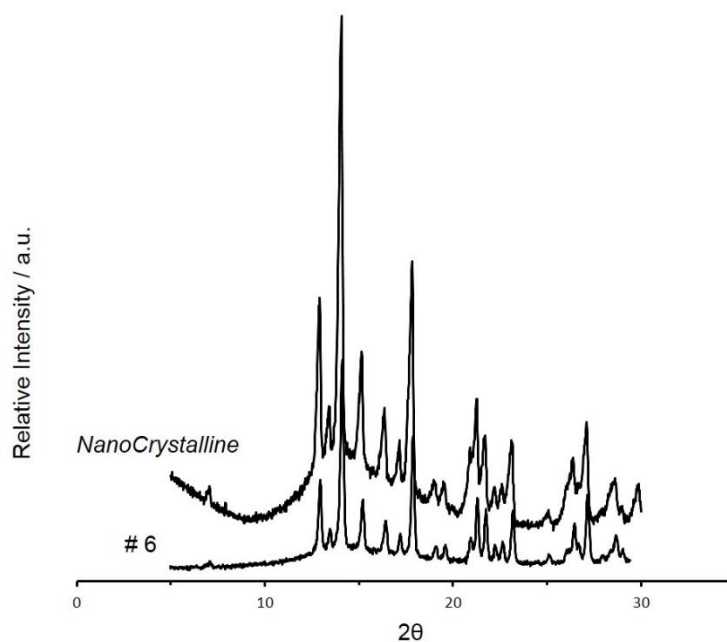


Figure C.2. Powder diffractograms correspondent to the 60% CBZ:Eudragit[®] L100 at 2% C_{feed} (Test 6) and the 60% CBZ:Eudragit[®] L100 at 8% C_{feed} (*NanoCrystalline*).

References

- [1] S.-Y. Lin, “Temperature-dependent anhydride formation of Eudragit L-100 films determined by reflectance FTi.r./d.s.c. microspectroscopy” *Polymer*. vol. 36, no. 16, pp. 3239-3241, 1995.
- [2] A. L. Grzesiakg, M. Lang, K. Kim and A. J. Matzger, “Comparison of the four anhydrous polymorphs of carbamazepine and the crystal structure of form I” *Journal of Pharmaceutical Sciences*. vol. 92, no. 11, pp. 2260-2271, 2003.

D. Chapter 5

- mDSC thermal analysis and XRPD profile of pure glutaric acid (GLU):

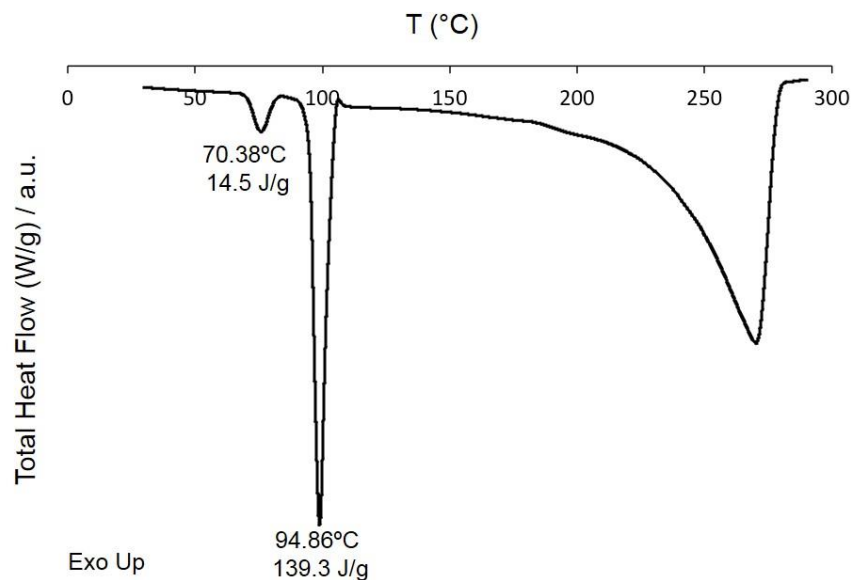


Figure D.1. Total heat flow thermogram correspondent to pure GLU. The onset temperatures and enthalpy values associated to the endothermic events are also indicated.

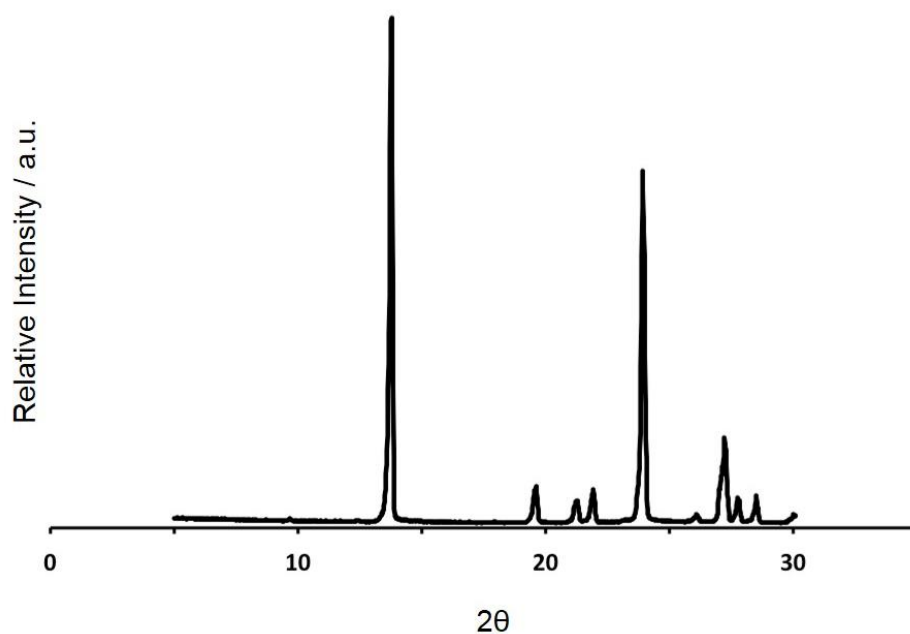


Figure D.2. XRPD diffractogram correspondent to pure GLU.

- Production of standard 1:1 CAF:GLU cocrystal using cooling recrystallization:

The cooling crystallization method employed to produce form II of the 1:1 CAF:GLU cocrystal was based on the work of Yu *et al.* [1]. According to the phase diagram of the CAF-GLU-acetonitrile (ACN) system reported and the crystallization method described, the critical step was to find the composition of the starting solution correspondent to “Run 1”, which led to the formation of form II of the cocrystal.

18.9 g of pure GLU (purity 99%, Sigma-Aldrich Quimica SA) and 12.6 g of pure CAF (β -caffeine anhydrous, purity 99%, Sigma-Aldrich Quimica SA) were dissolved in 250 mL of ACN, at 40°C. A 250 mL jacketed glass reactor with mechanical stirring at 410 rpm was used. The temperature in the reactor was controlled using a Huber thermostat. A silicone-based heat transfer fluid (SYLTHERM XLT, Dow Chemical Co.) circulated inside the jacket of the reactor. Temperature was cooled down from 40°C to 34°C quickly. No cocrystal seeds were added. Precipitation onset was observed. The suspension was cooled further down to 10 °C at 0.1 °C/min. The solid was isolated by filtration.

Figure D.3 shows the XRPD diffractogram obtained for the cocrystal obtained from cooling crystallization together with the diffractogram of the polymorphic form II of the 1:1 CAF:GLU cocrystal obtained from the Cambridge Software Database (CSD).

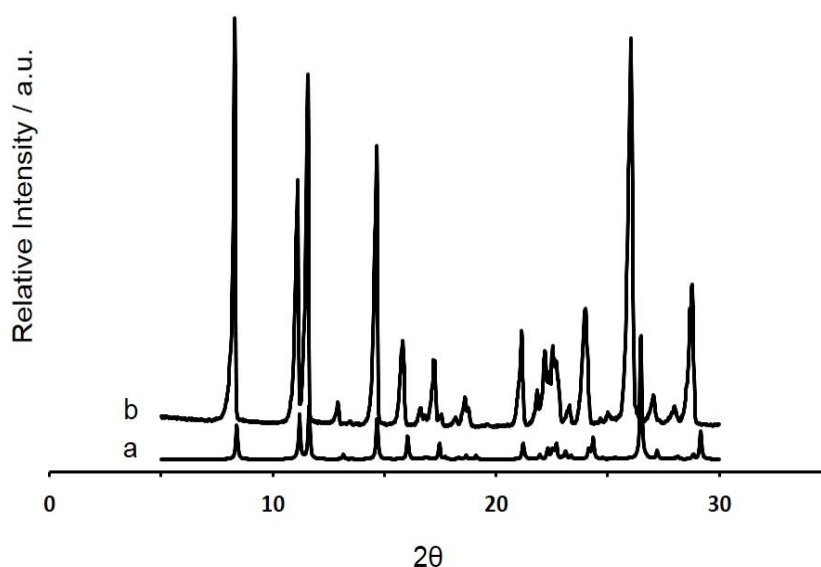


Figure D.3. XRPD diffractograms correspondent to the 1:1 CAF:GLU system: a - cocrystal data obtained from CSD, code EXUQUJ (form II), b - cocrystal obtained by cooling crystallization.

Figure D.4 shows the SEM images obtained for the cocrystal. Plate-shaped individual cocrystals were observed.

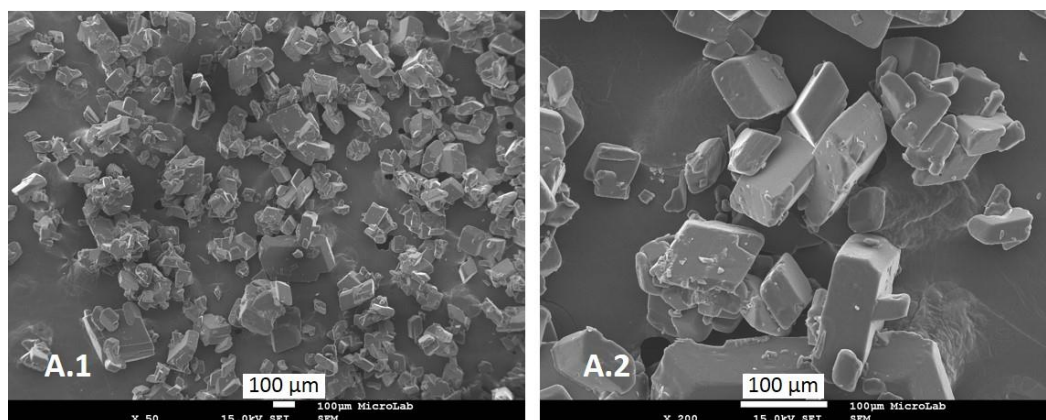


Figure D.4. Micrographs correspondent to the 1:1 CAF:GLU cocrystal produced by cooling crystallization.

- Development of a XRPD limit test for the evaluation of cocrystals purity:

The development of the XRPD limit test as regards to the CAF “impurity” involved two different stages: first, a peak selectivity and preferred orientation analysis was conducted, followed by a second stage that involved the optimization of the XRPD method, preparation of physical mixture and peak area analysis.

1. Peak selectivity and preferred orientation analysis:

Peak selectivity consisted of identifying one or more peaks, preferably with high intensity, in the diffractogram of pure CAF that were absent in the diffractogram of the standard cocrystal, and pure GLU. After this identification stage, an analysis of preferred orientation of the samples was conducted. Pure CAF was gently grinded with mortar and pestle one and two times, during approximately 1 min. After grinding, if the samples reveal preferred orientations, it means that the distribution of the crystallites in the holder is non-random, and the area and the intensity of the peaks will change [2]. The peak at $11.8\ 2\theta$ in the diffractogram of pure CAF was the one selected for being selective against the standard cocrystal and for not revealing preferred orientations, as can be seen in Figure D.5.

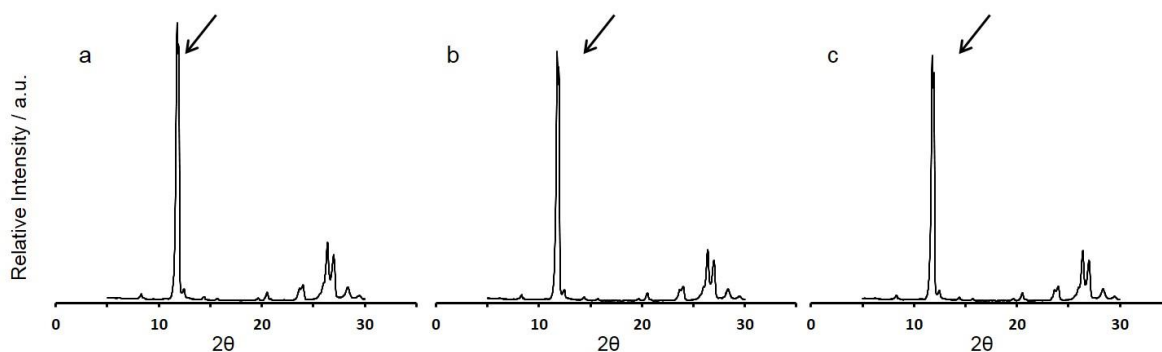


Figure D.5. XRPD diffractograms correspondent to pure CAF: a - as is, b – grinded once, c– grinded twice. The arrows indicate the high intensity 11.8 2θ peak.

2. Optimization of the XRPD method, preparation of the physical mixture and peak area analysis:

The optimization of the XRPD method involved the fine tune of XRPD parameters in order to improve the detection of the peaks in the 2θ range of interest, in this case around the position of the CAF peak selected. The samples were measured over a 2θ interval from 10 to 14° with a step size of 0.017° and step time of 1500 s.

A physical mixture of 1:1 CAF:GLU standard cocrystal (produced using cooling crystallization) and 5 wt.% CAF was prepared. The physical mixture was analyzed using the optimized XRPD method, and the area of the peak at 11.8 2θ was used as the reference. The reflection integration interval considered was from 11.7 to 12.1 2θ .

Figure D.6 shows the XRPD diffractograms of the pure standard cocrystal and 5 wt.% CAF:standard cocrystal physical mixture.

In order to estimate cocrystal purity of the spray-congealed samples, the powders correspondent to Test 1 to 5 were also analyzed using the optimized XRPD method, and the peaks integrated likewise. Figure D.7 shows the XRPD diffractograms at slow scan of Tests 1 to 5.

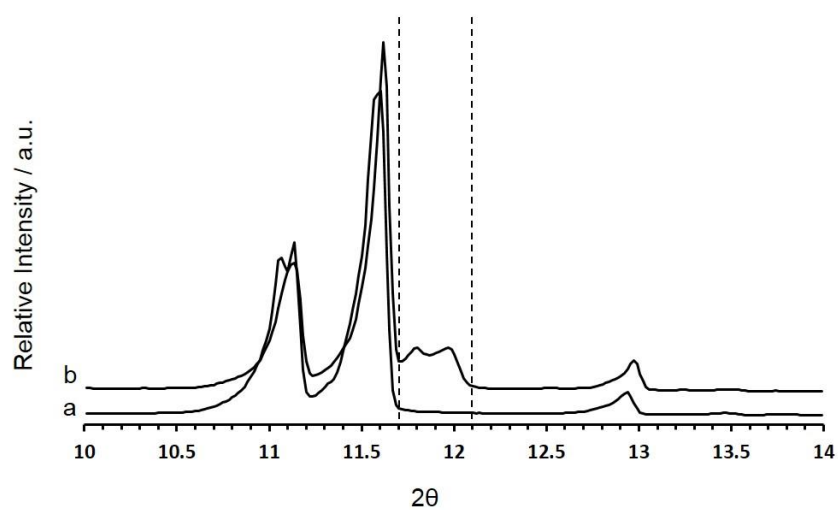


Figure D.6. XRPD diffractograms, at slow scan, correspondent to a - 1:1 CAF:GLU standard cocrystal produced by cooling crystallization and b - 5 wt.% CAF:standard cocrystal physical mixture. The dashed lines represent the integration interval (*i.e.* 11.7 to 12.1 2θ).

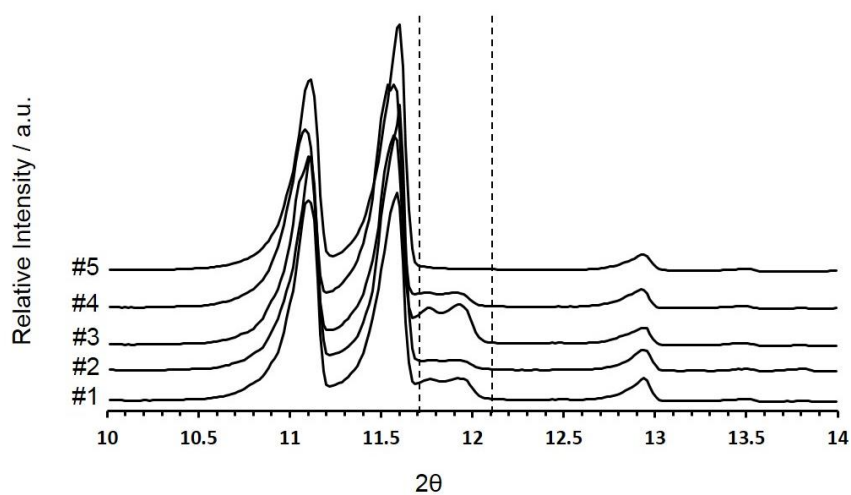


Figure D.7. XRPD diffractograms, at slow scan, correspondent to the spray-congealed 1:1 CAF:GLU cocrystals: #1 to #5 – different tests performed according to the experimental design. The dashed lines represent the integration interval (*i.e.* 11.7 to 12.1 2θ).

References

- [1] Z. Q. Yu, P. S. Chow and R. B. H. Tan, "Operating Regions in Cooling Cocrystallization of Caffeine and Glutaric Acid in Acetonitrile" *Crystal Growth & Design*, vol. 10, no. 5, pp. 2382-2387, 2010.
- [2] L. Padrela, E. Gomes de Azevedo and S. P. Velaga, "Powder X-ray diffraction method for the quantification of cocrystals in the crystallization mixture" *Drug Development and Industrial Pharmacy*, vol. 38, no. 8, pp. 923-929, 2012.